

USAARL Report No. 2016-22

# A Model of Human Orientation and Self-Motion Perception during Body Acceleration: The Orientation Modeling System

By Michael C. Newman<sup>1</sup>, Ben D. Lawson<sup>2</sup>, Angus H. Rupert<sup>2</sup>  
Brad J. McGrath<sup>3</sup>, Amanda M. Hayes<sup>2,4</sup>, Lana S. Milam<sup>1,4</sup>

<sup>1</sup>The National Aerospace Training and Research Center

<sup>2</sup>U.S. Army Aeromedical Research Laboratory

<sup>3</sup>Embry-Riddle Aeronautical University

<sup>4</sup>Laulima Government Solutions, LLC



**United States Army Aeromedical Research Laboratory**

**Auditory Protection and Performance Division  
Aircrew Health and Performance Division**

**September 2016**

Approved for public release; distribution unlimited.

## **NOTICE**

### **Qualified Requesters**

Qualified requesters may obtain copies from the Defense Technical Information Center (DTIC), Cameron Station, Alexandria, Virginia 22314. Orders will be expedited if placed through the librarian or other person designated to request documents from DTIC.

### **Change of Address**

Organizations receiving reports from the U.S. Army Aeromedical Research Laboratory on automatic mailing lists should confirm correct address when corresponding about laboratory reports.

### **Disposition**

Destroy this document when it is no longer needed. Do not return it to the originator.

### **Disclaimer**

The views, opinions, and/or findings contained in this report are those of the author(s) and should not be construed as an official Department of the Army position, policy, or decision, unless so designated by other official documentation. Citation of trade names in this report does not constitute an official Department of the Army endorsement or approval of the use of such commercial items.

<b>REPORT DOCUMENTATION PAGE</b>					<i>Form Approved</i> <i>OMB No. 0704-0188</i>	
<small>The public reporting burden for this collection of information is estimated to average 1 hour per response, including the time for reviewing instructions, searching existing data sources, gathering and maintaining the data needed, and completing and reviewing the collection of information. Send comments regarding this burden estimate or any other aspect of this collection of information, including suggestions for reducing the burden, to Department of Defense, Washington Headquarters Services, Directorate for Information Operations and Reports (0704-0188), 1215 Jefferson Davis Highway, Suite 1204, Arlington, VA 22202-4302. Respondents should be aware that notwithstanding any other provision of law, no person shall be subject to any penalty for failing to comply with a collection of information if it does not display a currently valid OMB control number.</small> <b>PLEASE DO NOT RETURN YOUR FORM TO THE ABOVE ADDRESS.</b>						
<b>1. REPORT DATE (DD-MM-YYYY)</b> 28-09-2016		<b>2. REPORT TYPE</b> Final			<b>3. DATES COVERED (From - To)</b>	
<b>4. TITLE AND SUBTITLE</b> A Model of Human Orientation and Self-Motion Perception during Body Acceleration: The Orientation Modeling System				<b>5a. CONTRACT NUMBER</b>		
				<b>5b. GRANT NUMBER</b>		
				<b>5c. PROGRAM ELEMENT NUMBER</b>		
<b>6. AUTHOR(S)</b> Newman, M. C. Lawson, B. D. Rupert, A. H. McGrath, B. J. Hayes, A. M. Milam, L. S.				<b>5d. PROJECT NUMBER</b>		
				<b>5e. TASK NUMBER</b>		
				<b>5f. WORK UNIT NUMBER</b>		
<b>7. PERFORMING ORGANIZATION NAME(S) AND ADDRESS(ES)</b> U.S. Army Aeromedical Research Laboratory P.O. Box 620577 Fort Rucker, AL 36362					<b>8. PERFORMING ORGANIZATION REPORT NUMBER</b> USAARL 2016-22	
<b>9. SPONSORING/MONITORING AGENCY NAME(S) AND ADDRESS(ES)</b> U.S. Army Medical Research and Materiel Command 504 Scott Street Fort Detrick, MD 21702					<b>10. SPONSOR/MONITOR'S ACRONYM(S)</b> USAMRMC	
					<b>11. SPONSOR/MONITOR'S REPORT NUMBER(S)</b>	
<b>12. DISTRIBUTION/AVAILABILITY STATEMENT</b> Approved for public release; distribution unlimited.						
<b>13. SUPPLEMENTARY NOTES</b>						
<b>14. ABSTRACT</b> Spatial disorientation (SD) is a common cause of human-error-related aircraft mishaps, especially during flight within degraded visual environments. Aviation accident investigators often conduct qualitative perceptual analyses of mishaps when spatial disorientation is inferred as a cause. We have developed a quantitative perceptual model of human spatial orientation and have employed it to evaluate data from a variety of acceleration situations, in order to predict the self-orientation and motion perceptions a person will experience when subjected to various accelerations. The model was able to produce successful simulations of moment-by-moment orientation and self-motion perception data from a variety of acceleration situations. The model also allows for comparison with the outputs of other published models. The features and performance of our model are described in this report. The model has potential applications for aviation modeling, simulation, and human balance maintenance.						
<b>15. SUBJECT TERMS</b> Modeling and simulation, equilibrium, balance, vestibular, spatial orientation, spatial disorientation, SD, DVE						
<b>16. SECURITY CLASSIFICATION OF:</b>			<b>17. LIMITATION OF ABSTRACT</b>  UU	<b>18. NUMBER OF PAGES</b>  91	<b>19a. NAME OF RESPONSIBLE PERSON</b> Loraine St. Onge, PhD	
a. REPORT UNCLAS	b. ABSTRACT UNCLAS	c. THIS PAGE UNCLAS			<b>19b. TELEPHONE NUMBER (Include area code)</b> 334-255-6906	

This page is intentionally blank.

## **Acknowledgements**

Report authors Newman and McGrath thank Charles Oman and Lawrence Young for their extensive mentorship in modeling and their contributions to the current orientation model. The authors thank Daniel Merfeld and Anthony Dietz for their contributions to some of the earlier spatial disorientation modeling efforts of report authors McGrath and Rupert. The authors thank Linda-Brooke Thompson and Shauna Legan for their assistance with this manuscript. The authors thank the following sponsors for supporting past and current aspects of this work: US Army Medical Research and Materiel Command (USAMRMC; In-House Laboratory Independent Research), Small Business Innovative Research program (PEO Aviation), and the Defense Health Program.

This page is intentionally blank.

## Table of Contents

	<b>Page</b>
Introduction.....	1
A Brief History of Orientation Modeling .....	1
Recent Modeling Efforts .....	3
The Current Modeling Effort .....	5
Vestibular Model .....	5
Orientation Angle Calculation .....	7
Hypothetical Limbic Coordinate Frame .....	7
Path Integration .....	8
Horizontal vs. Vertical Motion .....	8
Parameter Adjustment.....	9
Visual-Vestibular Interaction Model .....	9
Visual Observers .....	10
Coordinate Frames .....	10
Visual Sensors.....	11
Internal Model Sensory Dynamics.....	11
Error Calculations .....	11
Complete Orientation Modeling System (OMS) .....	12
Visual Sensory Switches.....	13
Visual Weighting Parameters .....	13
Parameter Calibration .....	14
Perception Toolbox Input .....	15
Perception Toolbox Graphic User Interface .....	17
Perception Models .....	18
Plotting Tools.....	19
Vector Visualization Tools .....	20
Virtual Reality (VR) Visualization Tools .....	20
Vestibulo-ocular Reflex (VOR) Tools.....	22
G-excess Tools.....	23
Summary List of Motion Stimuli.....	24
Sign Conventions and Plot Legends .....	25
Results & Discussion .....	26
Basic Sensory Paradigms.....	26
Earth vertical rotation (dark, light). .....	26
Earth vertical rotation (circularvection).....	27
Fixed radius centrifugation. ....	28
Post-rotational tilt .....	32
Novel Applications .....	34
Coriolis cross-coupling during accelerated rotation. ....	34
Coriolis cross-coupling during constant velocity rotation.....	36
Coriolis cross-coupling during decelerated rotation.....	39
G-Excess illusion.....	41
Somatogravic illusion (dark, light). ....	46
Optokinetic nystagmus (OKN) & optokinetic after-nystagmus (OKAN).....	47
Linearvection. ....	49

## Table of Contents (continued)

	Page
Roll circularvection .....	51
Practical Aviation Applications .....	52
Post-turn illusion in degraded visual conditions.....	52
Post-turn illusion with artificial visual orientation cue.....	54
Coriolis head movement during a coordinated turn. ....	55
Case Study: F18 Mishap Analysis .....	56
Mishap summary. ....	56
Data preparation.....	57
F18 mishap analysis (Isolated angular velocity cues). ....	59
F18 mishap analysis (Angular velocity + linear acceleration cues). ....	60
F18 mishap analysis (G-excess parameter adjustment).....	65
Visualization tool.....	66
Further considerations. ....	66
Conclusions.....	67
Recommendations.....	68
References.....	71

## List of Figures

1. Original Merfeld spatial orientation model (Merfeld et al., 1993). ....	3
2. Timeline of development of velocity storage, observer and optimal control (KF, EKF, UKF) perception models. ....	3
3. Merfeld et al. (1993) Spatial Orientation Model. ....	6
4. Extended vestibular model.....	6
5. Model response to sinusoidal vertical (A) and horizontal (B) displacement profiles.....	9
6. Block diagram representation for a generic visual model pathway.....	10
7. Orientation Modeling System (OMS) block diagram.....	13
8. Model stability assessment during a rollvection stimulus.. ....	15
9. Example Excel input file.....	16
10. Main graphical user interface.....	17
11. Plotting Tools graphical user interface. ....	19
12. Vector Visualization Tools graphical user interface.....	20
13. Virtual Reality Visualization Tools graphical user interface.....	21
14. Vestibulo-Ocular Reflex Tools graphical user interface. ....	22
15. Merfeld & Zupan (2002) Vestibulo-Ocular Reflex Model.....	23
16. G-excess Tools graphical user interface. ....	24
17. Model predictions for constant velocity rotation about an Earth-vertical axis.....	26
18. Model predictions for constant velocity yaw circularvection.....	27
19. Borah, Young, and Curry (1978) estimated angular velocity for Earth vertical constant velocity rotation in the dark and light and with a moving visual field (circularvection).....	28
20. Model response during 175°/s rotation in a 1m radius centrifuge.....	30
21. Merfeld and Zupan (2002) modeling results for fixed radius (1 m) centrifugation.....	31
22. Model response to a 90° post-rotational tilt (nose-down) following 100°/s constant velocity Earth vertical yaw rotation.....	32



## Table of Contents (continued)

### List of Figures (continued)

	Page
23. Merfeld and Zupan (2002) modeling results for a 90° post-rotational tilt (nose-down) .....	33
24. Model response to a 30° head tilt during Earth vertical accelerated rotation. ....	34
25. Model response to a 30° head tilt during accelerated rotation.....	35
26. Vector analysis of estimated angular velocity immediately following 30° roll tilt. ....	35
27. Model response to a 30° head tilt during Earth vertical constant velocity rotation.....	37
28. Model response to a 30° head tilt during constant velocity rotation.. ....	38
29. Vector analysis of estimated angular velocity immediately following 30° roll tilt. ....	38
30. Model response to a 30° head tilt during Earth vertical decelerated rotation. ....	39
31. Model response to a 30° head tilt during decelerated rotation.. ....	40
32. Vector analysis of estimated angular velocity immediately following 30 degree roll tilt. ....	41
33. Gravitoinertial force projection following a head turn made in normal (A, B, C) and hypergravity (D, E, F) conditions.. ....	42
34. Model response to a 45° head tilt during 2G vertical linear acceleration.....	43
35. Model response to a 45° head tilt during 2G vertical linear acceleration.....	44
36. Model response to a 45° head tilt during 2G vertical linear acceleration with modified Kaa parameter.....	45
37. Model response to a 45° head tilt during 2G vertical linear acceleration with modified Kaa parameter.....	45
38. Model response to a step in forward linear acceleration.....	46
39. Slow phase eye velocity in response to 180°/s rotation in the dark (A, D), circular vection (B, E) and rotation in the light (C, F).....	48
40. Model response during step changes in vection field velocity.. ....	50
41. Model response to a 45°/s circular roll vection stimulus.....	51
42. Perception Toolbox tilting and tumbling visualization tool during constant velocity roll circular vection.....	52
43. Model input to the semicircular canal (A) and otolith organs (B) during a coordinated 2-min turn. ....	53
44. Estimated roll angle during coordinated turn without visual sensory input. ....	54
45. Estimated roll angle during coordinated turn with a visual orientation cue from an artificial horizon indicator. ....	55
46. Angular velocity perception following a cross-coupled head movement during a coordinated turn. ....	55
47. Vector analysis of estimated angular velocity immediately following 30° roll tilt. ....	56
48. Spline fits for F18 mishap analysis.....	58
49. Orientation perception during F18 mishap (angular velocity).....	59
50. Orientation perception during F18 mishap (angular velocity + linear acceleration cues).....	60
51. Actual and estimated pilot orientation during F18 mishap (Part I of III). ....	61
52. Actual and estimated pilot orientation during F18 mishap (Part II of III).....	62
53. Actual and estimated pilot orientation during F18 mishap (Part III of III). ....	63
54. Errors in roll, pitch, and yaw perception.....	64
55. Comparison of orientation perception during F18 mishap with and without G-excess parameter adjustment. ....	65

## Table of Contents (continued)

### List of Figures (continued)

	Page
56. F18 mishap visualization tools.....	66

### List of Tables

1. Perception Model Applications & Validation Stimuli.....	4
2. Vestibular Parameters .....	14
3. Visual Parameters .....	14
4. Stability Ranges for Visual Weighting Parameters .....	15
5. Spatial Orientation Models Included in Perception Toolbox .....	18
6. List of Motion Profiles Included With Perception Toolbox .....	24
7. Plot Trace Color Legend .....	25
8. Sign Conventions .....	25
9. Sensory Cues.....	25

## Introduction

Afferent inputs concerning resultant gravitational and self-generated bodily accelerations are critical to the efferent control outputs one makes to skeletal musculature. Afferent, efferent, and reafferent signals are continually integrated to permit coordinated activity and build an accurate mental model of one's spatial orientation. The perception and control of body orientation evolved mainly in response to self-generated accelerations unlike those encountered during passive vehicle travel or other unusual motions frequently experienced in present times. Unusual accelerations and associated sensorimotor (e.g., visual-vestibular) discordances are common during aviation operations, sea travel, cross-country land travel, moving-based and centrifuge-based training, space flight, and extra-planetary surface exploration. These situations induce spatial disorientation, degraded dynamic visual acuity, motion sickness, and difficulty concentrating (Guedry & Oman, 1990; Graybiel & Knepton, 1976; Lawson & Mead, 1998; Lawson, Smith, Kass, Kennedy, & Muth, 2003; Gibb, Ercoline, & Scharff, 2011; Lawson, Rupert, Guedry, Grissett, & Mead, 1997; Cowings, Toscano, De Roshia, & Tauson, 2001; Lathan & Clement, 1997). Even during active voluntary movement, sensory disturbances may arise when the movement occurs in a non-terrestrial force environment (e.g., a space station, the Moon) or when the moving person is experiencing the aftereffects of specific insults to the vestibular system (e.g., due to head injury or vestibular disease). This paper concerns the application of mathematical modeling to the study of orientation perception and sensory illusions associated with movement. We describe past modeling efforts and our effort to refine the state of orientation modeling.

## A Brief History of Orientation Modeling

Static orientation models have been developed (e.g., Correia, Hixson, & Niven, 1968) that describe whole body tilt perception (which typically determines body control motor commands) and vestibular gaze reflexes (which determine functional dynamic visual acuity) during constant acceleration stimuli, such as acceleration due to gravity during body tilt or resultant (centripetal plus gravitational) acceleration during constant velocity centrifugation (off-center rotation). Relatively simple models of orientation during head movement also have been devised and empirically evaluated over the years (e.g., Guedry & Benson, 1978; Lawson, Guedry, Rupert, & Anderson, 1994).

As validated models of semicircular canal (SCC) and otolith dynamics became available in the 20<sup>th</sup> century (Goldberg & Fernandez, 1971; Fernandez & Goldberg, 1976a, 1976b, 1976c), it became evident that end organ response alone could not adequately account for the time course of the vestibulo-ocular reflex (VOR). Moreover, the duration of the illusory after-rotation sensation and the post-rotatory eye movements following constant velocity earth vertical rotation was found to extend well beyond that of the actual SCC afferent firing duration, a phenomenon that is called velocity storage (Raphan, Matsuo, & Cohen, 1979). Likewise, the gradual time course of the somatogravic illusion (i.e., the well-known pitch-up illusion that occurs in response to forward linear acceleration) could not be explained by otolith afferent dynamics alone. Early attempts to model these effects included the velocity storage models developed by Robinson (1977) and Raphan, Matsuo, and Cohen (1977, 1979) and the complementary filter model developed by Mayne (1974).

More advanced models, based on concepts from estimation theory in engineering, have been developed and applied primarily in the field of vestibular physiology (Borah, Young, & Curry, 1978; Merfeld, Young, Oman, & Shelhamer, 1993; Merfeld & Zupan, 2002; Haslwanter, Jaeger, Mayr, & Fetter, 2000; Vingerhoets, Van Ginsbergen, & Medendorp, 2007; Selva, 2009). Borah, Young and Curry (1978, 1988) developed a steady-state Kalman Filter (KF) to model the orientation perception of a human riding passively in a vehicle. Their model included vestibular motion cues as well as dynamic angular and linear visual velocity information. While the Borah model was capable of predicting responses to a number of vestibular and visual-vestibular motion paradigms, the linear nature of the KF restricted its application to small head deviations from the postural upright. Pommellet (1990) modified Borah's internal model and implemented a time varying Extended Kalman Filter (EKF) to account for full nonlinear motion dynamics. The EKF model was able to match Borah's predictions for simple stimuli; however, it exhibited numerical instabilities during more complex motion profiles involving larger estimated tilt angles. A follow-up EKF study by Bilien (1993) investigating the vestibular portions of the model encountered similar difficulties when modeling Coriolis cross-coupling responses.

Kynor (2002) and Selva (2009) developed stable implementations of the EKF (Selva also developed a stable Unscented Kalman Filter (UKF) version of the Borah model) and were able to successfully model a number of nonlinear, large angle perceptual responses, including centrifugation and the pitch-up illusion (during rapid forward acceleration such as a catapult launch takeoff). While the stabilized model was able to reproduce simple visual illusions, such as linearvection, its integration of visual sensory pathways did not appear to match the true architecture or behavior of the Central Nervous System (CNS). For example, the model relied on visual velocity information (via visual flow of the surrounding visual scene) to suppress the somatogravic illusion in the light, a response which was not found experimentally (Tokumaru, Kaida, Ashida, Misumoto, & Tatsuno, 1998). Results were also highly dependent on model parameter assumptions and were extremely sensitive to even small deviations in the assumed sensor bandwidths or noise covariance matrices. Finally, the model failed to reproduce sensations arising from contradictory vestibular sensory information. This finding led Bilien (1993) to conclude that the optimal implementation of the KF and EKF may actually be "too optimal" to model the central nervous system's spatial orientation processes.

Merfeld, Young, Oman, and Shelhamer (1993) developed a useful "Observer" model of human spatial orientation based on the state Observer framework proposed by Luenberger (1971). Merfeld's model (Figure 1) utilized nonlinear quaternion mathematics and internal models of semicircular canal and otolith dynamics to solve for central estimates of angular velocity, linear acceleration, and gravity. By empirical adjustment of the four internal weighting parameters in Figure 1 ( $k_\omega, k_{f\omega}, k_f, k_a$ ), this model was capable of predicting the orientation illusions that occur during a number of motion stimuli, including constant velocity earth-vertical rotation, off-vertical-axis rotation (OVAR), and post-rotational tilt. Refinements by Haslwanter, Jaeger, Mayr, & Fetter (2000), Merfeld & Zupan (2002) and Vingerhoets et al. (2007) provided further model validation (see Figure 2 for a brief history of Observer and optimal control model development).

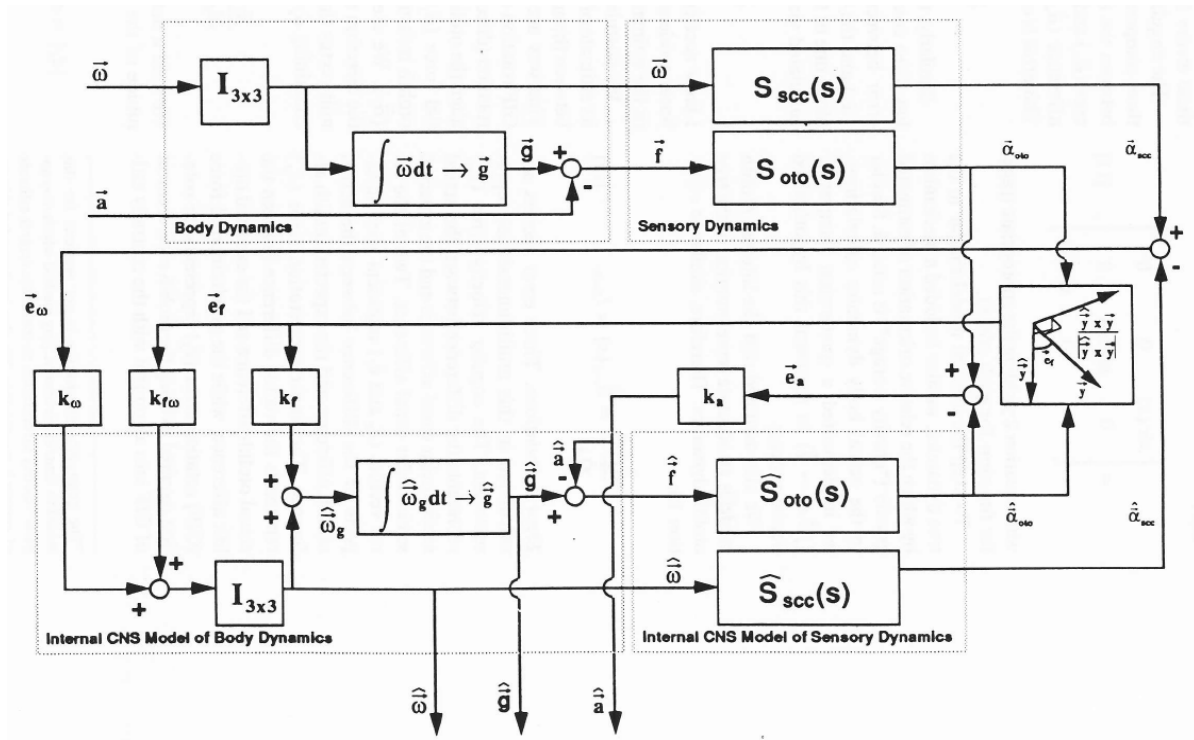


Figure 1. Original Merfeld spatial orientation model (Merfeld et al., 1993).

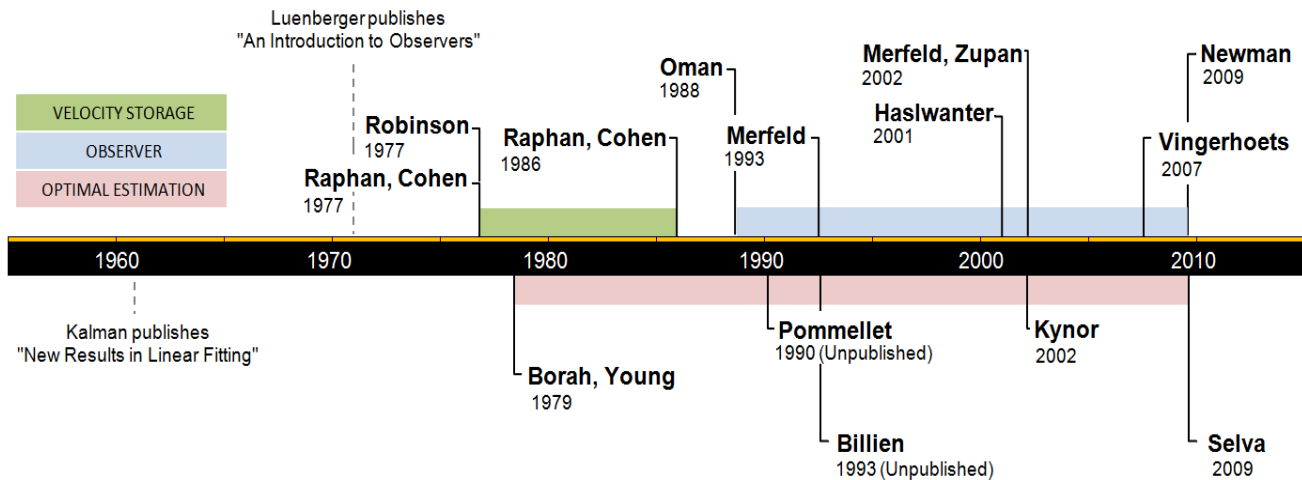


Figure 2. Timeline of development of velocity storage, observer and optimal control (KF, EKF, UKF) perception models.

## Recent Modeling Efforts

Newman (2009) attempted to add visual sensory information to the original Observer model framework and extend model predictions to include orientation, position and linear

velocity estimates. Newman's model was able to mimic orientation perceptions, linear and circular vection, rotation in the light, and acceleration in the light. A summary of the motion paradigms simulated successfully by this model and others is presented in Table 1.

*Table 1.* Perception Model Applications & Validation Stimuli

	Velocity Storage	OVAR	Post- rotational Tilt	Somatogravic Illusion (Centrifuge)	Somatogravic Illusion (Sled)	Roll Tilt	Circular Vection	Linear Vection	Coriolis
<b>Observer Models</b>									
Merfeld 1993	✓	✓	✓	-	-	-	-	-	-
Haslwanter 2001	-	✓	-	-	-	-	-	-	-
Merfeld & Zupan 2002	-	-	-	✓	-	✓	-	-	-
Vingerhoets 2007	-	✓	-	-	-	✓	-	-	-
Newman 2009	✓	✓	✓	✓	✓	-	✓	✓	✓
<b>Optimal Control Models</b>									
Borah 1979	✓	-	-	-	✓	-	✓	✓	-
Pommellet 1990	✓	-	-	✓	✓	-	✓	✓	-
Bilien 1993	-	-	-	✓	-	-	-	-	✓
Kynor 2002	✓	-	-	✓	✓	-	-	-	-
Selva 2009	✓	-	-	-	✓	-	✓	-	✓

Until recently, orientation perception modeling has not been applied extensively to large-amplitude or dynamic, multi-axis, three-dimensional motions such as those that occur during natural movement or during usual aircraft maneuvers. The Disorientation Analysis and Prediction System (DAPS) developed by Creare Inc. implemented the stable Kynor (2002) EKF algorithm into a MatLab<sup>®</sup>-based graphical user interface (GUI). DAPS was able to successfully predict SD during two A-10 accident scenarios. Since both of the chosen A-10 accidents were the result of underestimation of roll rate or roll angle, the general utility of DAPS for high-G, supra-threshold, tactical-flight analysis remains uncertain. Additionally, the aforementioned limitations of the Kynor (2002) EKF model should be considered when using DAPS to estimate perceptions during high otolith-canal conflict, especially in the presence of visual flow sensory input.

Small et al. (2006) of Alion Corp. developed a Spatial Disorientation Analysis Tool (SDAT) that included a sophisticated user interface, rules for classification of classic orientation illusions, and a rudimentary model for sensory cue interaction. Attempts to incorporate a more accurate Observer model of human perception into SDAT proved difficult due to the inherent differences between the two modeling techniques (Small et al., 2011).

Groen, Smaili, and Hosman (2007) proposed an alternative (non-Observer) model for human orientation perception and provided a toolbox of MatLab<sup>®</sup> routines and Simulink<sup>®</sup> block diagrams. Although comprehensive and well-documented, the result was ultimately only accessible to expert MatLab<sup>®</sup> users.

In order to improve upon these earlier efforts, a new perception model, the Orientation Modeling System (OMS), was developed and integrated into a GUI-based program called Perception Toolbox. The OMS is an extension of the Merfeld Observer family of models and the

subsequent visual-vestibular topology developed by Newman (2009). The methodology for extending the Merfeld model and adding the visual sensory components is detailed in sections “The current modeling effort” and “Visual-vestibular interaction model” of this report. The OMS was programmed in MatLab<sup>®</sup> and Simulink<sup>®</sup> and was designed specifically for direct integration with Perception Toolbox. Perception Toolbox is a suite of perception research and visualization tools. Perception Toolbox was designed to improve the accessibility and functionality of perception model use during sensorimotor research, and applied investigations of human error-related accidents. Specifically, Perception Toolbox attempts to:

- Improve visualization techniques of dynamic human perception;
- Facilitate comparison between existing perception models;
- Provide a broad set of predefined modeling applications, based on simulations from the laboratory and aviation settings;
- Provide specific tools to better visualize the complex dynamics of the Coriolis cross-coupling effect (Guedry & Benson, 1978);
- Extend model predictions to better account for and visualize the G-excess effect (Guedry & Rupert, 1991); and
- Provide general tools for prediction of reflexive vestibular gaze reactions.

The features of Perception Toolbox are outlined in the section “Perception toolbox,” beginning on page 15. In the next section, we discuss the key features of the model itself before returning to its visualization tools.

## **The Current Modeling Effort**

### **Vestibular Model**

The vestibular core of the OMS is based on Merfeld’s Spatial Orientation Model shown in Figure 3 (Merfeld et al., 1993). Note that the Merfeld model presented in Figure 3 has been rearranged so that it resembles the presentation format of Haslwanter et al. (2000). In the model in Figure 3, three-dimensional vectors of linear acceleration ( $\vec{a}$ ) and angular velocity ( $\vec{\omega}$ ) are input to the model in a head-fixed coordinate frame. Angular velocity is integrated using a quaternion integrator ( $\int \vec{\omega}$ ) to keep track of the orientation of gravity ( $\vec{g}$ ) with respect to the head. The otolith transfer functions (OTO) are modeled as unity and respond to the gravito-inertial force (GIF) ( $\vec{f} = \vec{g} - \vec{a}$ ).

The SCC are modeled as second-order high-pass filters with a cupula-endolymph long time constant of 5.7 s and a neural adaptation time constant of 80 s. Afferent signals from the canals and otoliths are compared in the CNS “Observer” against expected values from a similar set of internal sensory dynamics ( $\hat{SCC}$ ,  $\hat{OTO}$ ). The resultant error signals are weighted with four free parameters ( $k_\omega, k_{f\omega}, k_f, k_a$ ) highlighted in green. The model outputs are central estimates of linear acceleration ( $\hat{\vec{a}}$ ), gravity ( $\hat{\vec{g}}$ ), and angular velocity ( $\hat{\vec{\omega}}$ ). Note that hatted variables ( $\hat{\phantom{x}}$ ) represent estimated states.

The original Merfeld topology was designed to process only vestibular sensory information. In order to incorporate visual cues, several structural modifications and extensions

were required (Figure 4). These modifications are described in the section “Orientation angle calculation” and based on previous research conducted by the author (Newman, 2009).

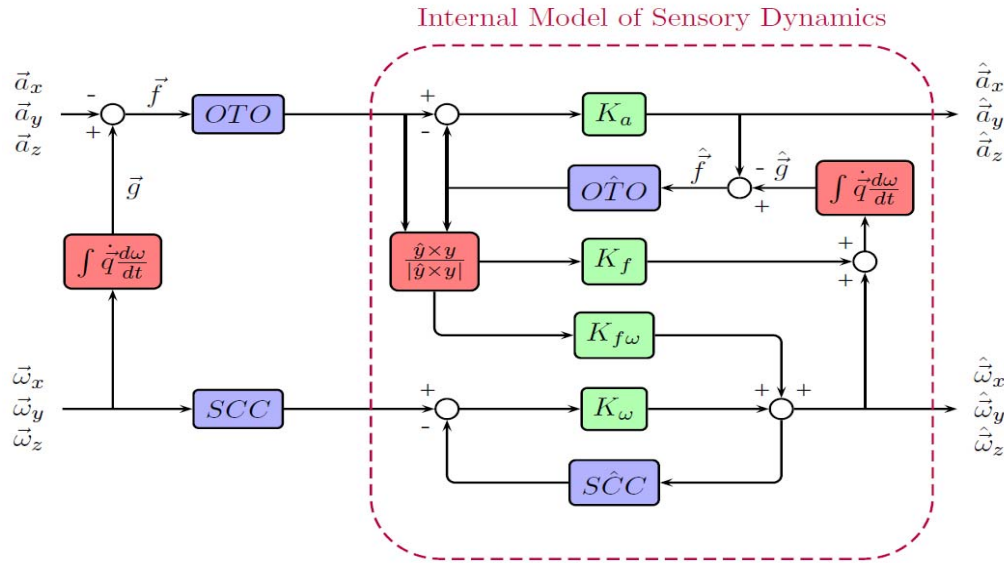


Figure 3. Merfeld et al. (1993) Spatial Orientation Model.

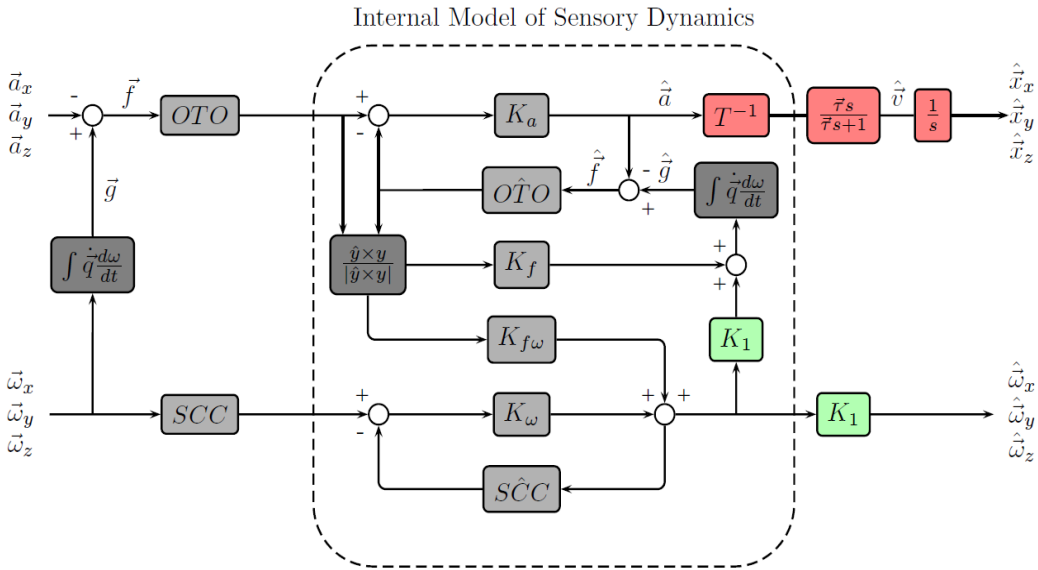


Figure 4. Extended vestibular model. Blocks highlighted in red and green have been added to the original Merfeld model topology. See page 12 for further explanation.



## Orientation Angle Calculation

Although the original Merfeld model provides a representation of gravity, it does not provide a direct calculation of the roll, pitch, and yaw angle of the simulated subject. We can derive true roll ( $\phi$ ), pitch ( $\theta$ ), and yaw ( $\psi$ ) Euler angles from the quaternion integrator used to keep track of the true gravitational vector, ( $\vec{g}$ ) (see Appendix for a full description of the quaternion mathematics used throughout this report).

$$\begin{aligned}\phi &= \text{atan}\left(\frac{2(q_0q_1 + q_2q_3)}{q_0^2 - q_1^2 - q_2^2 + q_3^2}\right) \\ \theta &= \text{asin}(-2(q_3q_1 - q_2q_0)) \\ \psi &= \text{atan}\left(\frac{2(q_2q_1 + q_0q_3)}{q_0^2 + q_1^2 - q_2^2 - q_3^2}\right)\end{aligned}$$

Likewise, we can derive estimated roll ( $\hat{\phi}$ ), pitch ( $\hat{\theta}$ ), and yaw ( $\hat{\psi}$ ) Euler angles from the quaternion integrator used to keep track of the estimated gravitational vector ( $\hat{\vec{g}}$ ).

$$\begin{aligned}\hat{\phi} &= \text{atan}\left(\frac{2(\hat{q}_0\hat{q}_1 + \hat{q}_2\hat{q}_3)}{\hat{q}_0^2 - \hat{q}_1^2 - \hat{q}_2^2 + \hat{q}_3^2}\right) \\ \hat{\theta} &= \text{asin}(-2(\hat{q}_3\hat{q}_1 - \hat{q}_2\hat{q}_0)) \\ \hat{\psi} &= \text{atan}\left(\frac{2(\hat{q}_2\hat{q}_1 + \hat{q}_0\hat{q}_3)}{\hat{q}_0^2 + \hat{q}_1^2 - \hat{q}_2^2 - \hat{q}_3^2}\right)\end{aligned}$$

## Hypothetical Limbic Coordinate Frame

Many visual and vestibular perceptions require erroneous estimates of one's position, velocity, and/or acceleration. Brownout during a vertical helicopter landing and helicopter rotor wash are examples of disorienting situations wherein position and velocity information becomes confusing or erroneous. In order to estimate perception of linear velocity and position with the model, we must integrate our estimate of linear acceleration in the proper coordinate frame used for human navigation.

To accomplish this, we assume that the CNS integrates the perceived linear acceleration vector ( $\hat{\vec{a}}$ ) in an allocentric reference frame oriented to the local vertical. We refer to this frame, which is aligned with the perceived gravitational horizontal, as the “limbic coordinate frame,” since a variety of physiological evidence suggests that estimates of azimuth and direction originate in limbic areas of the brain, including the hippocampus, thalamus, and medial entorhinal cortex. Neural coding of place and grid cells (Best, White, & Minai, 2001; Hafting, Fyhn, Molden, Moser, & Moser, 2005; Calton & Taube, 2005; Knierim, McNaughton, & Poe, 2000; Knierim, Poe, & McNaughton, 2003; Oman, 2007), along with orientation and wayfinding experiments performed in 1G (Aoki, Ohno, & Yamaguchi, 2003; Aoki, Ohno, & Yamaguchi, 2005) and 0G (Vidal, Lipshits, McIntyre, & Berthoz, 2003; Vidal, Amorim, & Berthoz, 2004), suggest that natural perception is designed for terrestrial 2D navigation with reference to a gravitationally upright body axis (Vidal et al., 2004).

This limbic coordinate frame is defined by the quaternion vector ( $\hat{q}$ ) from the estimated gravitation state ( $\hat{g}$ ). At each time step of the simulation, the estimated linear acceleration vector is transformed to the limbic coordinate system (represented by the red T-1 block in Figure 4) and integrated twice to obtain estimates of position and velocity (represented by the red transfer functions shown earlier in Figure 4). For a detailed description of the quaternion mathematics and transformation methods employed, the reader is referred to the Appendix.

### Path Integration

Integration of estimated acceleration ( $\hat{a}$ ) to estimated velocity ( $\hat{v}$ ) is accomplished with leaky integration with individual time constants for motion about each limbic coordinate axis. The transfer function for this leaky integration is displayed below.

$$\hat{v} = \frac{\vec{\tau}s}{\vec{\tau}s + 1} \hat{a}$$

$$\vec{\tau} = \begin{bmatrix} 16.67 \\ 16.67 \\ 1.0 \end{bmatrix}$$

A standard integrator was implemented for the velocity-to-position integration to ensure that a static visual position input would result in a dynamic response with zero steady-state error. Leaky dynamics initiate phase and magnitude estimation errors, which do not correspond to perceived reality (e.g., displacement estimates for sinusoidal horizontal translatory motion should remain accurate with a visual position reference). The transfer function for this integration is displayed below.

$$\hat{x} = \frac{1}{s} \hat{v}$$

### Horizontal vs. Vertical Motion

It should be noted that time constants for motion within the horizontal plane differ substantially from those associated with vertical motion along the actual or perceived direction of gravity ( $\tau = 16.66s$  vs.  $\tau = 1.0s$ ). Position and velocity estimation within the horizontal plane has been shown to be fairly accurate for a range of motion amplitudes and frequencies (Israël, Grasso, Georges-Francois, Tsuzuki, & Berthoz, 1989; Mittelstaedt & Mittelstaedt, 2001; Seidman, 2008; Guedry & Harris, 1963; Mittelstaedt & Glasauer, 1991; Loomis et al., 1993).

Large-amplitude studies performed in helicopters and vertical motion devices (Walsh, 1964; Malcolm & Jones, 1973; Jones & Young, 1978) have shown a fundamental limitation in the ability of humans to integrate inertial acceleration cues along a gravitationally vertical axis. Experimental subjects were found unable to correctly indicate the magnitude or direction of motion, often eliciting phase errors of 180°. While aware of vertical displacement, subjects could indicate the proper direction of travel only slightly better than chance. To model these large

phase and magnitude estimation errors, the leaky integration time constant about the perceived vertical has been substantially shortened (Figure 5).

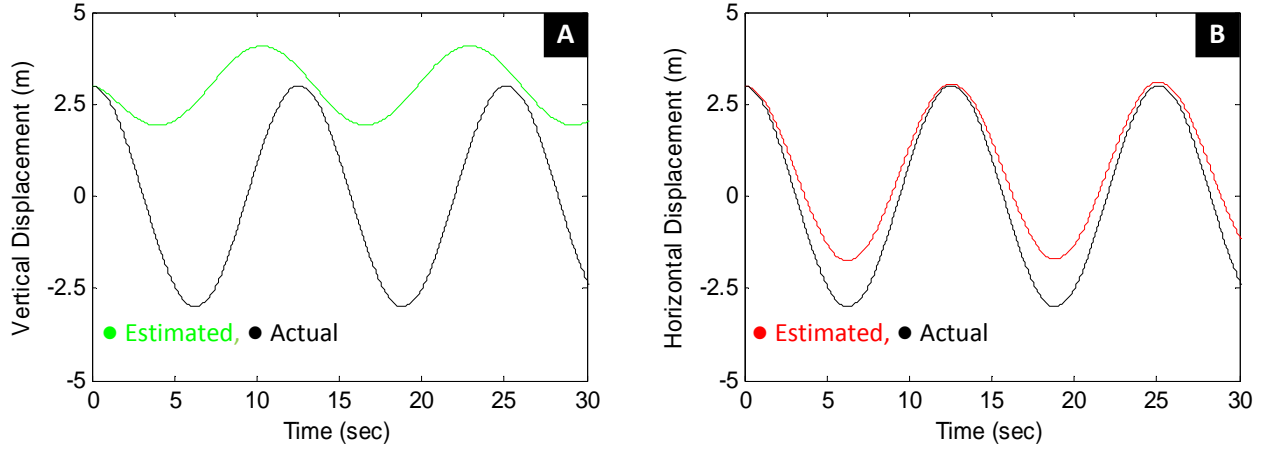


*Figure 5.* Model response to sinusoidal vertical (A) and horizontal (B) displacement profiles. Horizontal motion is perceived fairly accurately with a slight magnitude misestimation. Vertical motion exhibits larger phase and magnitude errors.

### Parameter Adjustment

An additional feedback gain ( $k_1$ ) has also been added to the model (highlighted in green in Figure 4). This parameter is a function of the angular velocity feedback gain ( $k_\omega$ ) and cannot be set or modified directly.  $k_1$  is required to make the loop gain of the angular velocity feedback loop unity. We calculate  $k_1$  as;

$$k_1 = \frac{k_\omega + 1}{k_\omega}$$

The loop gain for the angular velocity pathway is calculated as the reciprocal of the above equation,  $k_\omega / (k_\omega + 1)$ . Using the Merfeld & Zupan (2002) parameter ( $k_\omega = 3$ ), the loop gain is found to be 0.75. This gain was intentionally set to mimic the 70% angular VOR response for eye movement data, yet is inconsistent with perceptual responses for many simple experiments (e.g., static tilt, constant velocity yaw rotation), where the initial response to sudden head movements is veridical.

### Visual-Vestibular Interaction Model

The preceding vestibular model extensions described in the last section (“Vestibular model development”) are essential prerequisites for the addition of visual sensory information. We describe here this modified visual-vestibular sensory interaction model.

## Visual Observers

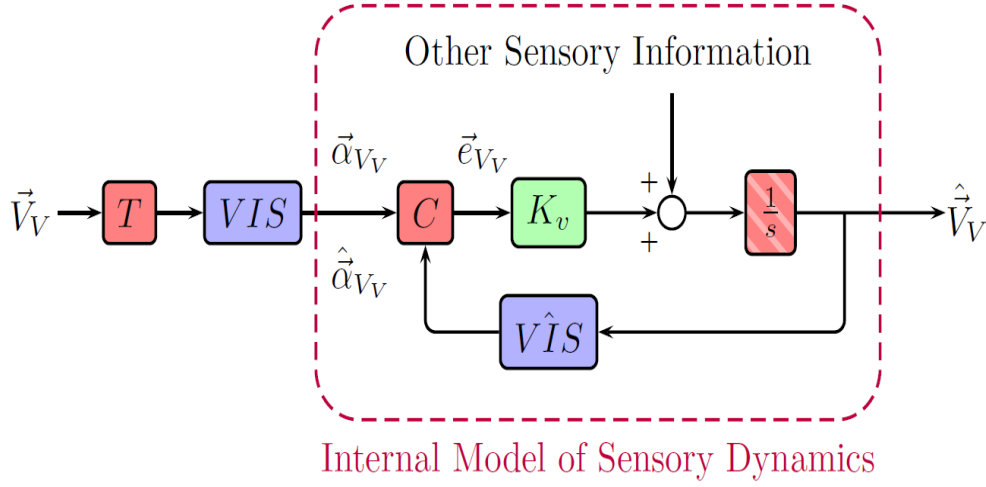


Figure 6. Block diagram representation for a generic visual model pathway. See text for explanation.

To keep the model structure and notation consistent with the original Merfeld model (Merfeld et al., 1993), each visual pathway is constructed as shown in Figure 6. For a generic visual pathway  $V$ , a visual input ( $\vec{V}_v$ ) is processed by the visual sensor ( $VIS$ ) to generate a visual sensory estimate ( $\vec{\alpha}_{V_v}$ ). This estimate is compared ( $C$ ) to an expected visual sensory estimate ( $\hat{\alpha}_{V_v}$ ) from an internal model of the visual sensor ( $\hat{VIS}$ ). The comparative difference ( $\vec{e}_{V_v}$ ) (sensory conflict) is weighted with a residual weighting parameter ( $K_v$ ) and added to the rate of change of the estimated state ( $\hat{\vec{V}}_v$ ). The weighted conflict vector is added to the derivative of the state in order to keep the visual model additions consistent with the structure of a classic Luenberger Observer. Since Merfeld et al. did not include an integrator in the forward loop of the angular velocity feedback pathway, we added the weighted visual angular velocity error directly to the state itself.

## Coordinate Frames

We assume that the visual system is capable of extracting four visual cues from its environment. These are position ( $\vec{x}_v$ ), linear velocity ( $\dot{\vec{x}}_v$ ), angular velocity ( $\vec{\omega}_v$ ), and gravity/orientation ( $\vec{g}_v$ ). The visual input variables are represented by three-dimensional vectors in a right handed, orthogonal, world-fixed, frame of reference ( $XW, YW, ZW$ ). To ensure congruency with the vestibular model's head and limbic coordinate frames, the visual cues are transformed to their respective frames of interaction prior to sensory processing. Visual gravity and angular velocity are transformed to the head-fixed coordinate axes and visual position and velocity are transformed to the perceived limbic frame.

## Visual Sensors

For simplicity, we assume that the visual system sensory dynamics can be approximated as unity for both static and dynamic visual inputs. We do not yet distinguish between focal and ambient vision or account for visual saturation limits for linear and circular vection cues. These are planned future modifications to the model. The current simplified visual model allows for a baseline assessment of the usefulness and practicality of Observer theory for modeling multi-sensory interaction. In three-dimensional space, we can represent each visual sensor as a 3x3 identity matrix. Since dynamic inputs illicit a sensation of motion in the opposite direction of the visual field (e.g., linear vection and circular vection), the dynamic sensors are modeled as negative 3x3 identity matrices. Each sensor transforms visual input ( $\vec{x}_V \ \dot{\vec{x}}_V \ \vec{\omega}_V \ \vec{g}_V$ ) to visual sensory estimates ( $\vec{\alpha}_{x_V} \ \vec{\alpha}_{\dot{x}_V} \ \vec{\alpha}_{g_V} \ \vec{\alpha}_{\omega_V}$ ).

Static Visual Cues	Dynamic Visual Cues
$\frac{\vec{\alpha}_{x_V}}{\vec{x}_V} = VIS_x = \begin{bmatrix} 1 & 0 & 0 \\ 0 & 1 & 0 \\ 0 & 0 & 1 \end{bmatrix} = I_{3 \times 3}$	$\frac{\vec{\alpha}_{\dot{x}_V}}{\dot{\vec{x}}_V} = VIS_{\dot{x}} = \begin{bmatrix} -1 & 0 & 0 \\ 0 & -1 & 0 \\ 0 & 0 & -1 \end{bmatrix} = -I_{3 \times 3}$
$\frac{\vec{\alpha}_{g_V}}{\vec{g}_V} = VIS_g = \begin{bmatrix} 1 & 0 & 0 \\ 0 & 1 & 0 \\ 0 & 0 & 1 \end{bmatrix} = I_{3 \times 3}$	$\frac{\vec{\alpha}_{\omega_V}}{\vec{\omega}_V} = VIS_{\omega} = \begin{bmatrix} -1 & 0 & 0 \\ 0 & -1 & 0 \\ 0 & 0 & -1 \end{bmatrix} = -I_{3 \times 3}$

## Internal Model Sensory Dynamics

We assume that the CNS possesses accurate internal models for each visual sensor. Since the CNS already accounts for the proper direction of the visual estimate, we can represent all internal models of visual sensory dynamics as positive 3x3 identity matrices. The internal model of the visual sensors transform the central state estimates ( $\hat{\vec{x}}_V \ \hat{\dot{\vec{x}}}_V \ \hat{\vec{g}}_V \ \hat{\vec{\omega}}_V$ ) to expected visual sensory estimates ( $\hat{\vec{\alpha}}_{x_V} \ \hat{\vec{\alpha}}_{\dot{x}_V} \ \hat{\vec{\alpha}}_{g_V} \ \hat{\vec{\alpha}}_{\omega_V}$ ).

$\frac{\hat{\vec{\alpha}}_{x_V}}{\hat{\vec{x}}_V} = V\hat{I}S_x = \begin{bmatrix} 1 & 0 & 0 \\ 0 & 1 & 0 \\ 0 & 0 & 1 \end{bmatrix} = I_{3 \times 3}$	$\frac{\hat{\vec{\alpha}}_{\dot{x}_V}}{\hat{\dot{\vec{x}}}_V} = V\hat{I}S_{\dot{x}} = \begin{bmatrix} 1 & 0 & 0 \\ 0 & 1 & 0 \\ 0 & 0 & 1 \end{bmatrix} = I_{3 \times 3}$
$\frac{\hat{\vec{\alpha}}_{g_V}}{\hat{\vec{g}}_V} = V\hat{I}S_g = \begin{bmatrix} 1 & 0 & 0 \\ 0 & 1 & 0 \\ 0 & 0 & 1 \end{bmatrix} = I_{3 \times 3}$	$\frac{\hat{\vec{\alpha}}_{\omega_V}}{\hat{\vec{\omega}}_V} = V\hat{I}S_{\omega} = \begin{bmatrix} 1 & 0 & 0 \\ 0 & 1 & 0 \\ 0 & 0 & 1 \end{bmatrix} = I_{3 \times 3}$

## Error Calculations

A sensory conflict vector is calculated for each visual input based on the relative error between the actual and expected visual sensory estimates. The visual position, velocity, and angular velocity errors are calculated through vector subtraction. Each error is represented as a vector containing an individual sensory conflict for each orthogonal axis.

$$\vec{e}_{x_V} = \vec{\alpha}_{x_V} - \hat{\vec{\alpha}}_{x_V}$$

$$\begin{aligned}\vec{e}_{\dot{x}_V} &= \vec{\alpha}_{\dot{x}_V} - \hat{\alpha}_{\dot{x}_V} \\ \vec{e}_{\omega_V} &= \vec{\alpha}_{\omega_V} - \hat{\alpha}_{\omega_V}\end{aligned}$$

The gravitational error requires both a magnitude and directional component. We calculate the conflict vector between the actual and expected gravitational sensory estimates by computing the rotation required to align both vectors. For the directional component, we use a cross product to calculate a unit vector perpendicular to the plane formed by the two vectors.

$$\frac{\vec{e}_{g_V}}{|\vec{e}_{g_V}|} = \frac{\vec{\alpha}_{g_V} \times \hat{\alpha}_{g_V}}{|\vec{\alpha}_{g_V} \times \hat{\alpha}_{g_V}|}$$

For the magnitude, we use a dot product to calculate the angle required to align both vectors within the previously calculated plane. Note that this implementation is identical to Merfeld's GIF rotational error.

$$|\vec{e}_{g_V}| = \cos^{-1} \left( \frac{\vec{\alpha}_{g_V}}{|\vec{\alpha}_{g_V}|} \cdot \frac{\hat{\alpha}_{g_V}}{|\hat{\alpha}_{g_V}|} \right)$$

### Complete Orientation Modeling System (OMS)

The complete block diagram for the OMS is shown in Figure 7. Static and dynamic visual inputs are added to the extended vestibular model denoted in Figure 4. Model inputs now include static visual position ( $\vec{x}_V$ ), gravity ( $\vec{g}_V$ ), dynamic visual velocity ( $\dot{\vec{x}}_V$ ), and angular velocity ( $\vec{\omega}_V$ ). All cues are centrally combined and used to generate internal estimates of angular velocity ( $\hat{\vec{\omega}}$ ), acceleration ( $\hat{\vec{a}}$ ), velocity ( $\hat{\vec{v}}$ ), position ( $\hat{\vec{x}}$ ), and gravity ( $\hat{\vec{g}}$ ). The four new visual free parameters are highlighted in green. Values for the free parameters are shown in the section “Parameter calibration.”

This space is intentionally blank.

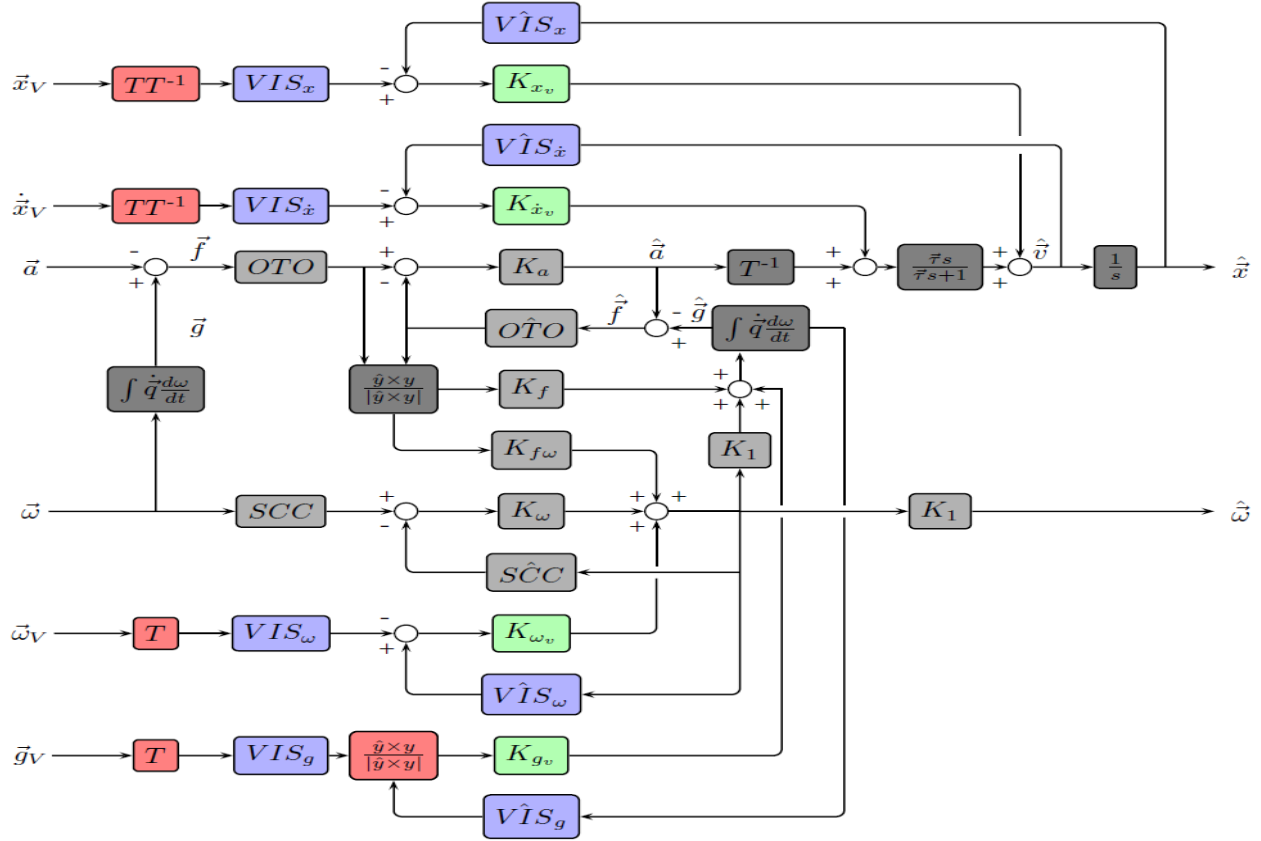


Figure 7. Orientation Modeling System (OMS) block diagram. Blocks highlighted in red, blue, and green have been added to the extended vestibular model developed in the section “Vestibular model development.”

### Visual Sensory Switches

All four visual sensory cues can be enabled or disabled dynamically during a simulation via a series of sensory switches. Switches are useful to model changes in visual sensory information that develop in a situation being simulated (e.g., a person closes or opens his eyes, a pilot gazes at an aircraft attitude indicator or suddenly enters brownout visual conditions). Disabling a visual sensor is not equal to simply setting visual input to zero. A zero-value visual velocity input, for example, can be interpreted as a static visual scene that is not translating with respect to the subject. This is quite different from a scenario in which a visual velocity cue is not available. Visual sensory switches are set as Boolean time history vectors in the input data file.<sup>1</sup>

### Visual Weighting Parameters

Visual error signals are individually weighted with residual weighting parameters that can be adjusted by the modeler to fit the data. The visual gravity residual weighting parameter ( $K_{gv}$ ) determines the influence of the visual gravitational error ( $\vec{e}_{gv}$ ) on the rate of change of the internal estimate of gravity ( $\hat{g}$ ). The visual angular velocity residual weighting parameter ( $K_{\omega v}$ )

<sup>1</sup> See section “Perception Toolbox.”

determines the influence of the visual angular velocity error ( $\vec{e}_{\omega_v}$ ) on the internal estimate of angular velocity ( $\hat{\omega}$ ). The visual position residual weighting parameter ( $K_{xv}$ ) determines the influence of the visual position error ( $\vec{e}_{g_v}$ ) on the rate of change of the internal estimate of position ( $\hat{x}$ ). The visual velocity residual weighting parameter ( $K_{\dot{x}v}$ ) determines the influence of the visual velocity error ( $\vec{e}_{\dot{x}_v}$ ) on the rate of change of the internal estimate of velocity ( $\hat{v}$ ). The values and methodologies used to set the weighting parameters are detailed in the section “Parameter calibration,” below.

## Parameter Calibration

Table 2. Vestibular Parameters

$K_a$	$K_f$	$K_{f\omega}$	$K_\omega$
-4	-4	8	8

Table 3. Visual Parameters

$K_{xv}$	$K_{\dot{x}v}$	$K_{gv}$	$K_{\omega v}$
0.75	0.75	5	10

The OMS has a total of eight free parameters that can be adjusted to tune the dynamic response of the perceptual estimates (see Tables 2 and 3). The four vestibular parameters (Table 2) match those originally calculated by Vingerhoets et al. (2007). Vingerhoets et al.’s (2007) parameters reflect the only Observer model vestibular weighting scheme validated entirely on perceptual data, and were thus chosen over the eye movement based parameter sets of Merfeld et al. (1993), Merfeld and Zupan, (2002) and Haslwanter et al. (2000). Parameters were tuned to minimize the sum of squares error (SSE) between model output and recorded translation perception during OVAR. A limited parameter space search method was used to test all possible vestibular parameter combinations within the Set A, shown below.

$$\text{Set A} = [-8 \quad -4 \quad -2 \quad -1 \quad -0.5 \quad 0.5 \quad 1 \quad 2 \quad 4 \quad 8]$$

A general stability analysis was conducted to determine the range of valid visual parameter values. Visual parameters were adjusted in increments of  $\pm 0.1$  during a series of simple visual sensory paradigms (i.e., linear vection, circular vection, static orientation cue, and a basic forward translation simulation). As visual parameters became marginally or completely unstable the resulting perceptual estimates would contain large amplitude overshoots or high frequency sinusoidal oscillations (shown in Figure 8B).



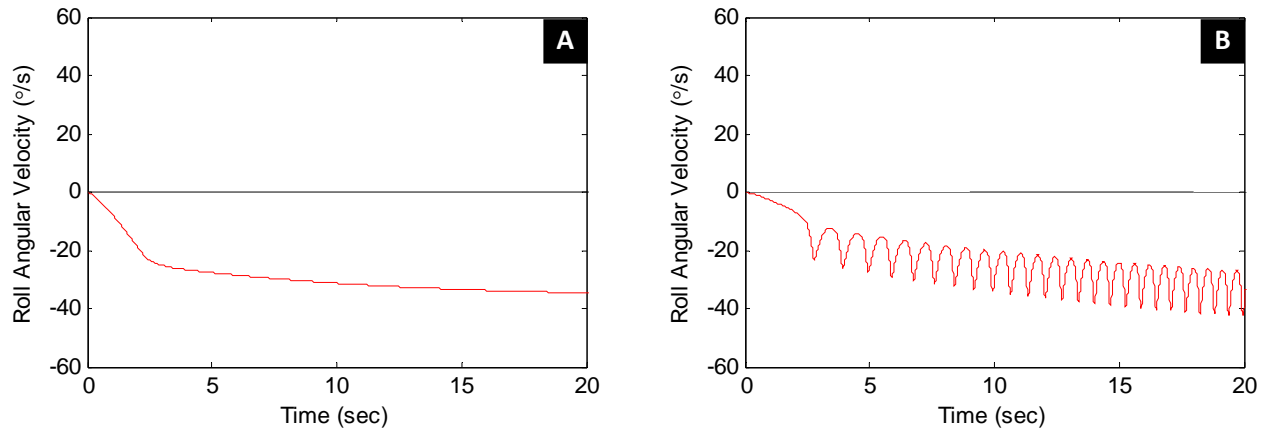


*Figure 8. Model stability assessment during a roll vection stimulus. (A): Stable roll vection response. (B): Unstable roll vection response. The unstable response exhibits oscillations that increase in frequency as the simulation progresses.*

Calculated stability ranges are shown in Table 4. The visual position parameter ( $K_{xv}$ ) and the visual velocity parameter ( $K_{\dot{x}v}$ ) were tuned to match the linear vection data of Chu (1976). (See section “Linear vection.”) The visual angular velocity parameter ( $K_{\omega v}$ ) was tuned to match experimental data for circular vection and rotation in the light (Waespe & Henn, 1977). (For further analysis, see the section on “Earth vertical rotation [dark, light]” and “Earth vertical rotation [circular vection].”) The tuning process was accomplished with a trial and error method based on the pertinent data characteristics responsive to parameter adjustment (e.g., rise times, steady state values, amplitudes, and phase angles). The remaining parameter ( $K_{gv}$ ), which weights the strength of the visual orientation error, is dependent on the situation being modeled. A sloping cloud bank, fully furnished tilted room, or simple illuminated, tilted line will each produce different strength orientation cues and resulting perceptions of tilt (Singer, Purcell, & Austin, 1970). The modeler should consider the strength of the visual cue being modeled and refer to the stability Table (see Table 4) to properly set  $K_{gv}$ .

*Table 4. Stability Ranges for Visual Weighting Parameters*

$0 < K_{xv} \leq 1$	$0 < K_{\dot{x}v} \leq 1$	$0 < K_{gv} < 330$	$0 < K_{\omega v} < 178$
---------------------	---------------------------	--------------------	--------------------------

## Perception Toolbox Input

Perception Toolbox is a MATLAB<sup>®</sup>-based program developed to aid in the processing, simulation, and visualization of human perception in response to three-dimensional, complex, multisensory motion stimuli. Vestibular and visual data is entered into the model through comma-separated-value (CSV) text files or Excel spreadsheets (Figure 9). These data files contain time histories of vestibular and visual sensory information, head movement dynamics, and sensory switches that indicate when certain cues are enabled during the simulation.

Time			
Variable name	Coordinate frame	Unit	Description
Time	n/a	s	Time vector denotes rate of input
Vestibular Linear Acceleration			
Variable name	Coordinate frame	Unit	Description
Ax	Head	m/s	X-axis, forward, linear acceleration
Ay	Head	m/s	Y-axis, lateral, linear acceleration
Az	Head	m/s	Z-axis, vertical, linear acceleration
Vestibular Angular Velocity			
Variable name	Coordinate frame	Unit	Description
wx	Head	°/s	Roll angular velocity about X-axis
wy	Head	°/s	Pitch angular velocity about Y-axis
wz	Head	°/s	Yaw angular velocity about Z-axis
Visual Position			
Variable name	Coordinate frame	Unit	Description
xv	World	m	Position of subject in Xw axis
yv	World	m	Position of subject in Yw axis
zv	World	m	Position of subject in Zw axis
Visual Velocity			
Variable name	Coordinate frame	Unit	Description
x_dotv	World	m/s	Velocity of subject in Xw axis
y_dotv	World	m/s	Velocity of subject in Yw axis
z_dotv	World	m/s	Velocity of subject in Zw axis
Visual Angular Velocity*			
Variable name	Coordinate frame	Unit	Description
wxv	Head	°/s	Visual roll angular velocity about X-axis
wyv	Head	°/s	Visual pitch angular velocity about Y-axis
wzv	Head	°/s	Visual yaw angular velocity about Z-axis
Visual Orientation			
Variable name	Coordinate frame	Unit	Description
Gxv	World	n/a	X component of "down" direction in Xw axis
Gyv	World	n/a	Y component of "down" direction in Yw axis
Gzv	World	n/a	Z component of "down" direction in Zw axis
G Magnitude			
Variable name	Coordinate frame	Unit	Description
g	n/a	G	Magnitude of gravity vector
Visual Sensory Switches			
Variable name	Coordinate frame	Unit	Description
Pos ON	n/a	Boolean (0 or 1)	Visual position cue ON = 1, OFF = 0
Head Movement			
Variable name	Coordinate frame	Unit	Description
θ <sub>xh</sub>	Head	°	Head roll angle
θ <sub>yh</sub>	Head	°	Head pitch angle
θ <sub>zh</sub>	Head	°	Head yaw angle
(s = seconds; m = meters; ° = degrees; G = G-units)			
* The input for a rotating scene is the negative of the vestibular angle velocity input since vection is induced in the direction opposite of the visual scene motion.			

Figure 9. Example Excel input file.

After a file has been loaded into the main GUI, it is processed through a Simulink<sup>®</sup>-based mathematical perception model that estimates what an individual would perceive given the current sensory information and motion.

The Perception Toolbox has three tools for data visualization: 2D time history plots, 3D animated vector plots, and virtual reality simulation. The virtual reality (VR) simulation in particular, is a powerful tool for sensorimotor researchers, human factors engineers, and accident investigators. Users can visualize the actual motion of a simulated VR avatar side-by-side with the predicted orientation derived from the perception models.

Two additional modeling tools are included and accessible from the main GUI: the VOR Toolbox, used to model eye movement dynamics, and the G-excess Toolbox, used to predict orientation perception under various acceleratory and gravitational states.

### Perception Toolbox Graphic User Interface

Figure 10 shows the Perception Toolbox main GUI window. From this window, a user can set and modify all model parameters, input motion data files, select individual models for simulation, export perceptual estimates to CSV or Excel and access the five other Perception Toolbox visualization and data processing tools.

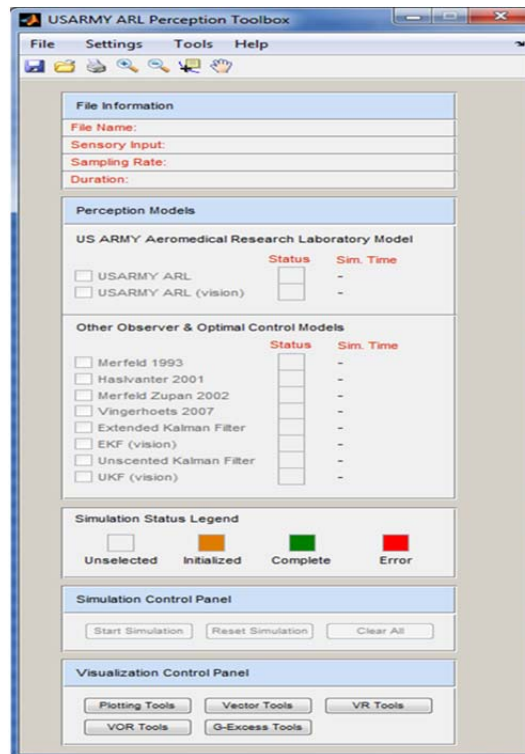


Figure 10. Main graphical user interface.

The simulation time for each model is also calculated and displayed on the main GUI. This value provides a rough estimate of model efficiency. Efficiency is particularly important for

potential future applications that involve real-time integration of a perception model into a given process, sensor, or display (Lawson, McGrath, Newman, and Rupert, 2015).

## Perception Models

In addition to the OMS outlined in this report, six other classic perception models have been preprogrammed into the Perception Toolbox (see Table 5). These additional models facilitate comparison with previous research and modeling results. To our knowledge, this is the only orientation model with this capability.

*Table 5. Spatial Orientation Models Included in Perception Toolbox*

<b>Models Included</b>	<b>Reference(s)</b>	<b>Notes</b>
Orientation Modeling System (OMS)	Newman, 2009	Two implementation (with and without visual cues)
Merfeld	Merfeld et al., 1993	Vestibular cues only
Haslwanter	Haslwanter et al., 2000	Vestibular cues only
Merfeld & Zupan	Merfeld & Zupan, 2002	Vestibular cues only
Vingerhoets	Vingerhoets et al., 2007	Vestibular cues only
Extended Kalman Filter <sup>2</sup>	Borah et al., 1978; Pommellet, 1990; Kynor, 2002; Selva, 2009	Two implementation (with and without visual cues)
Unscented Kalman Filter <sup>3</sup>	Selva, 2009	Two implementation (with and without visual cues)

Each model is implemented in its own Simulink<sup>®</sup> block diagram and can be selected independently for simulation. The Perception Toolbox correctly formats input data for each perception model and stores outputted estimates of spatial orientation perception in MATLAB<sup>®</sup> structures for future comparison and visualization. The parameters and feedback gains for each

<sup>2</sup> The family of Kalman Filter & Extended Kalman Filter (EKF) models that began with Borah, Young, and Curry's (1978) Sensory Mechanism Model and progressed to the latest nonlinear models by Kynor (2002) and Selva (2009) all maintain a very similar mathematical foundation to solve for estimates of spatial orientation perception. The more recent implementations have added more advanced nonlinear estimation techniques and therefore have been chosen for implementation in the Perception Toolbox.

<sup>3</sup> The Unscented Kalman Filter (UKF) model implemented by Selva (2009) addresses several of the approximation issues intrinsic to Extended Kalman Filters. Unlike the EKF, the UKF does not explicitly approximate the nonlinear process and observation models. This approximation can yield very large errors in the estimated statistics of the posterior distribution of the states. The UKF uses the true nonlinear model and an unscented transformation for mean and covariance propagation. Accuracy of mean and covariance estimates for the UKF are third order (assuming Gaussian statistics), compared to only first order with the EKF.

model are fully customizable via the main GUI. Default parameters correspond to those published in the original manuscripts listed in Table 4.

## Plotting Tools

The Plotting Tools GUI is shown in Figure 11. From this window, users can plot the actual motion stimuli against estimates of acceleration, angular velocity, gravity, gravitoinertial force, linear velocity, displacement, head angle, head velocity, and head acceleration for each of the perception models listed in Table 4. Users can plot the results for a single model or compare estimates for all models by selecting the desired checkboxes in the plot legend side panel. More advanced MATLAB® plotting features, such as zoom, data tips, regression analysis, and plot scroll are accessible in a convenient toolbar. Plots can be printed and saved to image files for offline analysis.

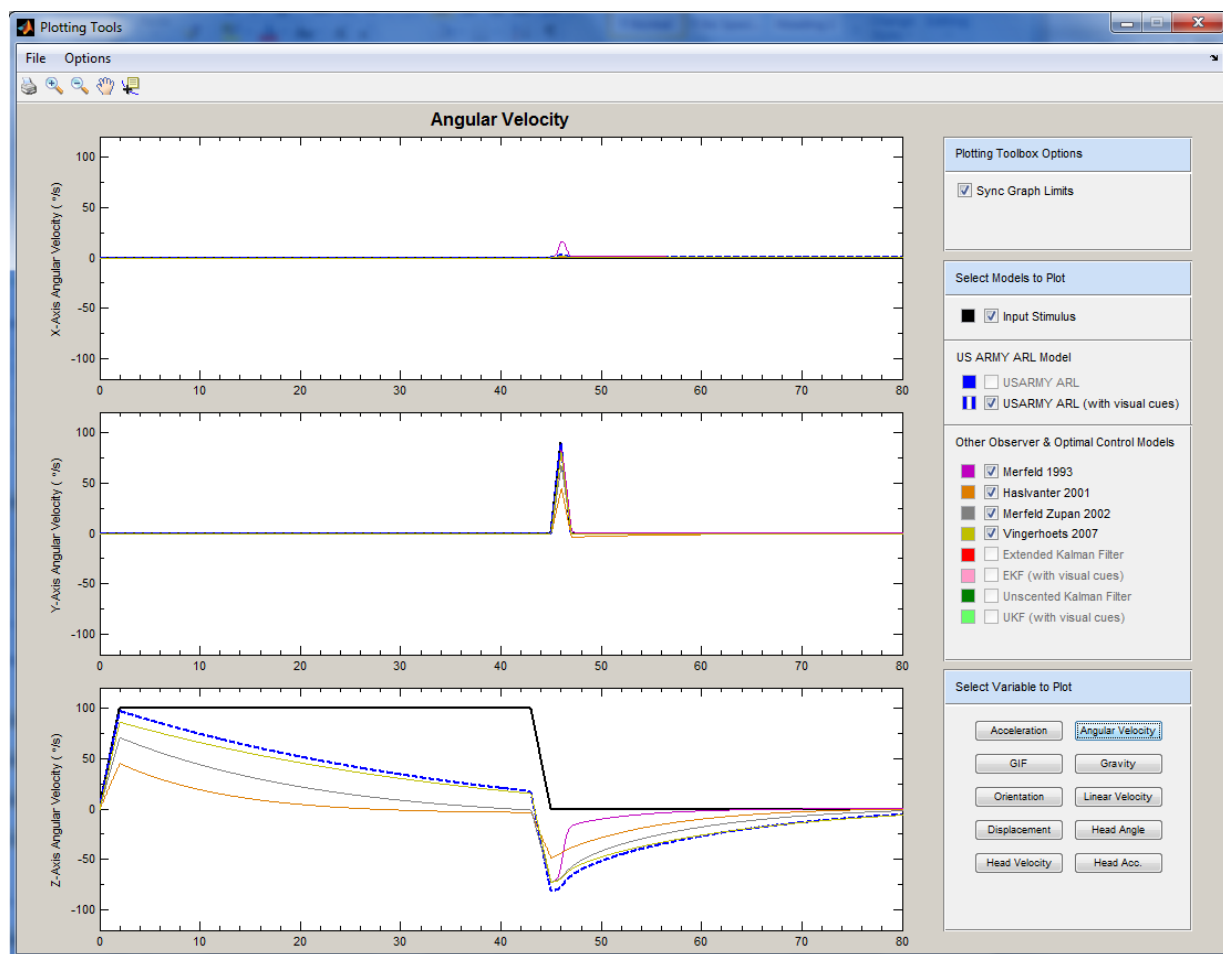


*Figure 11.* Plotting Tools graphical user interface. Results for multiple perception models are shown. Each trace represents the response of an individual perception model. Trace colors correspond to the perception model listed in model legend in the right center sidebar panel.

## Vector Visualization Tools

The Vector Tools GUI is shown in Figure 12. Vector Tools displays animated 2D and 3D plots for any of the variables calculated by the Perception Toolbox. Users are presented with a 2D time history of the chosen variable, a polar plot of estimated and actual azimuth angle, and a vector plotted in 3D vector space. Users can modify the perspective of the 3D vector plot during the simulation to isolate the XY, YZ, and XZ vector planes.

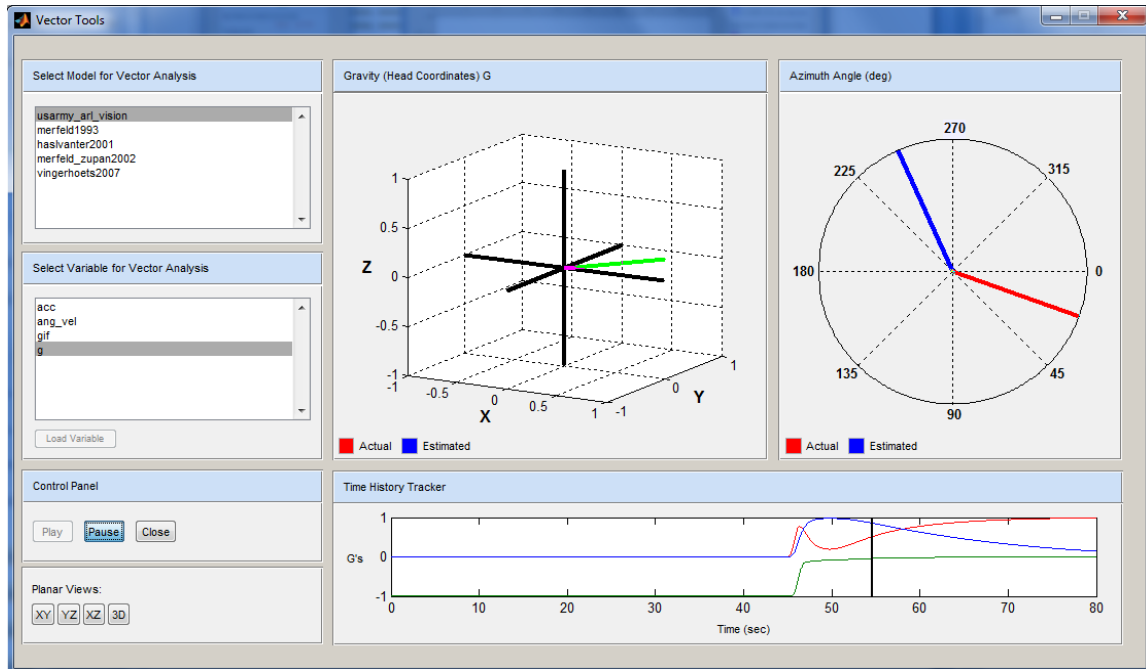
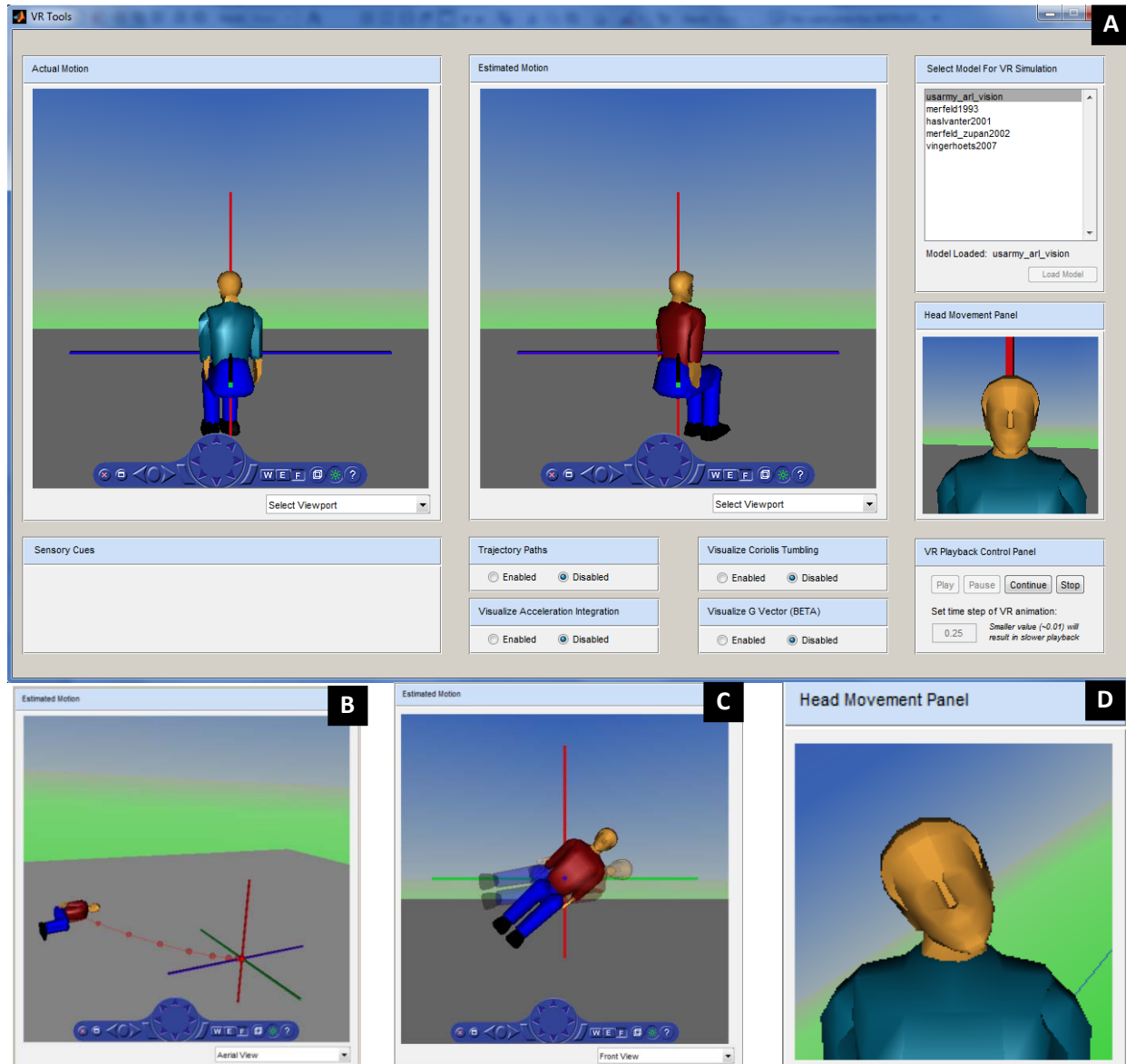


Figure 12. Vector Visualization Tools graphical user interface.

## Virtual Reality (VR) Visualization Tools

Virtual reality playback is accomplished using MATLAB<sup>®</sup>'s 3D Animation Toolbox and the VRML (Virtual Reality Modeling Language) 3D World Blaxxon Freeware. The VR Tools GUI is composed of three independent virtual worlds. World one displays the actual motion of the simulated subject. World two displays the estimated motion driven by a selected perception model. World 3 provides a close-up view that displays head movements made throughout the simulation (Figure 13D). These worlds are integrated into a MATLAB<sup>®</sup> GUI as shown in Figure 13A. From this GUI, users can select the perception model that they wish to visualize and set a number of important options and settings for VR playback.



*Figure 13.* Virtual Reality Visualization Tools graphical user interface. **(A):** Main interface. **(B):** Example of the path trajectory visualization. **(C):** Example of the Coriolis tumbling visualization. **(D):** Example of the head movement model visualization.

The path trajectory visualization option (Figure 13B) displays the motion path for the simulated subject in virtual space. The Coriolis tumbling visualization option (Figure 13C) allows users to view the paradoxical sensation of limited tilt displacement accompanied by a persistent velocity tumbling sensation that is often reported during the Coriolis cross-coupled illusion. A similar visualization can be done for some other illusions with paradoxical displacement/velocity characteristics, such as a roll tilt sensation due to circular rollvection. Selecting this option converts the estimated orientation into two individual sensations: a) static tilt, represented by the solid avatar in Figure 13C, and b) tumbling velocity, represented by the translucent rotating avatar. When viewed in real time, this visualization tool provides a powerful illustration of the combined perceptual response.

## Vestibulo-Ocular Reflex (VOR) Tools

Eye movements provide another physiological measure that can be used to validate and tune a perception model's dynamic response. Unlike verbal reports or estimates of orientation that rely on the psychophysical setting of a vertical line, eye movements are a direct, reflexive response to angular and horizontal motion. It is important, however, to note that the link between orientation perception and eye movements is complicated and not fully understood. What a subject perceives or reports may not agree with eye movement response.

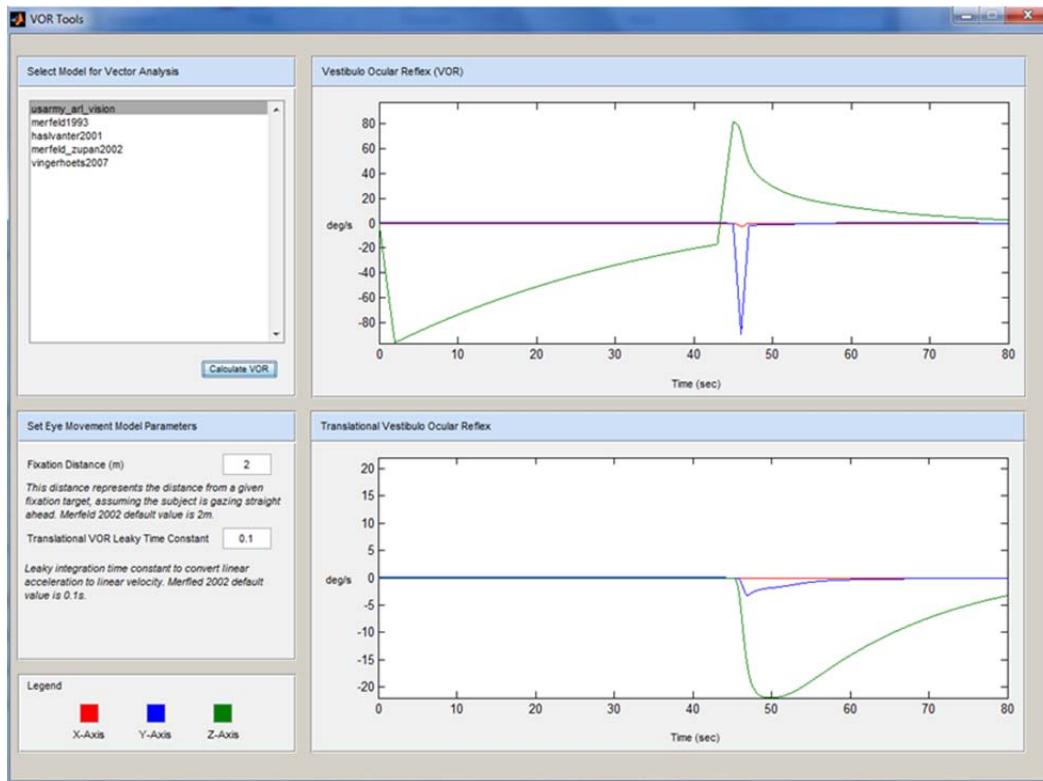


Figure 14. Vestibulo-Ocular Reflex Tools graphical user interface.

We dissociate eye movement predictions from spatial orientation perception predictions using a separate VOR toolbox (Figure 14). The VOR Toolbox uses a basic eye movement model (Figure 15) to calculate the slow phase eye velocity of the VOR (Merfeld et al., 1993; Merfeld & Zupan, 2002). VOR is modeled as the sum of angular VOR (AVOR) driven by the perception model's estimate of angular velocity, and translational VOR (TVOR) driven by estimated linear acceleration. The VOR Toolbox allows users to plot the AVOR, TVOR, and total VOR, and adjust the two free parameters of the eye movement model.



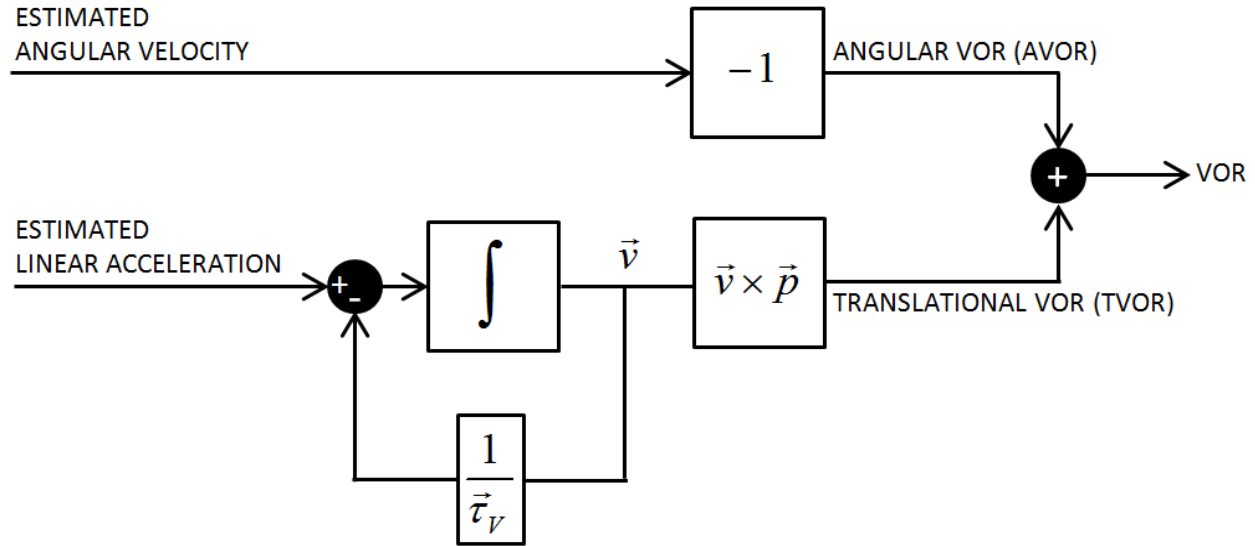


Figure 15. Merfeld & Zupan (2002) Vestibulo-Ocular Reflex Model.

The VOR is modeled as the sum of the AVOR and the TVOR. The TVOR is derived from the estimate of linear acceleration by leaky integration followed by a cross product with an estimated target proximity vector  $\vec{p}$ , which accounts for distance and gaze direction influences. The leaky integration time constant  $\vec{\tau}_v$  is set at a default value of 0.1s. The proximity vector is equal to  $[1/d, 0, 0]$ , where  $d$  is equal to the distance from the given focal target. By default  $d$  is set equal to 2 meters to correspond with the parameter set used by Merfeld and Zupan (2002).

## G-excess Tools

In hypergravity, the excess G-forces acting on the otolith organs can produce sensations of tilt over-estimation, tumbling and disorientation. These “G-excess” phenomenon are particularly important in aviation, where changes in the magnitude and direction of the GIF vector are frequent, abrupt, and often occur during mission critical tasks such as air combat (Gilson, Guedry, Hixson, & Niven, 1973; Guedry & Rupert, 1991). The Perception Toolbox provides a separate tool for visualizing G-excess effects.

The G-excess Tools GUI is shown in Figure 16. G-excess Tools allows users to modify the relative sensitivity or weighting of the utricle versus saccule organs in hypergravity and re-simulate motion profiles with the adjusted parameter set.<sup>4</sup> Estimates of roll and pitch angle can be reviewed and animated in real time against the simulated subject’s true orientation. A dynamic representation of the forces acting on the otoliths in both hyper- and normal-G environments is also provided.

<sup>4</sup> This feature allows modelers to distinguish different planes of motion (Clark, 2013), where previously they had to assume all planes of motion were weighted the same.

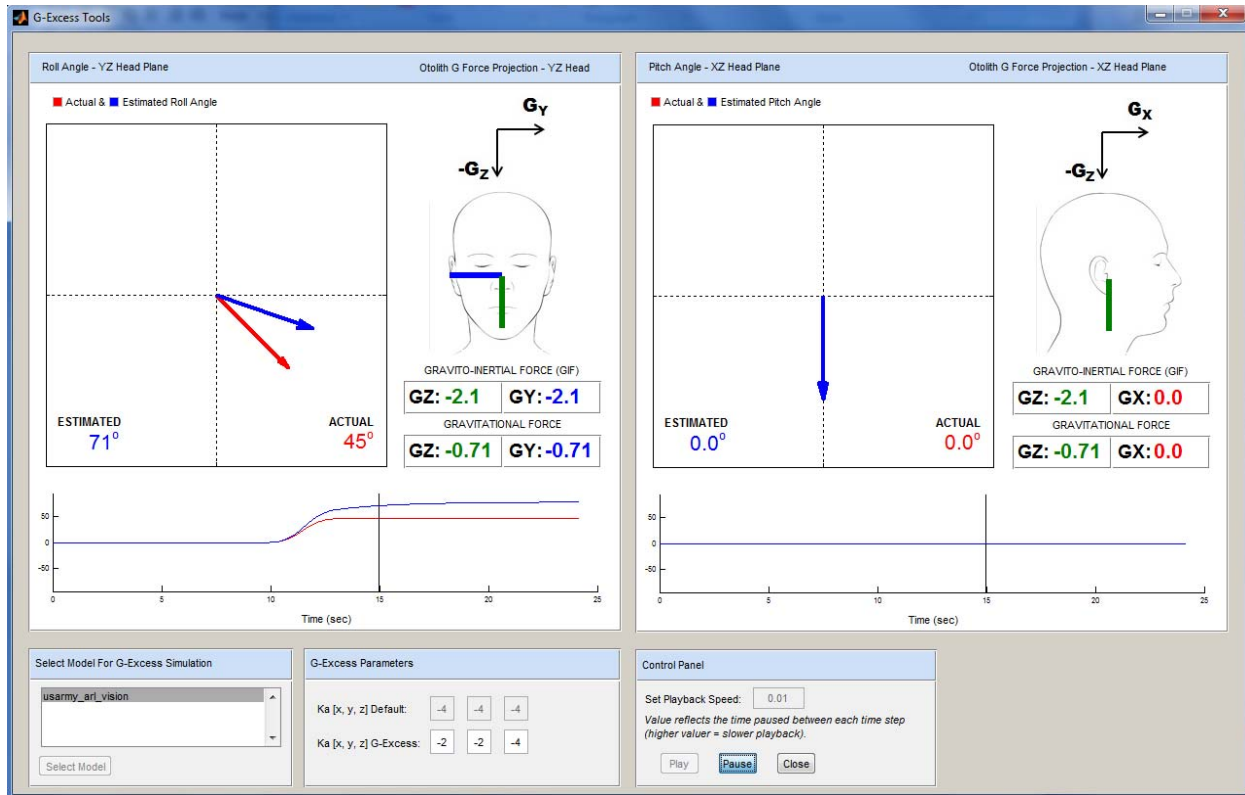


Figure 16. G-excess Tools graphical user interface.

## Summary List of Motion Stimuli

Table 6 lists the 19 motion profiles incorporated into the Perception Toolbox and for which model findings are described in this report.

Table 6. List of Motion Profiles Included With Perception Toolbox

1	Constant Velocity Rotation in the Dark	2	Constant Velocity Rotation in the Light
3	Yaw Circular Vection	4	Fixed Radius Centrifugation
5	Post-Rotational Tilt	6	Coriolis during Accelerated Rotation
7	Coriolis during Constant Velocity Rotation	8	Coriolis during Decelerated Rotation
9	G-Excess Illusion	10	Somatogravic Illusion in the Dark
11	Somatogravic Illusion in the Light	12	Optokinetic Nystagmus & After-Nystagmus
13	Linear Vection	14	Roll Circular Vection
15	Post-Turn Illusion in Degraded Visual Conditions	16	Post-Turn Illusion w/ Artificial Visual Horizon Cue
17	Coriolis Head Movement in a Coordinated Turn	18	F18 Mishap with Angular Cues
19	F18 Mishap with Angular Cues and Acceleration Cues		

## Sign Conventions and Plot Legends

The plot legend (x, y, z, roll, pitch, yaw) and sign conventions used for all simulations in this report are shown in Table 7 and Table 8, respectively. For each simulation presented, the sensory information available to the simulated subject is summarized in a Table similar to the one shown in Table 9. The two vestibular cues (VEST) correspond to angular velocity from the semicircular canals ( $\vec{\omega}$ ) and linear acceleration from the otolith organs ( $\vec{a}$ ). The four visual cues (VISUAL) correspond to visual position ( $\vec{x}$ ), visual linear velocity ( $\vec{v}$ ), visual angular velocity ( $\vec{\omega}$ ), and visual orientation or gravity ( $\vec{g}$ ). Cues highlighted in yellow ■ are available to the subject during each simulation. Cues highlighted in red ■ are available to the subject during one of the experimental conditions of the simulation (see captions for further disambiguation). Cues in white ■ represent sensory information that are not used or available (i.e., the eyes are closed, the room is darkened, or a clear visual horizon line is not present).

Table 7. Plot Trace Color Legend

<span style="color: red;">—</span> X, ROLL	<span style="color: blue;">—</span> Y, PITCH	<span style="color: green;">—</span> Z, YAW
--	--	---

Table 8. Sign Conventions

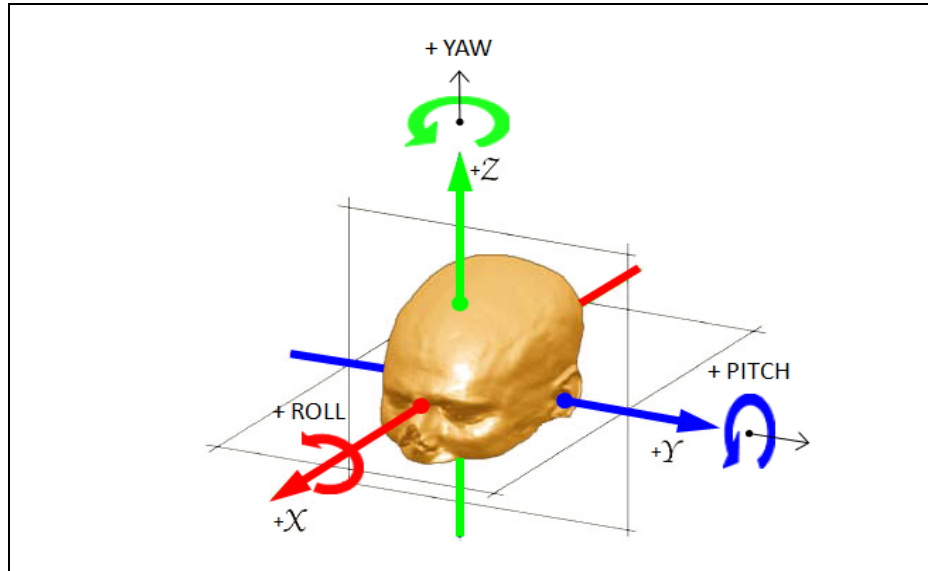


Table 9. Sensory Cues

VEST		VISUAL			
$\vec{\omega}$	$\vec{a}$	$\vec{x}$	$\vec{v}$	$\vec{g}$	$\vec{\omega}$

## Results & Discussion

### Basic Sensory Paradigms

#### Earth vertical rotation (dark, light).

VEST		VISUAL			
$\vec{\omega}$	$\vec{a}$	$\vec{x}$	$\vec{v}$	$\vec{g}$	$\vec{\omega}$

Figure 17 shows the model response for constant velocity rotation about an Earth vertical axis under dark (i.e., vestibular) and light (i.e., visual-vestibular) experimental conditions. Velocity perception in the dark (Figure 17A and 17C) displays the typical exponential decay of angular sensation and the lengthened time constant attributed to central velocity storage. Since visual information is not present in this condition, the simulation results are similar to Merfeld et al.'s (1993) 1D velocity storage model. When a stationary visual surround is present (Figure 17B and 17D), the model predicts a sustained sensation of rotational motion which slightly decays to a value close to the actual input stimuli.

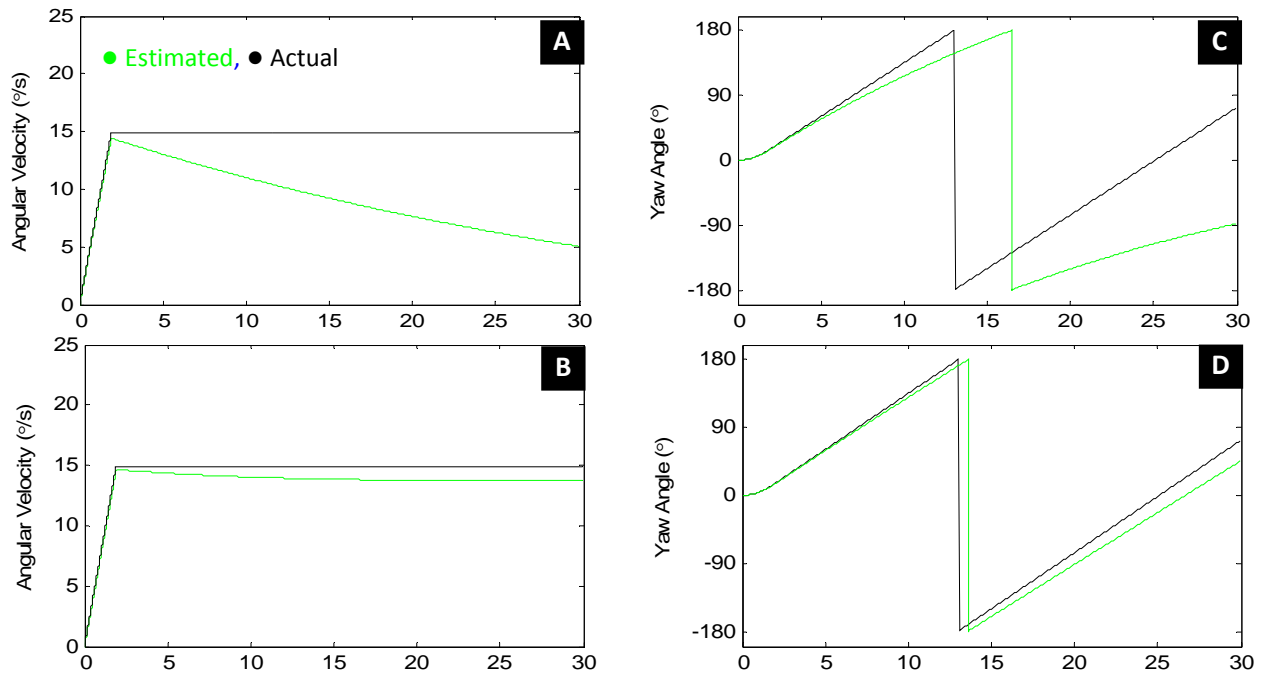


**Figure 17.** Model predictions for constant velocity rotation about an Earth-vertical axis. The simulated subject was seated upright in a rotary chair and rotated in the dark (**A, C**) and light (**B, D**) at = 0.26 radian/s (14.89°/s) for a duration of 30 s. (**A, B**): Estimated yaw angular velocity for darkness and lighted conditions. (**C, D**): Estimated yaw angle for darkness and lighted conditions. The Rotation in the light response was tuned to mimic the modeling results of Borah et al. (1978) and the experimental data of Waespe and Henn (1977). Also shown is the input 0.26 radian/s stimulus and subsequent yaw angle during rotation.

## Earth vertical rotation (circular vection).

VEST		VISUAL			
$\vec{\omega}$	$\vec{a}$	$\vec{x}$	$\vec{v}$	$\vec{g}$	$\vec{\omega}$

In response to pure yaw rotation of a moving visual surround, the model predicts an illusory sensation of angular velocity in the opposite direction of the visual scene (i.e., circular vection) (Figure 18A and 18B). The circular vection response curve shows two distinct components associated with the time course of the perceived self-motion; a fast-rising component responsible for the quick initial onset followed by a slow rising component that levels out to a value slightly below the velocity of the visual field. The fast-rising component accounts for 70% of the total angular velocity estimate ( $0^\circ/\text{s} \rightarrow 10^\circ/\text{s}$  in 2.5 s) and is driven by the visual system and the dynamics of the visual velocity residual feedback loop. As the internal model's estimate of angular velocity increases, visual-vestibular interactions begin to slow down the neurological processing of rotational motion. These more gradual dynamics result from the velocity storage time constant associated with the canals and CNS, and account for the remaining 30% of velocity perception ( $10^\circ/\text{s} \rightarrow 14.5^\circ/\text{s}$  in 37.75 s). The existence of these separate components has been demonstrated experimentally (Cohen, Henn, Raphan, & Dennett, 1981; Jell, Ireland, & Lafortune, 1984; Lafortune, Ireland, Jell, & DuVal, 1986).

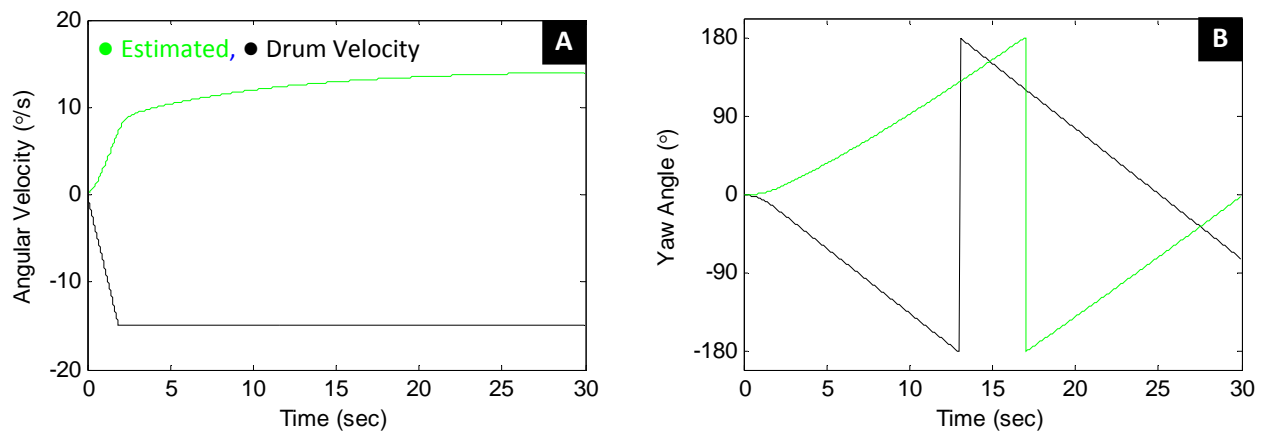


*Figure 18.* Model predictions for constant velocity yaw circular vection. The subject is stationary and placed inside an optokinetic drum that rotates in the light at  $= -0.26$  radian/s ( $14.89^\circ/\text{s}$ ). Drum rotation is in the opposite direction of the angular velocity stimulus to illicit an illusory sensation of rotation which has a consistent direction with the angular motion in the Light/Dark example. **(A):** Estimated yaw angular velocity. **(B):** Estimated yaw angle. The circular vection response was tuned to mimic the modeling results of Borah (1978) and the experimental data of Waespe and Henn (1977). Also shown is the input  $-0.26$  radian/s drum rotation and the yaw angle of the drum.

Although the overall circular vection simulation is good, like the Borah (1978) (Figure 19 curve labeled “CV”), Pommellet (1990), and Kynor (2002) models, the OMS predicts an immediate onset of circular vection sensation at the start of visual field motion. This is inconsistent with the delay typically observed in human subjects (Lawson, 2005). To account for

vection delays and inter-subject variability, Borah implemented a nonlinear ad-hoc conflict mechanism that could distinguish and schedule gains for pure rotational field motion. A similar ad-hoc augmentation is being considered for future modifications of our model.

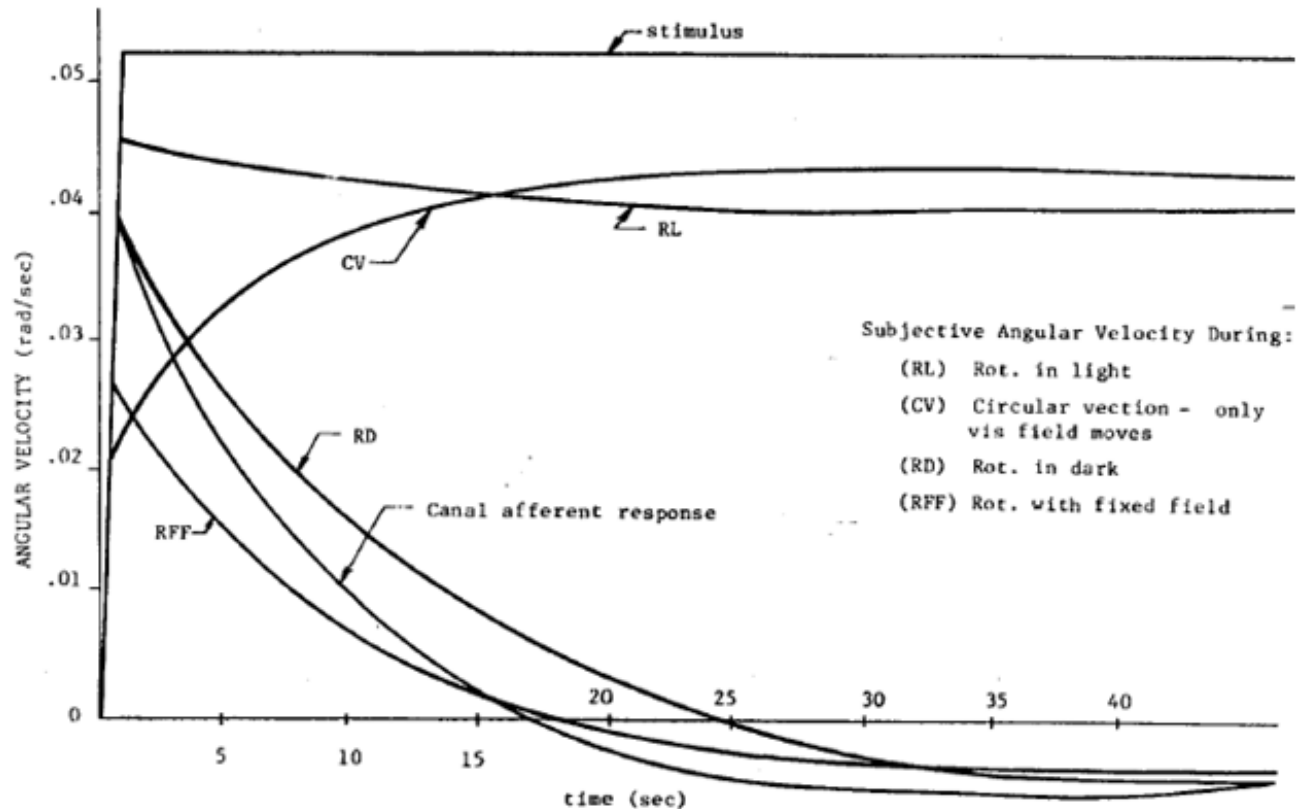


Figure 19. Borah, Young, and Curry (1978) estimated angular velocity for Earth vertical constant velocity rotation in the dark and light and with a moving visual field (circular vection).

### Fixed radius centrifugation.

VEST	VISUAL
$\vec{\omega}$ $\vec{a}$	$\vec{x}$ $\vec{v}$ $\vec{g}$ $\vec{\omega}$

During fixed radius centrifugation the CNS must dissociate between conflicting cues from the semicircular canals and otoliths. The shifting gravito-inertial force vector along the body produces an illusory sensation of body tilt that contrasts to the pure yaw rotational stimulation of the horizontal semicircular canals (i.e., true body tilt would stimulate the roll or pitch canal). Data from both perceptual reports and eye movement recordings (Clark & Graybiel, 1963; Clark & Graybiel, 1966; Graybiel & Brown, 1951; Haslwanter, Curthoys, Black, Topples, & Halmagyi, 1996; Merfeld, Zupan, & Gifford, 2001; McGrath, Oman, Guedry, & Rupert, 1993) suggest that the illusory tilt will exhibit two distinct characteristics during acceleration and deceleration of the centrifuge. During acceleration the illusory tilt angle will lag well behind the actual GIF vector, slowly building up to a steady state value with a time constant that varies depending on the GIF

level and onset rate of the centrifuge. In contrast, during deceleration from elevated G, little or no lag is typically reported. Additionally, a vertical component of the VOR has been shown to persist during centrifugation, gradually building to a constant value as the centrifuge reaches a steady-state velocity.

Model results (Figure 20) appear to match these findings. The inter-aural (y-axis) linear acceleration stimulus (Figure 20C) and estimated response (Figure 20D) show a rapid rise as the angular velocity (Figure 20A) of the centrifuge increases. The perceived tilt angle (represented by the estimated direction of the gravitational vector in Figure 20F), however, lags considerably behind the acceleration onset, reaching a steady state in approximately 60 s (opposed to the actual acceleration onset time of 5 s). Therefore, this aspect of our model requires refinement. During deceleration (from time  $t = 135$  s to 140 s) no such lag is evident. The model also predicts the expected steady-state, vertical, slow phase eye velocity component of the VOR (Figure 20H) when the centrifuge has reached a constant angular rate.

This space is intentionally blank.

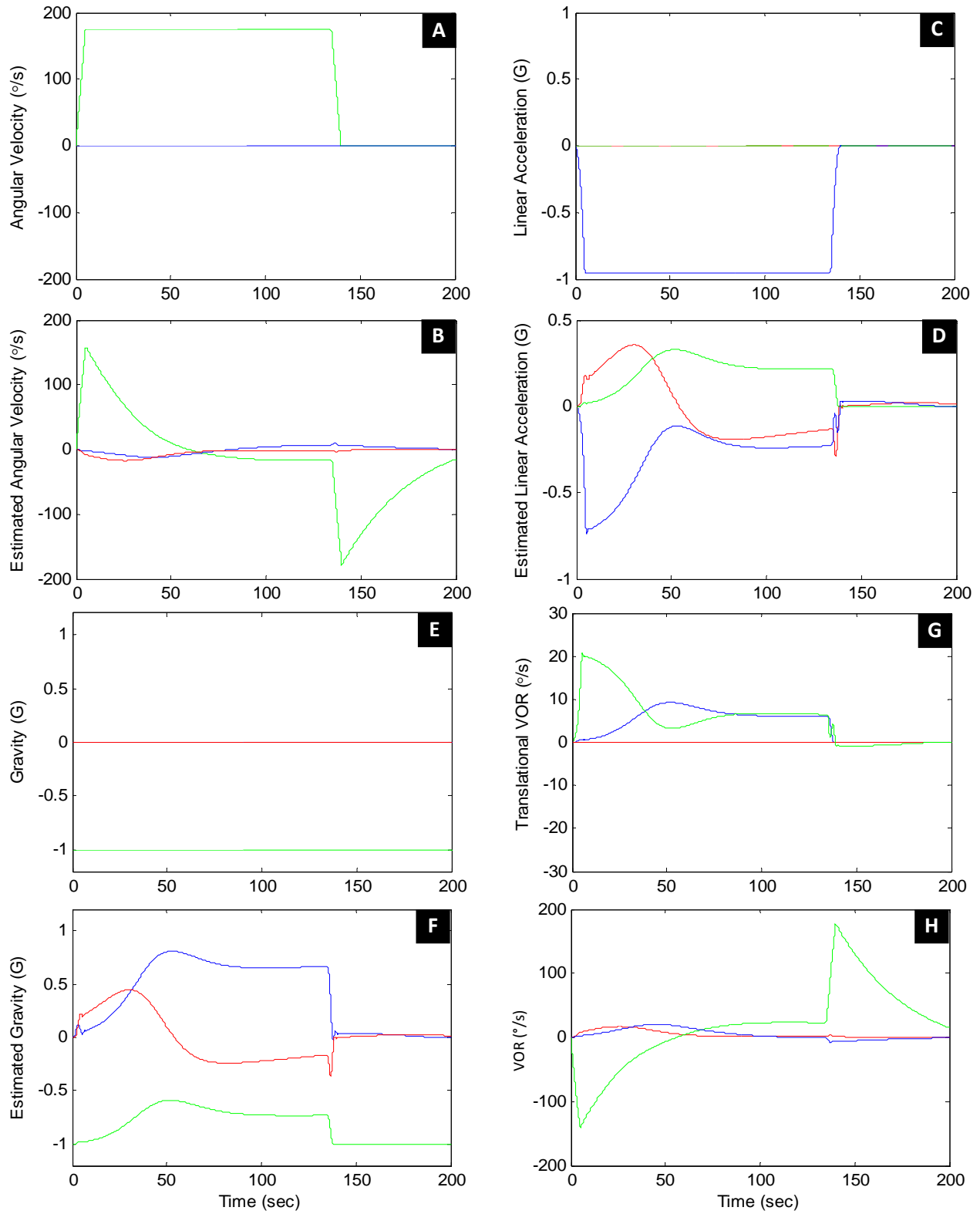
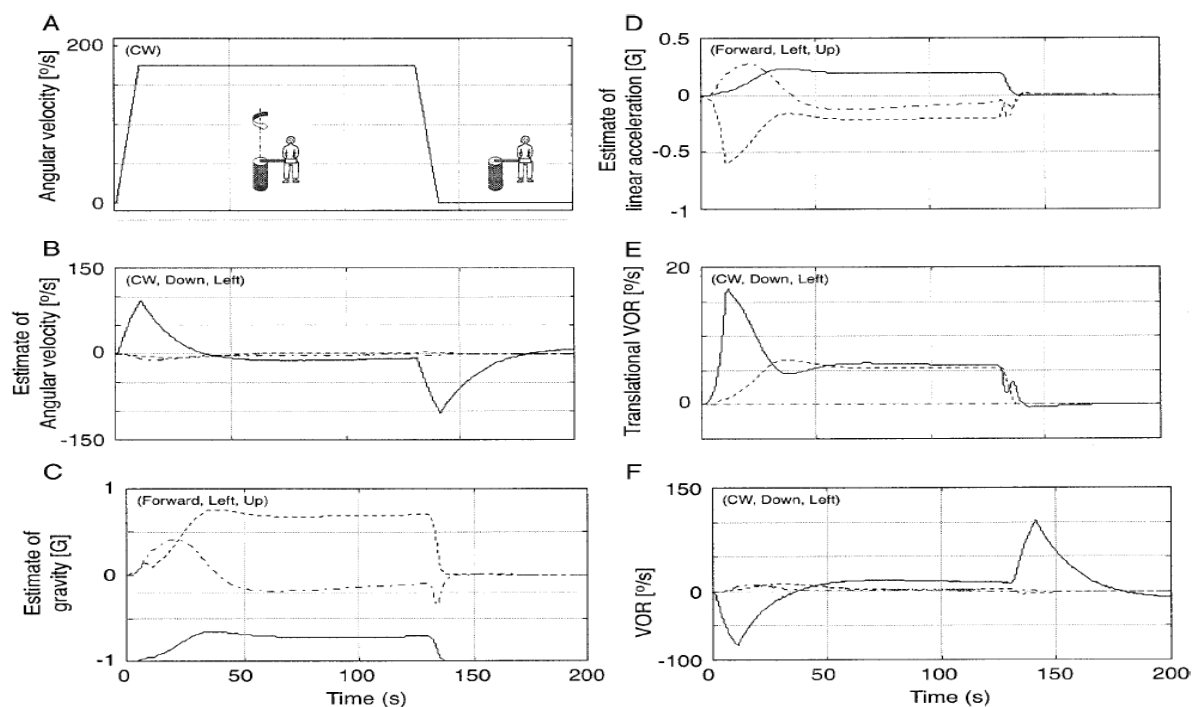


Figure 20. Model response during 175°/s rotation in a 1-m radius centrifuge.



The subject was situated upright, facing away from the direction of rotation, and aligned such that the resultant centripetal acceleration during centrifugation was pointed radially inward (-y) towards the axis of rotation. Figure 21 shows Actual (**A**) and Estimated (**B**) angular velocity, as well as Actual (**C**) and Estimated (**D**) linear acceleration. To allow for a direct comparison with the modeling results of Merfeld and Zupan (2002) and the published data of Merfeld, Zupan, and Gifford (2001), the simulated conditions precisely match the 175°/s fixed-radius centrifuge trials. Also shown in Figure 21 are the Actual (**E**) and Estimated (**F**) gravitational vector, and the TVOR (**G**) and total (**H**) VOR. For the TVOR and total VOR, an eye movement model was implemented with a fixation distance (2 m) and leaky integration time constant (0.1 s). These values are identical to those used by Merfeld and Zupan (2002).

These results are in agreement with the data cited above and the modeling results of Merfeld and Zupan (2002) (Figure 21). As noted previously, the vestibular core of the OMS has been adapted from the Observer Model developed by Merfeld et al. (1993). Agreement between these two efforts is therefore expected. We present this motion paradigm and the post-rotational tilt paradigm in the following section (“Post-rotational tilt”) to demonstrate that the new parameter set chosen for the visual-vestibular interaction model is robust, and can reproduce both the novel simulations considered in this report and the previously validated sensory paradigms considered in past modeling efforts.



*Figure 21.* Merfeld and Zupan (2002) modeling results for fixed radius (1 m) centrifugation. The angular velocity input (**A**) is shown, along with the model estimate of angular velocity (**B**), gravity (**C**), and linear acceleration (**D**), and predicted the translational (**E**) and total (**F**) VOR.

## Post-rotational tilt.

VEST	VISUAL
$\vec{\omega}$ $\vec{a}$	$\vec{x}$ $\vec{v}$ $\vec{g}$ $\vec{\omega}$

Head or body tilt following prolonged constant velocity rotation has been shown to produce dramatic effects on the post-rotatory tilt perception and VOR response. Benson and colleagues (Benson, Bodin, & Bodin, 1966; Benson, 1966a; Benson, 1966b) demonstrated that the time constant of the post-rotatory VOR is reduced in response to a change in the static otolith representation of gravity. Merfeld, Zupan, and Peterka (1999) and Zupan, Peterka, and Merfeld (2000) also demonstrated that the illusory tilt that results from post-rotatory tilt stimulation will produce a small central estimate of linear acceleration, and a measureable translational VOR.

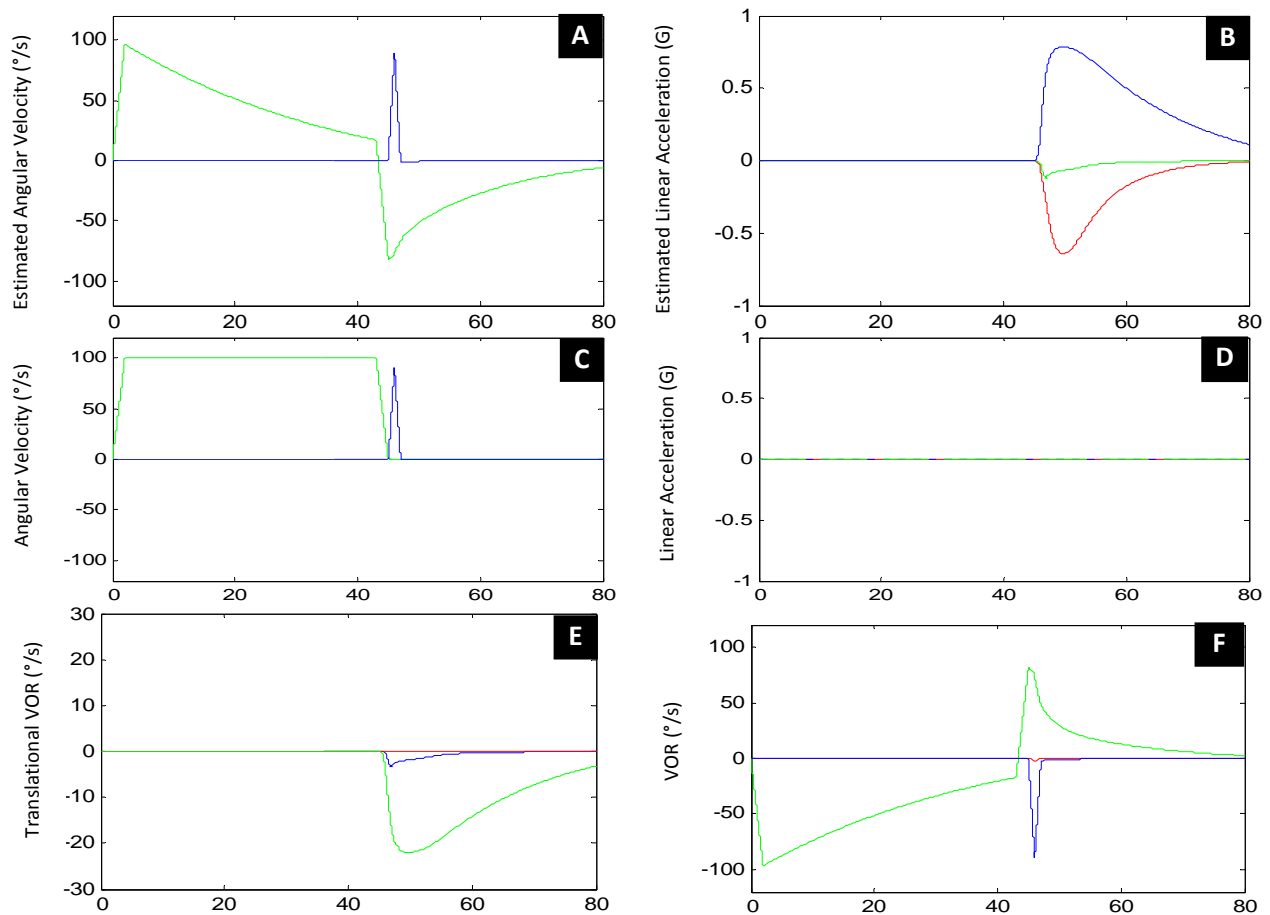


*Figure 22.* Model response to a 90° post-rotational tilt (nose-down) following 100°/s constant velocity Earth vertical yaw rotation.

The yaw angular velocity trapezoid profile (acceleration/deceleration rates of 50 °/s<sup>2</sup>) and pitch down angular velocity spike (peak pitch rate of 90°/s) are shown in pane A (green and blue trace, respectively). Figure 22 shows Actual (A) and Estimated (B) angular velocity, Actual (C) and Estimated (D) linear acceleration, and Translational (E) and total (F) VOR. For the TVOR

and total VOR, an eye movement model was implemented with a fixation distance (2 m) and leaky integration time constant (0.1 s). These values are identical to those used by Merfeld and Zupan (2002). To allow for a direct comparison with the modeling results of Merfeld and Zupan (2002) and the published data of Zupan et al. (2000), the simulated conditions precisely match the 100°/s post-rotational tilt trials.

Modeling predictions are in agreement with these findings (Figure 22). The predicted post-rotatory time constant for the VOR (Figure 22F) of the simulated trial is shown to be considerably shorter than the VOR time constant during initial rotation (5 s vs. 27 s, respectively). Likewise, the model predicts a small illusory linear acceleration response (Figure 22D) following the post-rotational tilt and a subsequent translational VOR (Figure 22E). The modeling results of Merfeld and Zupan (2002) are reproduced below for comparison (Figure 23). Overall, considerable agreement between the two models has been shown for both the fixed-radius centrifuge and post-rotational tilt motion paradigms.

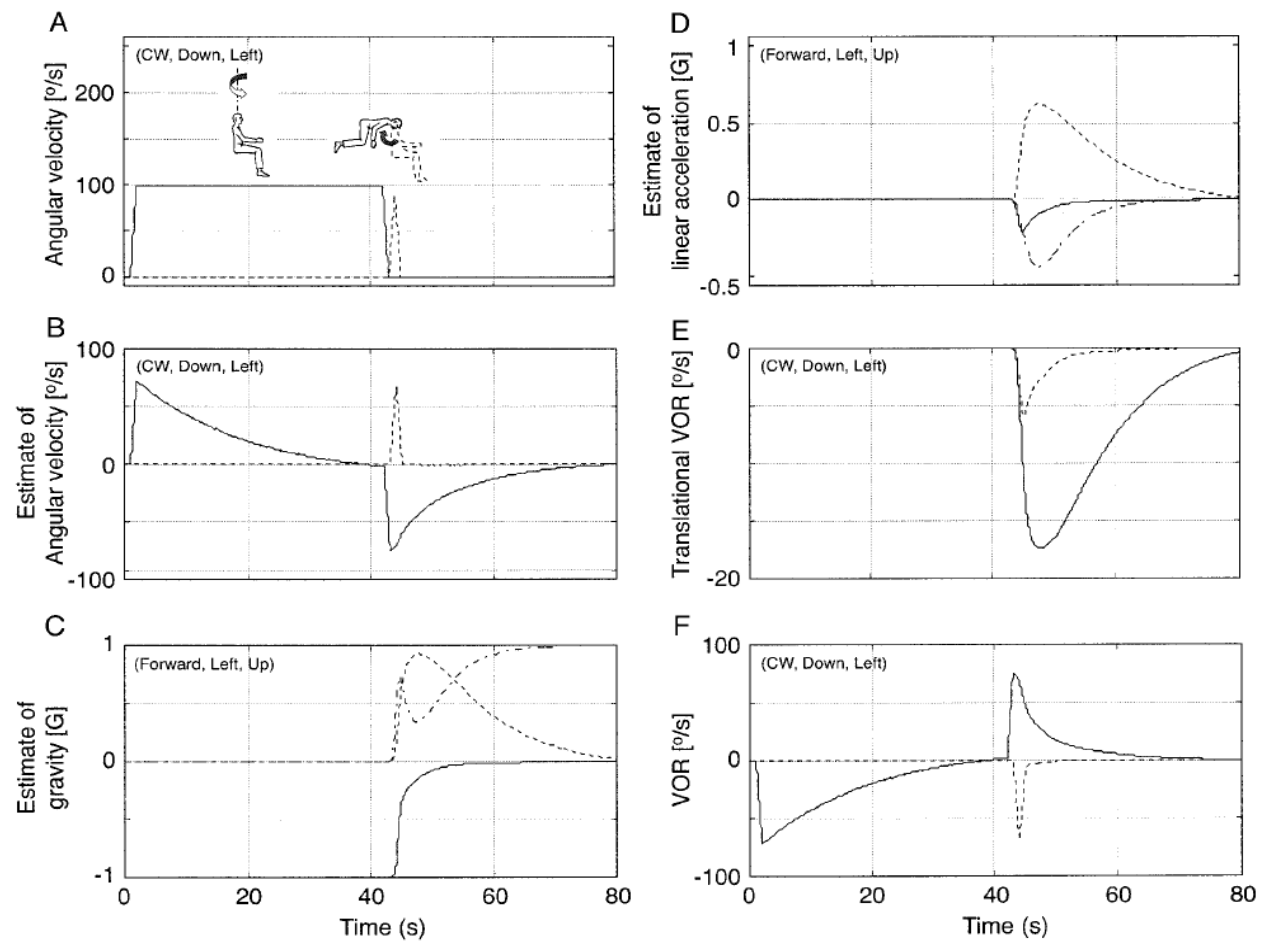


*Figure 23.* Merfeld and Zupan (2002) modeling results for a 90° post-rotational tilt (nose-down). The angular velocity input (**A**) is shown, along with the model estimate of angular velocity (**B**), gravity (**C**), and linear acceleration (**D**), and predicted the translational (**E**) and total (**F**) VOR.

## Novel Applications

Guedry and Benson (1978) demonstrated that the nauseogenicity and tumbling sensations that result from a Coriolis cross-coupled head movement are different depending on the orientation and magnitude of the resultant angular velocity impulse acting on the semicircular canals. In this classic experiment, volunteer subjects made head movements during three distinct experimental conditions: accelerated rotation, constant velocity rotation, and decelerated rotation. Each head movement was made at a rotary chair velocity of 1 rad/s. Using vector analysis, Guedry and Benson (1978) proposed a simple model to understand why these three seemingly identical head movements produced such drastically different perceptual responses. Input for the simulations are shown in sections “Coriolis cross-coupling during accelerated rotation,” “Coriolis cross-coupling during constant velocity rotation,” and “Coriolis cross-coupling during decelerated rotation.” They were chosen to match each of the three experimental conditions considered by Guedry and Benson (1978).

### Coriolis cross-coupling during accelerated rotation.

VEST	VISUAL
$\vec{\omega}$ $\vec{a}$	$\vec{x}$ $\vec{v}$ $\vec{g}$ $\vec{\omega}$

The predicted response to a cross-coupled head movement made during accelerated rotation is shown in Figure 24. Comparing the actual (Figure 24A) and estimated (Figure 24B) angular velocity response shows a near-perfect estimation of head velocity both before and after the 30° head tilt. As the head tilt is initiated, the horizontal semicircular canal cues have not had time to substantially decay and therefore the angular velocity vector is rotated properly into the new head orientation with minimal transient illusory linear acceleration (Figure 24D).

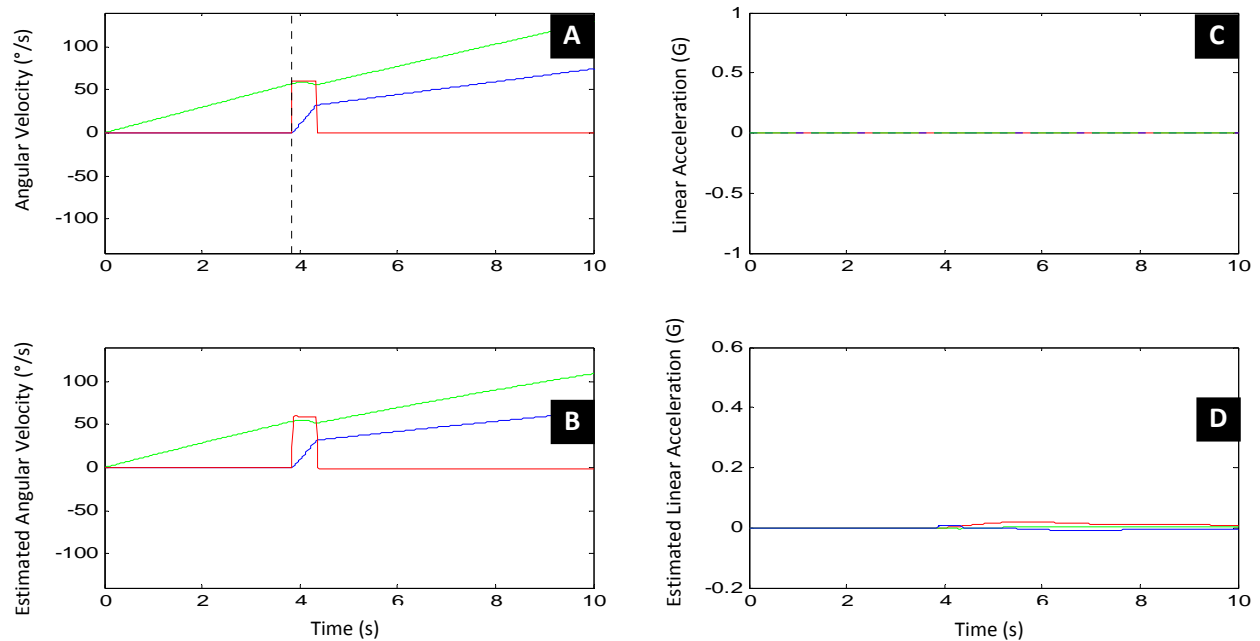


Figure 24. Model response to a 30° head tilt during Earth vertical accelerated rotation. Actual (A) and Estimated (B) angular velocity. Actual (C) and Estimated (D) linear acceleration.

The simulated subject was seated upright in a rotary chair and accelerated at a constant angular rate of  $0.26 \text{ radian/s}^2$  ( $14.89^\circ/\text{s}^2$ ) for 10 seconds. At 3.85 seconds, when the angular velocity of the rotary chair was equal to  $1 \text{ rad/s}$  ( $57.3^\circ/\text{s}$ ), the subject made a  $30^\circ$  roll head tilt (Right Ear Down) at a rate of  $60^\circ/\text{s}$  (red trace). The simulation was modeled to match the classic Coriolis cross-coupling experiment (Case I) performed by Guedry and Benson (1978).

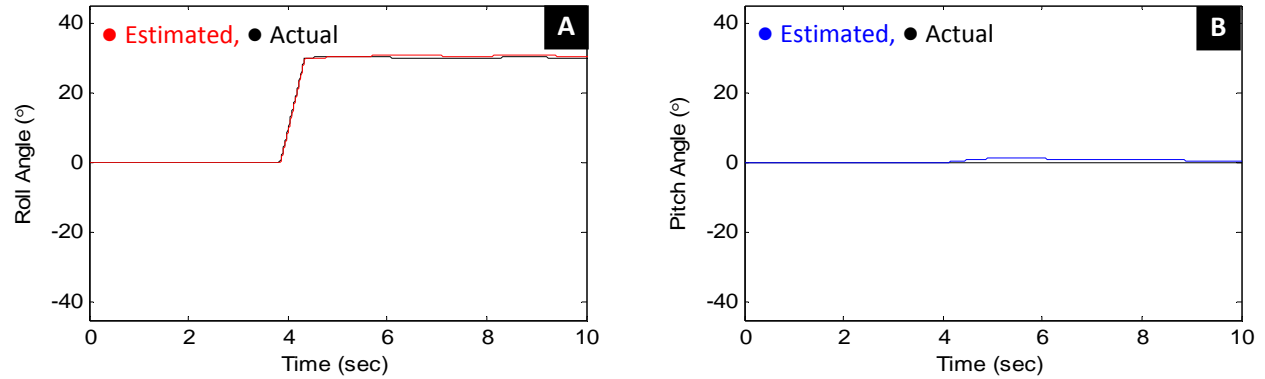


Figure 25. Model response to a  $30^\circ$  head tilt during accelerated rotation. Estimated Roll (A) and Pitch (B) angle.

As is seen in Figure 25, proper estimation of angular velocity and linear acceleration will produce a correct perception of roll (Figure 25A) and pitch (Figure 25B) angle. A comparison between Guedry and Benson's (1978) vector analysis and our modeling results is shown in Figure 26. The vector analysis shows the y- and z-axis angular velocity components, and the resultant impulse vector, immediately following the  $30^\circ$  head tilt.

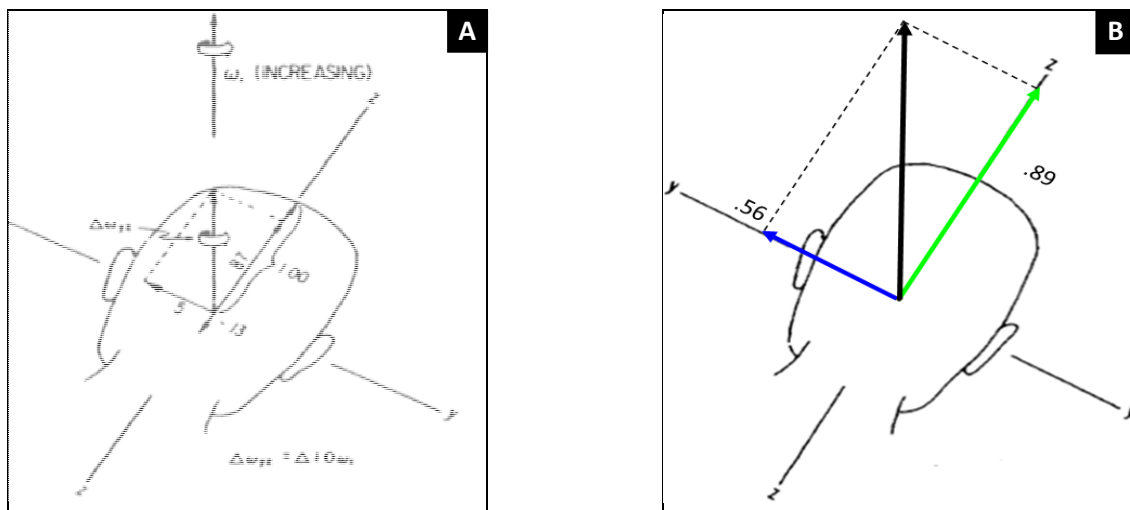


Figure 26. Vector analysis of estimated angular velocity immediately following  $30^\circ$  roll tilt. (A): Predicted response from Guedry and Benson (1978). (B): Predicted model response of our OMS.

Considerable agreement is demonstrated between the two models, in terms of vector orientation and magnitude. The OMS predicts a resultant angular velocity impulse vector offset from the axis of chair rotation by  $2.2^\circ$  (compared with  $0^\circ$  for the Guedry and Benson [1978] model). This small difference in offset angle would be expected to produce minimal illusory sensations of tilting/tumbling, which differ negligibly from Guedry and Benson's (1978) model, but which are in agreement with the subjective reports of motion sickness and perceptual disturbances recorded during the original experiment. Some vestibular syndromes have highly predictable effects on velocity sensation, which should be amenable to modeling (e.g., certain types of unilateral vestibular maladies) and targeted therapies or prostheses.

### **Coriolis cross-coupling during constant velocity rotation.**

VEST		VISUAL			
$\vec{\omega}$	$\vec{a}$	$\vec{x}$	$\vec{v}$	$\vec{g}$	$\vec{\omega}$

The predicted response to a cross-coupled head movement made during constant velocity rotation is shown in Figure 27. In this simulation, the  $30^\circ$  head tilt is made when angular velocity perception of the horizontal semicircular canal has effectively decayed to zero (Figure 27B). As the head tilts out of the rotation plane, the resultant stimuli to the superior and horizontal semicircular canals produce a response traditionally referred to as the Coriolis cross-coupling illusion or the vestibular Coriolis Effect. The result is an illusory sensation of angular velocity and tilt about a third axis of rotation; this illusion can be highly nauseogenic when a gravity cue is present.

This space is intentionally blank.

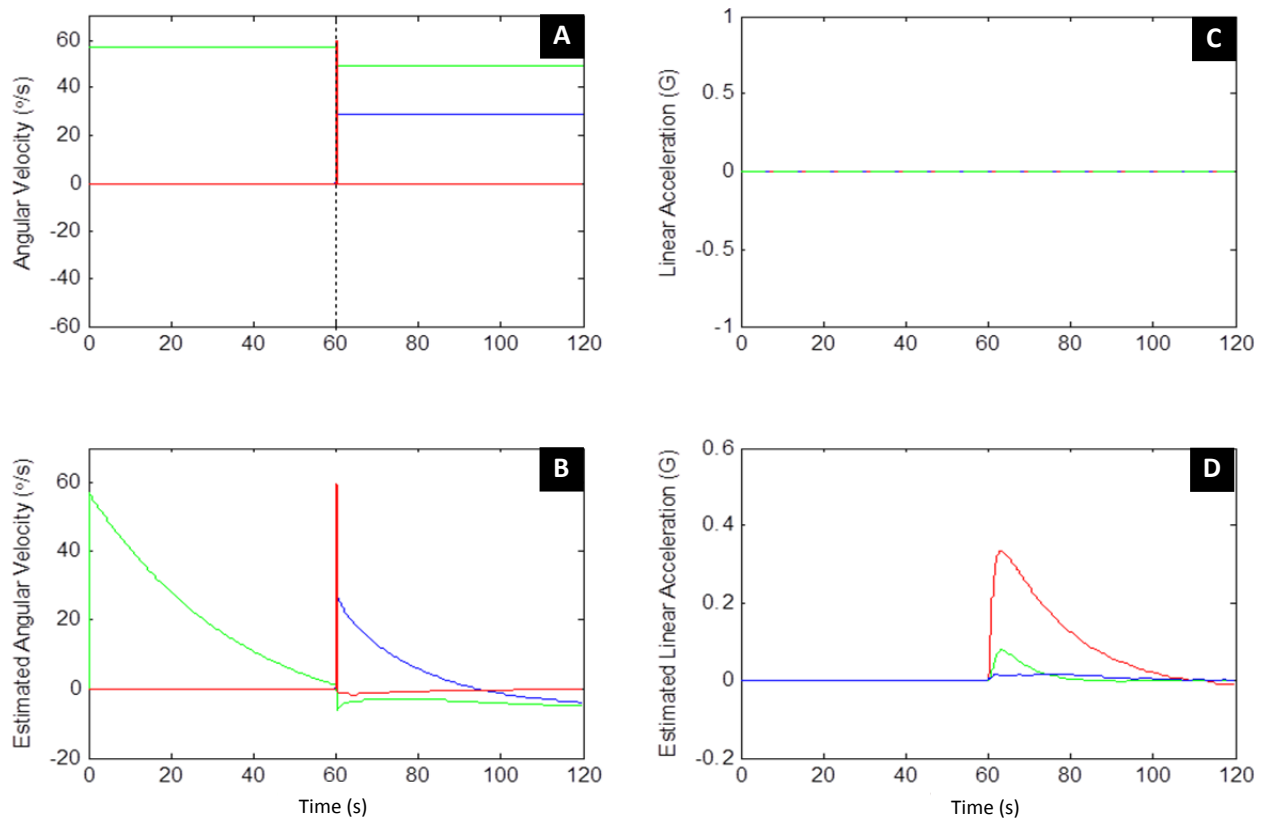


*Figure 27.* Model response to a 30° head tilt during Earth vertical constant velocity rotation. The simulated subject was seated upright in a rotary chair and accelerated at a constant angular rate of  $0.26 \text{ radian/s}^2$  ( $14.89^\circ/\text{s}^2$ ) to a terminal velocity of  $1 \text{ rad/s}$  ( $57.3^\circ/\text{s}$ ). At 60 s, when the horizontal canal cue has decayed to near zero, the subject made a 30° roll head tilt (Right Ear Down) at a rate of  $60^\circ/\text{s}$  (red trace). The simulation was modeled to match the classic Coriolis cross-coupling experiment (Case II) performed by Guedry and Benson (1978). Actual (A) and Estimated (B) angular velocity. Actual (C) and Estimated (D) linear acceleration.

During accelerated rotation, the angular velocity perception immediately preceding the 30° tilt was nearly veridical and the cross-coupled axis was aligned properly with the axis of the rotating chair. In this prolonged constant-velocity example, the cross-coupled axis is not aligned with the axis of chair rotation and thus illusory sensations of tumbling (Figure 27B), acceleration (Figure 27D), and tilting (Figure 27A and 27B) are experienced.

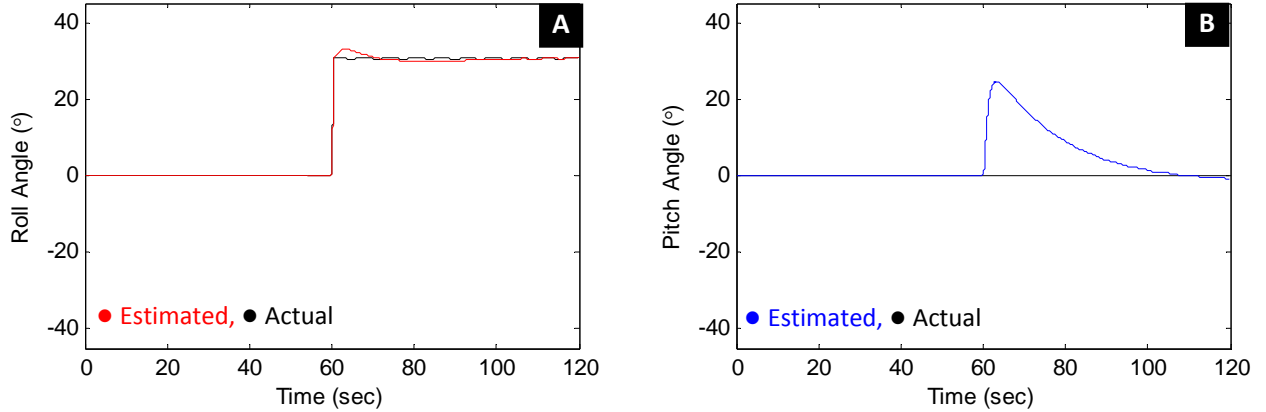


Figure 28. Model response to a 30° head tilt during constant velocity rotation. Estimated Roll (A) and Pitch (B) angle.

These simulation results are in good agreement with the vector analysis of Guedry and Benson (1978) (Figure 29). For an identical simulation, their vector analysis predicted an estimated angular velocity magnitude of 0.52 rad/s with individual components of 0.5 rad/s and -0.13 rad/s for y- and z-axis angular velocity, respectively. This corresponds to an illusory pitch down sensation about an axis shifted 74.6° from the true vertical. The OMS predicts an angular impulse vector of magnitude 0.49 rad/s with 0.48 rad/s and -0.11 rad/s y- and z-axis components, respectively. The OMS also predicts that the axis of illusory tumbling will be shifted 72.9° from the true vertical. The small differences between our modeling results and Guedry's theoretical calculations can be attributed to the 0.5 s latency in the rolling head tilt. Guedry and Benson (1978) made a simplifying assumption that the tilt was accomplished instantaneously, whereas we do not.

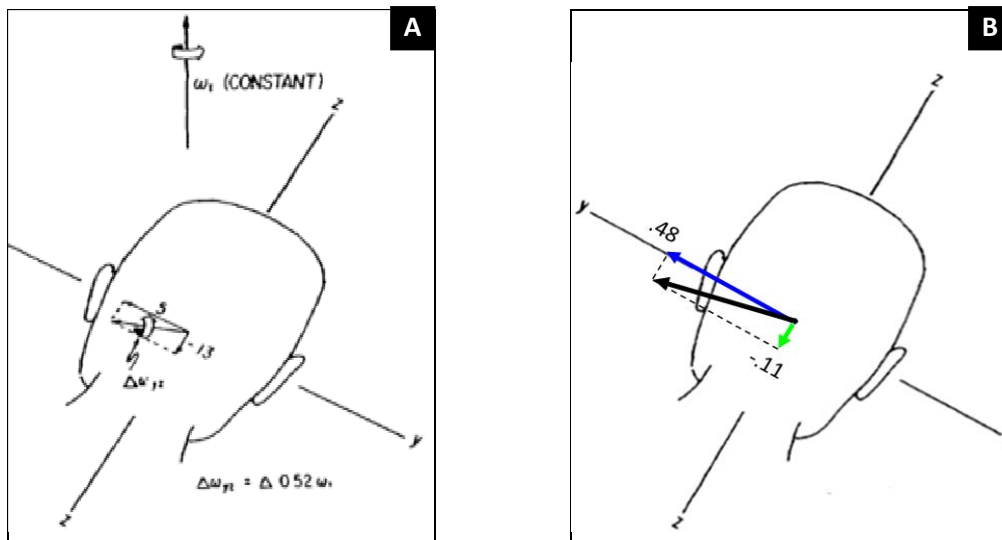


Figure 29. Vector analysis of estimated angular velocity immediately following 30° roll tilt. (A): Predicted response from Guedry and Benson (1978). (B): Predicted model response.



The Guedry and Benson analysis predicted the axis of tilt sensation, and the time course of angular velocity based on semicircular canal cues, but did not explicitly quantify the interaction with gravireceptor cues, or predict the magnitude and duration of illusory pitch (Figure 28B). It is clear from subjects' descriptions that the perceived pitch angle is not the integral of perceived rotational velocity (Figure 27B). Instead, the resulting sensation is one of continuous tumbling, but limited tilt. The OMS is able to successfully mimic this paradoxical sensation.

### Coriolis cross-coupling during decelerated rotation.

VEST	VISUAL
$\vec{\omega}$ $\vec{a}$	$\vec{x}$ $\vec{v}$ $\vec{g}$ $\vec{\omega}$

During decelerated rotation, reports of illusory tumbling, perceptual disturbances, and motion sickness were graded most severe, (as compared with the accelerated and constant velocity conditions), for 9 of the 11 subjects who experienced all 3 motion profiles (Guedry & Benson, 1978). The remaining two subjects reported the constant velocity and deceleration condition as equally nauseogenic (Guedry & Benson, 1978). Model results for the deceleration simulation are shown in Figure 30.

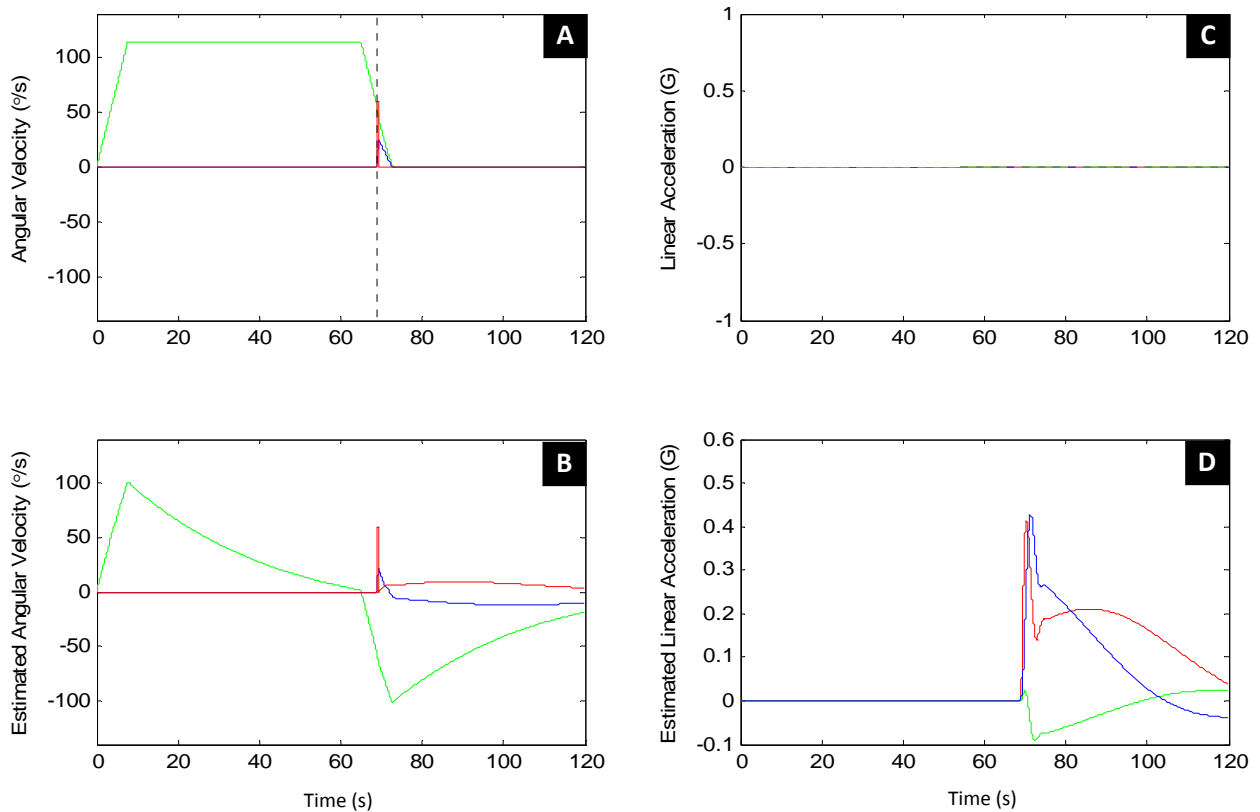


Figure 30. Model response to a 30° head tilt during Earth vertical decelerated rotation. Actual (A) and Estimated (B) angular velocity. Actual (C) and Estimated (D) linear acceleration.

The simulated subject was seated upright in a rotary chair and accelerated counter-clockwise at a constant angular rate of  $0.26 \text{ radian/s}^2$  ( $14.89^\circ/\text{s}^2$ ) to a terminal velocity of  $2 \text{ rad/s}$  ( $114.6^\circ/\text{s}$ ). At  $65 \text{ s}$  the rotary chair was decelerated at a rate of  $-0.26 \text{ radian/s}^2$  ( $-14.89^\circ/\text{s}^2$ ) until it was brought to a stop at  $72.7 \text{ s}$ . At  $68.8 \text{ s}$ , when the angular velocity of the rotary chair was equal to  $1 \text{ rad/s}$  ( $57.3^\circ/\text{s}$ ), the subject made a  $30^\circ$  roll head tilt (Right Ear Down) at a rate of  $60^\circ/\text{s}$  (red trace). The simulation was modeled to match the classic Coriolis cross-coupling experiment (Case III) performed by Guedry and Benson (1978).

At time  $t = 65 \text{ s}$ , as the chair begins to decelerate from  $2 \text{ rad/s}$ , the angular velocity sensation of the horizontal semicircular canal has effectively decayed to zero (Figure 30B). The deceleration of the chair is therefore interpreted as angular velocity in the opposite direction of true chair motion. At the moment before the  $30^\circ$  head tilt, the central estimate of angular velocity is equal to  $-54.6^\circ/\text{s}$  vs. the true angular velocity of  $57.2^\circ/\text{s}$ . As was seen in the constant velocity simulation, this misestimation results in an impulse vector that produces a strong Coriolis cross-coupling illusion and illusory sensations of tumbling (Figure 30B), acceleration (Figure 30D), and tilting (Figure 31A and 31B).

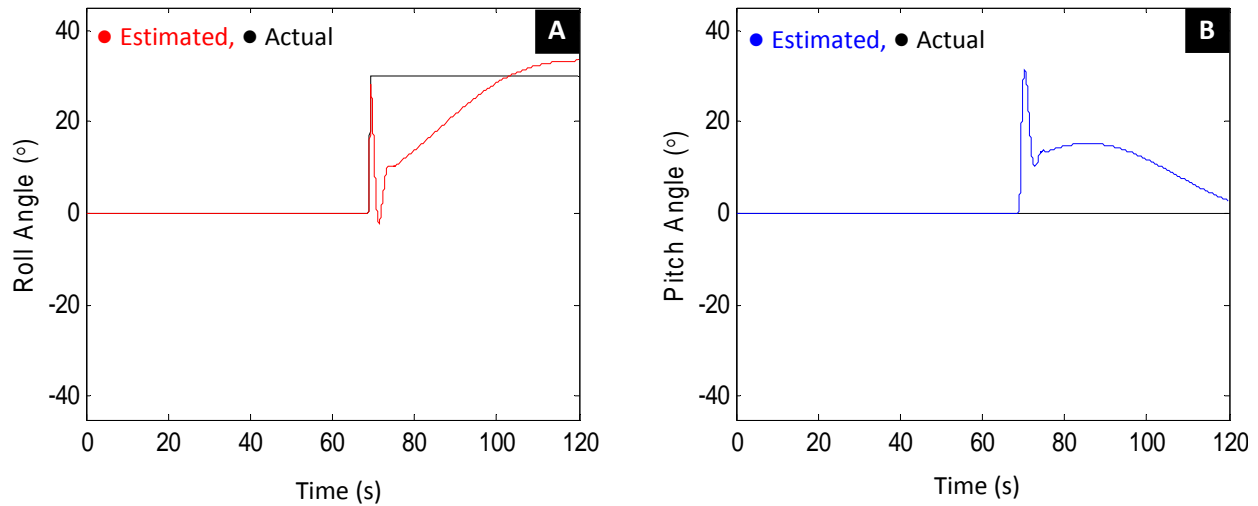


Figure 31. Model response to a  $30^\circ$  head tilt during decelerated rotation. Estimated Roll (A) and Pitch (B) angle.

Once again, our simulation results are in good agreement with the data and analysis of Guedry and Benson (1978) (Figure 32A). The OMS predicts an angular impulse vector of magnitude  $1.23 \text{ rad/s}$  (vs.  $1.24 \text{ rad/s}$ ) and an axis of illusory tumbling shifted  $130.9^\circ$  (vs.  $126.1^\circ$ ) from the true vertical (Figure 33B). The magnitude of the angular velocity impulse vector during deceleration (Figure 30B) is much greater than the vector that was produced during the constant velocity scenario (Figure 27B). The magnitude of the tumbling sensation and the degree of axis shift from true vertical correctly predict that the deceleration condition produces the most perceptual disturbances and instances of nausea and discomfort.

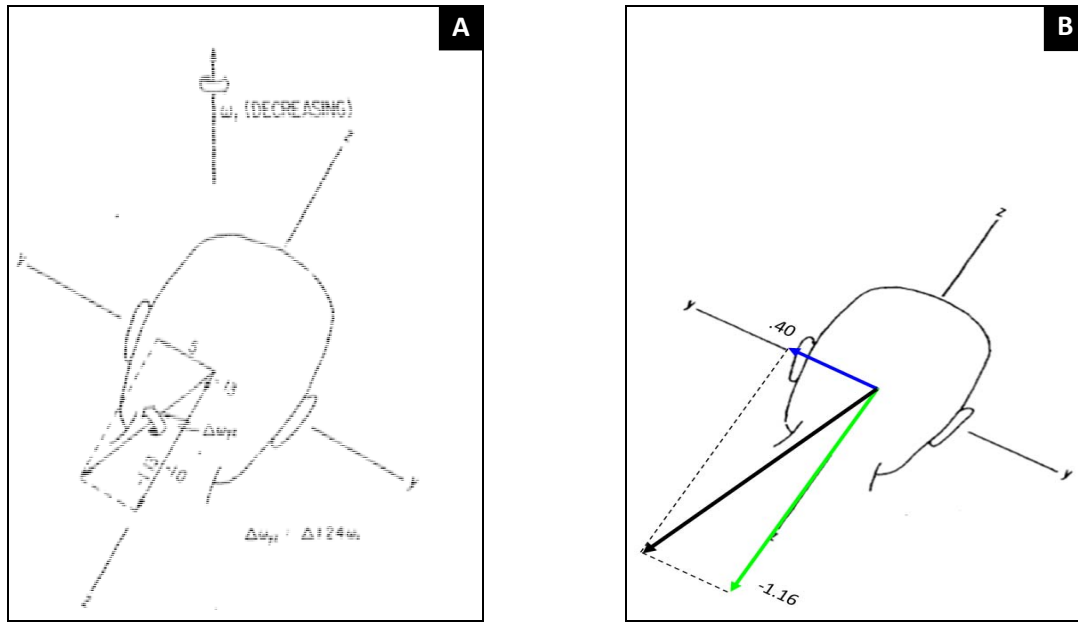


Figure 32. Vector analysis of estimated angular velocity immediately following 30° roll tilt. **(A):** Predicted response from Guedry and Benson (1978). **(B):** Present model response.

### G-Excess illusion.

VEST	VISUAL
$\vec{\omega}$ $\vec{a}$	$\vec{x}$ $\vec{v}$ $\vec{g}$ $\vec{\omega}$

When a pilot makes a head tilt in hypergravity, the excess gravito-inertial force acting on the otolith organs can produce non-veridical sensations of aircraft banking and spatial disorientation (Figure 33). This phenomenon is typically referred to as the G-Excess illusion or G-Excess Tilt Illusion.

This section is intentionally blank.

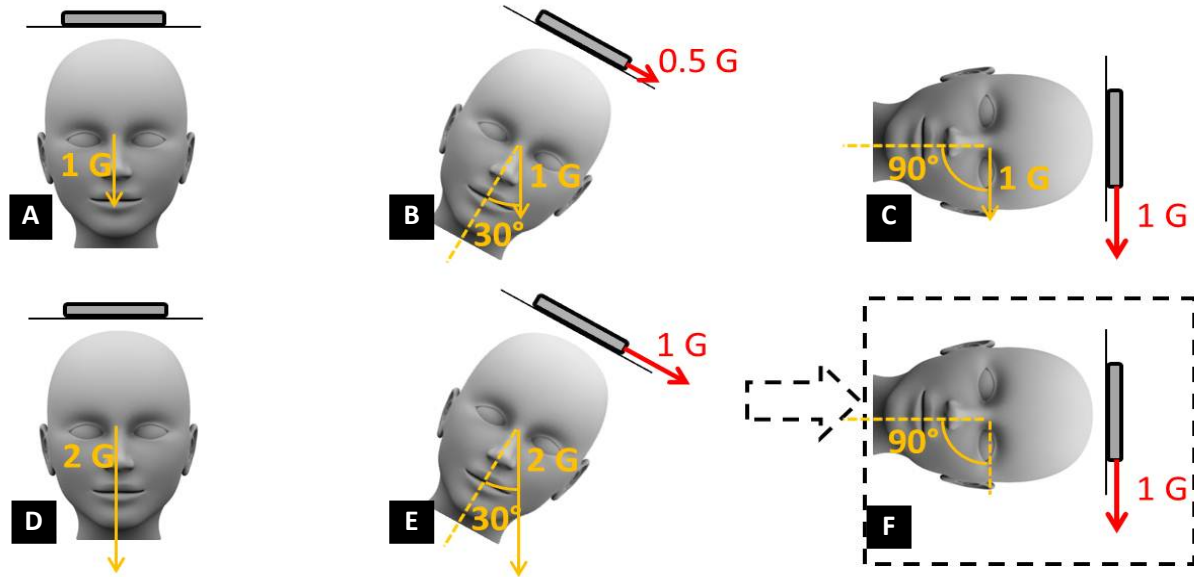


*Figure 33. Gravito-inertial force projection following a head turn made in normal (A, B, C) and hypergravity (D, E, F) conditions. (A): Head upright at 1G. (B): Tilting the head 30° will result in a 0.5G shear force acting along the inter-aural utricular plane of the otoliths. (C): At 90° the utricular plane is aligned with gravity and a 1.0G shear force is experienced. (D): Head upright at 2G. (E): Tilting the head 30° will now result in a 1.0G inter-aural shear force ( $2.0G \sin 30^\circ = 1.0G$ ) which is identical to force experienced during the 90° head tilt at 1.0G (C). (F): In the absence of strong visual or proprioceptive cues, this elicits an illusory overestimation of head tilt of up to 90° (commonly referred to as the G-Excess illusion), which is partially generalized to one's body, seat, and vehicle. (Reproduced from Clark [2013].)*

Experiments investigating the G-Excess illusion have used centrifugation (Chelette, Martin, & Albery, 1995; Schöne, 1964; Correia, Hixson, & Niven, 1968; Miller & Graybiel, 1971) to produce G forces. While this method is appropriate to study this phenomenon, it relies on strong angular velocity stimulation of the semicircular canals to produce the required hyper-gravimic environment. The resulting illusion is a combination of both G-excess and Coriolis cross-coupling, which makes modeling and understanding the dynamics of the pure G-Excess illusion very difficult.

Coordinated aircraft turning maneuvers have been employed to reduce semicircular canal contributions greatly (Gilson, Guedry, Hixson, & Niven, 1973; Guedry & Rupert, 1991). To dissociate between these two components (angular versus linear), we instead model G-excess during sustained, purely vertical linear acceleration (Figure 34). The simulated subject would be seated upright in a darkened, very tall elevator shaft and accelerated upwards at 2Gs for 25 s (Figure 34A). The resulting gravito-inertial force acting along the long body (z) axis is equal to  $-3.0 \text{ Gz}$  ( $f = g - a = -1G - 2G = -3Gz$ ). At 10 s, the simulated subject makes a smooth 45° right-ear-down rolling head movement (head angular velocity profile shown in Figure 34C). This head orientation is held for 7 s and then returned back to the neutral spine position.

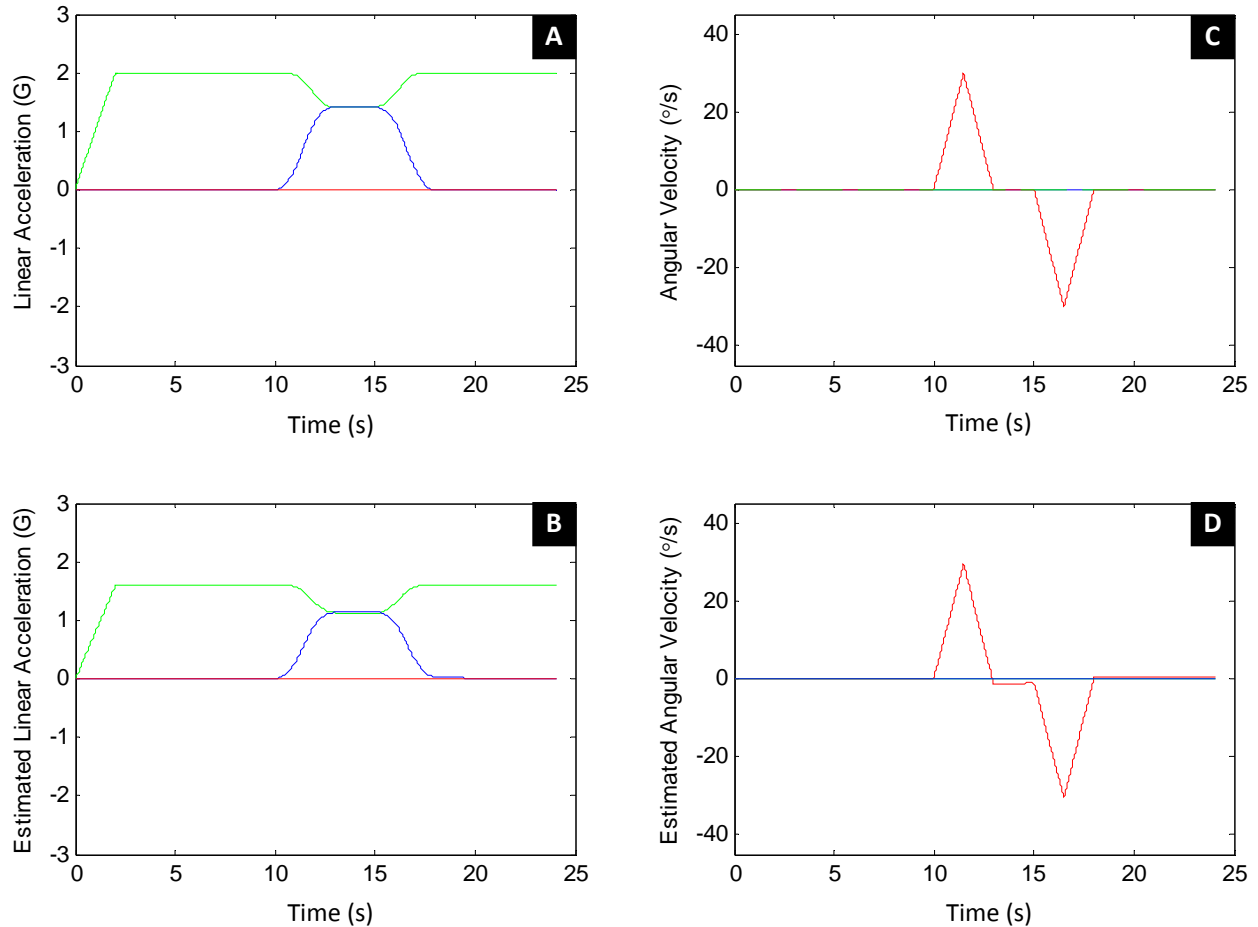


*Figure 34.* Model response to a 45° head tilt during 2G vertical linear acceleration. Actual (**A**) and Estimated (**B**) linear acceleration. Actual (**C**) and Estimated (**D**) angular velocity.

The model predicts that the subject will estimate both components of the linear acceleration force acting along the body (Figure 34B) and the roll angular velocity of the head with considerable accuracy (Figure 34D). While the individual components of the linear acceleration vector (Figure 34B) are slightly under-reported in terms of magnitude (the 2.0 Gz sustained upward acceleration is estimated as 1.6 Gz), the relative orientation of the vector is precisely aligned with the true orientation of the head. The resulting perception of roll angle is therefore accurate (Figure 34A) and no G-Excess illusion is experienced. This is not concordant with the literature.

In order to produce the overestimation of roll angle that we would expect (Gilson et al., 1973; Guedry & Rupert, 1991) during this hyper-G simulation, we must modify an internal parameter of the vestibular system model. The original model, based on Merfeld et al.'s (1993) Observer structure, was developed, tested and verified strictly under 1-G normal gravity conditions. That model implicitly assumes that the central nervous system has an internal representation of gravity and can distinguish tilt from translation with equal ability in all gravitoinertial force conditions. Furthermore, the model assumes that the utricle and saccule otolith feedback parameters are equally weighted during deconstruction of the estimated linear

acceleration vector. In other words, as the head is tilted  $45^\circ$  during our vertical acceleration simulation, the CNS, by design, properly extracts the vector components of the GIF that represent gravity (due primarily to correct estimation of the angular velocity of the head by the canals) and interprets the remaining GIF as acceleration in the proper direction of motion. Significant overestimation of tilt angle is therefore impossible with the original Merfeld model.

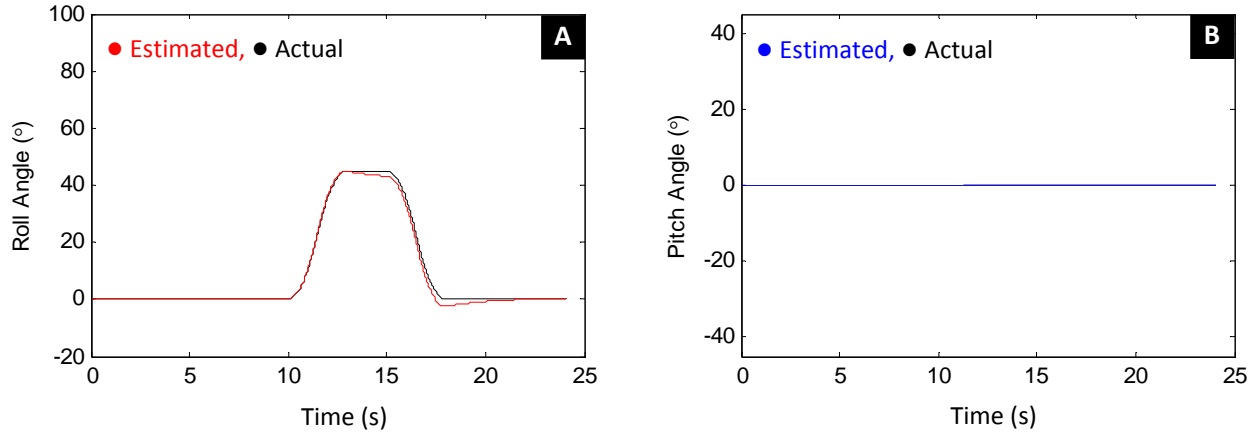


*Figure 35.* Model response to a  $45^\circ$  head tilt during 2G vertical linear acceleration. **(A):** Estimated roll angle. **(B):** Estimated pitch angle. The true roll and pitch angle are also shown.

We extended the original vestibular model to process utricle and saccule shearing forces differently by simply modifying the *Kaa* parameter of the CNS model. This approach was originally suggested by Clark (2013) and has been implemented here using a simplified version of his approach. For all of the present simulations *Kaa* was set to -4 for feedback along the x-axis, y-axis, and z-axis. Errors, therefore, in estimation of the individual components of linear acceleration were equally weighted. If the x- and y-components of *Kaa* are instead set to -2 during elevated G simulations, and the z-component is left at -4, misestimation of tilt is possible. Modifying *Kaa* implies that the CNS will weight utricle and saccule information differently when estimating gravity and acceleration in hyper-G and will allow shifts in the relative orientation of the central linear acceleration estimate to affect the resultant GIF direction independently from the central estimate of gravity (or tilt angle).

Results for model simulations using this modified parameter set are shown in Figures 21 and 36. The experimental setup for this simulation is identical to the previous example. Notice that angular velocity perception (Figure 36D) remains veridical. However, due to the modification of *Kaa*, the central estimate of linear acceleration (Figure 36B) now produces a large overestimation of roll angle (Figure 37A). The model predicts an initial G-excess overestimation of tilt angle of  $15.6^\circ$ , and this misperception slowly worsens to a  $25.6^\circ$  overestimation as the head turn is held under G. The model also predicts a lag in tilt angle estimation that lasts for 4 s following the head turn back to neutral spine orientation.

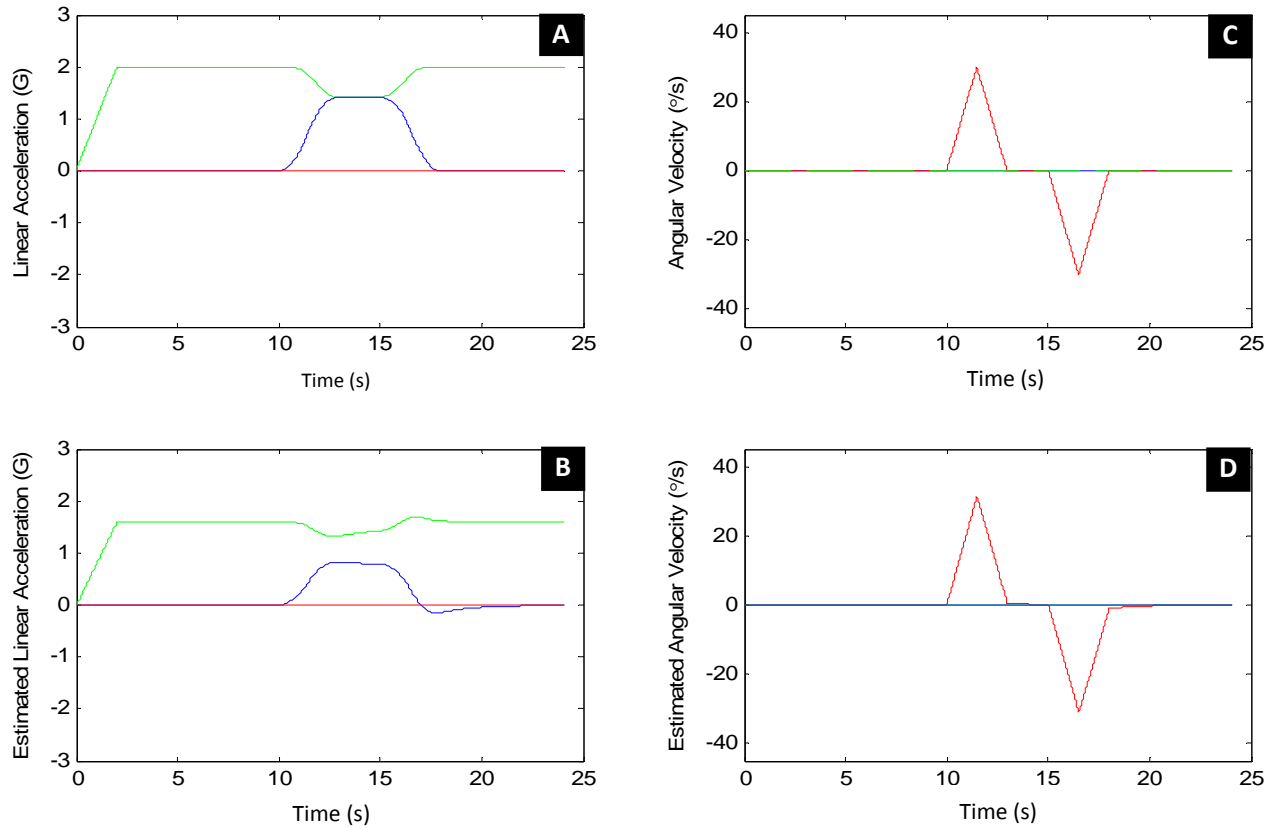


Figure 36. Model response to a 45° head tilt during 2G vertical linear acceleration with modified  $K_{aa}$  parameter. Actual (A) and Estimated (B) linear acceleration. Actual (C) and Estimated (D) angular velocity.

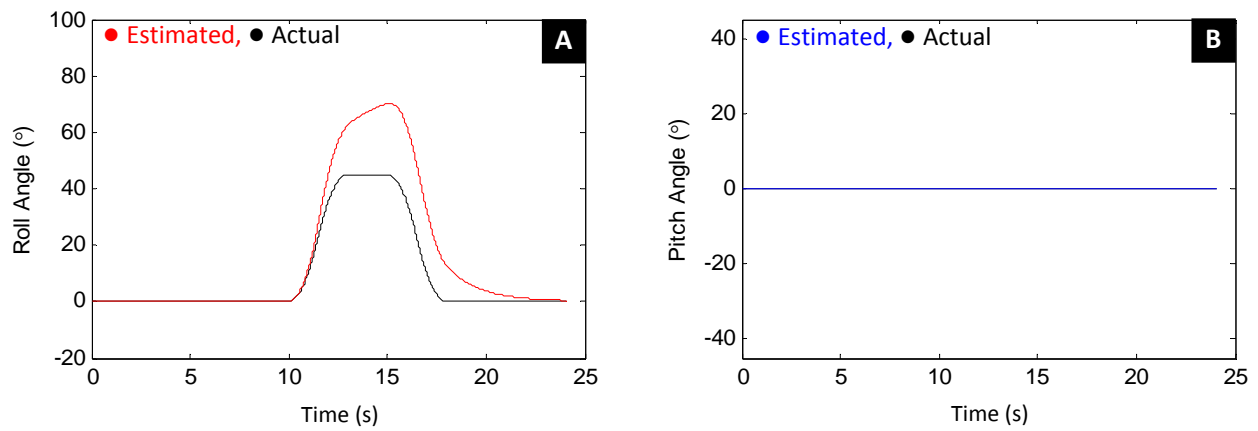
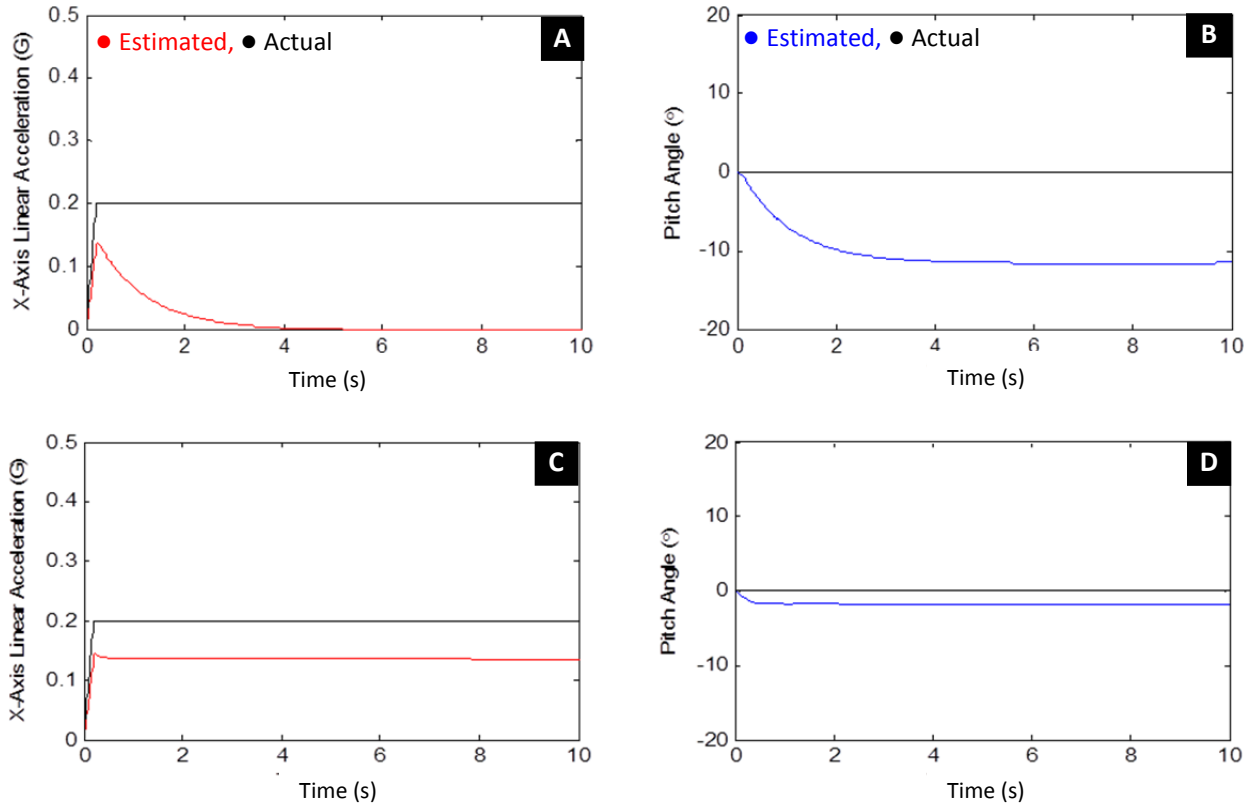


Figure 37. Model response to a 45° head tilt during 2G vertical linear acceleration with modified  $K_{aa}$  parameter. (A): Estimated roll angle. (B): Estimated pitch angle. The true roll and pitch angle are also shown.

## Somatogravic illusion (dark, light).

VEST	VISUAL
$\vec{\omega}$ $\vec{a}$	$\vec{x}$ $\vec{v}$ $\vec{g}$ $\vec{\omega}$

The model successfully predicts the somatogravic (pitch-up) illusion for forward linear acceleration in the dark (Figures 38A and 38B) and the suppression of the illusion in the light (Figures 38C and 38D). The somatogravic illusion in the dark has been well-documented experimentally (Cohen, Crosby, & Blackburn, 1973; Graybiel & Brown, 1951; Graybiel, 1966) and is predicted by many perception models (Borah et al., 1978; Pommellet, 1990; Kynor, 2002; Bilien, 1993). It is worth comparing the implementation of the visual pathways for these models in order to understand how the OMS works differently than previous modeling efforts.



*Figure 38.* Model response to a step in forward linear acceleration. The simulated subject was seated upright and accelerated forward (+x) on a horizontal sled at 0.2 G/s for 10 s in both darkness (**A, B**) and lighted (**C, D**) conditions. The time course and dynamics of the predicted pitch-up sensation were set to match the experimental centrifuge data from Graybiel and Brown (1951) and the Borah et al. (1978) KF response curves. (**A, C**): Estimated linear acceleration for darkness and lighted conditions. (**B, D**): Estimated pitch angle for darkness and lighted conditions. Also shown is the 0.2 G input stimulus.

The OMS uses visual angular velocity and visual gravity information, along with canal and otolith cues from the vestibular system, to estimate acceleration and pitch angle. While visual linear velocity and position information are also available, the structure of the OMS posits



that these quantities do not appreciably affect the lower derivatives of acceleration or the relative orientation of the simulated subject. This constrained visual capability is quite different from past modeling implementations, which did not incorporate visual cues for the direction of gravity. These models assumed that only visual velocity information, resulting from linear motion of the moving scene, would suppress the somatogravic illusion and permit correct estimates of forward linear acceleration. In a study addressing this specific issue, Tokumaru et al. (1998) found that subjects who underwent linear acceleration with isolated visual vection cues lacking visual gravity cues reported sensations of tilt with equal likelihood and magnitude as those without any visual information at all. The researchers additionally found that when subjects were provided with a visual gravity reference they felt significantly reduced magnitudes of the pitch-up sensation. These findings imply that while many models properly predict visual suppression of the somatogravic illusion, the implementation made by the OMS is more consistent with the findings and with the actual visual-vestibular interaction mechanism responsible.

The somatogravic illusion is common in aviation; it is particularly hazardous during flight in degraded visual conditions and during rapid ascent or catapult-assisted take off. In these conditions, a proper representation of visual-vestibular sensory interaction is required in order to predict the onset and intensity of the resulting pitch-up sensation. Unlike previous modeling efforts, the OMS can predict the somatogravic illusion in light, as long as a strong visual orientation cue is not present (e.g., a clear horizon line).

### **Optokinetic nystagmus (OKN) & optokinetic after-nystagmus (OKAN).**

VEST		VISUAL			
$\vec{\omega}$	$\vec{a}$	$\vec{x}$	$\vec{v}$	$\vec{g}$	$\vec{\omega}$

Results for a simulation of optokinetic nystagmus (OKN) and optokinetic after-nystagmus (OKAN) are shown in Figure 39. The predicted model dynamics for OKN and OKAN (Figures 39D, 39E, and 39F) are compared against data from Raphan et al. (1979) (Figures 39A, 39B, and 39C). The model response to the rotation in the dark (Figure 39D) demonstrates the expected exponential decay of slow phase velocity during constant velocity rotation and the post-rotatory response in the opposite direction as the chair is stopped at  $t = 60$  s. During pure rotation of the visual surround (circular vection), the model correctly predicts the fast and slow dynamics of the optokinetic nystagmus onset and the saturation of slow phase eye velocity that immediately occurs once the visual vection field is turned off (Figure 39E). The model estimates a rapid saturation of velocity to about  $90^\circ/\text{s}$ , which is slightly lower than the  $120^\circ/\text{s}$  OKAN saturation level reported by Raphan et al. (1979). Finally, during constant velocity rotation in the light (Figures 39C and 39F), the model accurately predicts the rapid rise and nearly veridical initial estimate of slow phase eye velocity, the slight decline in perception during constant velocity rotation, and the small negative velocity recorded as the chair is brought to a stop.

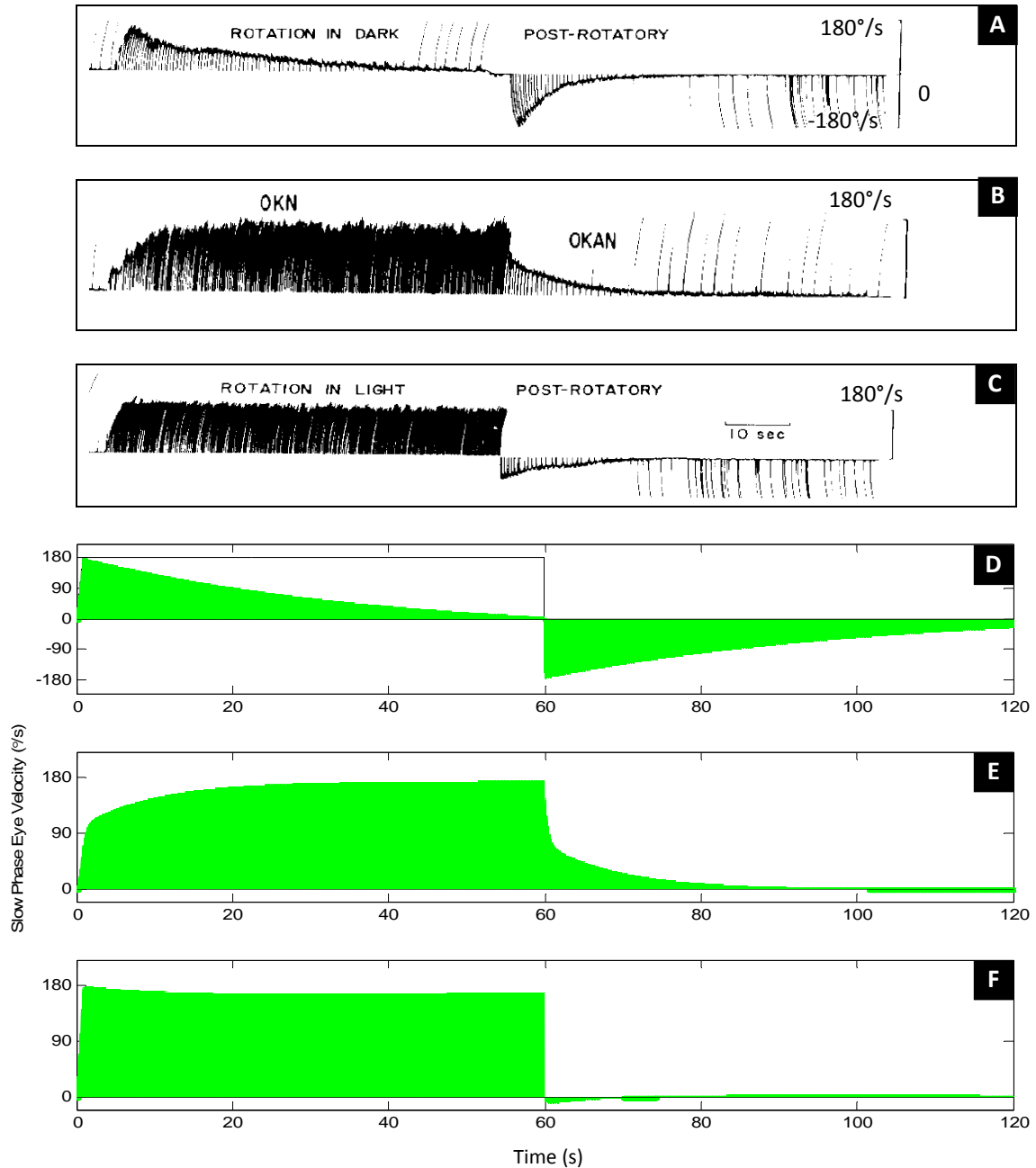


*Figure 39.* Slow phase eye velocity in response to 180°/s rotation in the dark (**A, D**), circular vection (**B, E**) and rotation in the light (**C, F**). (**A, B, C**): Experimental data from Raphan et al. (1977). (**D, E, F**): Predicted model response. **Note:** Model output is represented as stem plots to provide a better visual comparison with the Raphan et al. (1977) data. Slow phase eye velocity was calculated with an eye movement model that used a fixation distance of (2 m) and a leaky integration time constant of (0.1 s). These values are identical to those used by Merfeld and Zupan (2002).

## Linear vection.

VEST		VISUAL			
$\vec{\omega}$	$\vec{a}$	$\vec{x}$	$\vec{v}$	$\vec{g}$	$\vec{\omega}$

In this simulation, the subject sat upright and viewed a high fidelity translating visual scene. Input to the model is represented as  $\pm 15$  cm/s and  $\pm 7$  cm/s steps in visual linear velocity (Figure 40A). As the CNS gradually accepts the visual input, an illusory sensation of linear self-motion (linear vection) develops in a direction opposite to visual field motion (Figure 40B). To allow for a direct comparison with Chu (1976) (Figure 40D), we plotted the negative of the visual field velocity in Figure 55A. While the model yields useful predictions concerning the Chu (1976) data, as with the circular vection simulation, the model will require modification to predict vection onset delays and the complex dynamics that result from such delays during step changes in the visual vection field (Figure 40E). A more complicated visual system, perhaps one which dissociates focal and peripheral vision or implements nonlinear visual dynamics, would be required to produce these characteristics.

Due to the structure of the visual residual pathways assumed in the OMS, changes in visual flow velocity are not interpreted as acceleration, and do not influence the estimated direction of gravity or pitch (Figure 40C). This is why in this example, a step change in visual field velocity does not result in any transient tilt sensation, which was accurate. As was noted during the somatogravic illusion simulation section “Somatogravic illusion (dark, light),” previous attempts to model the interactions of the visual and vestibular systems did not account for this important structural distinction. A step change in linear field velocity therefore could result in transient acceleration and a sensation of pitching forward or backwards, which is not observed experimentally.

This space is intentionally blank.

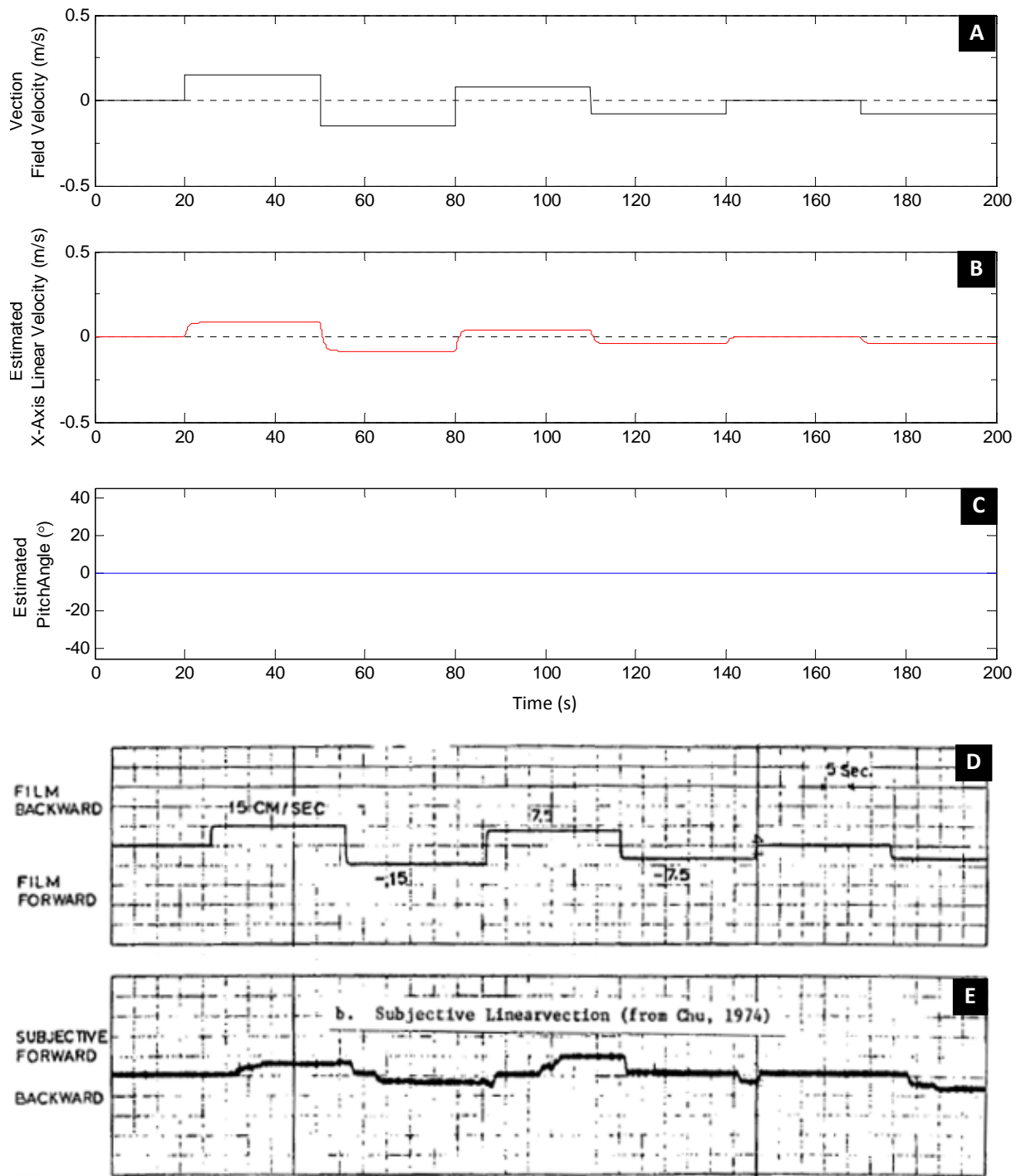


Figure 40. Model response during step changes in vection field velocity. To allow for a direct comparison with the published data of Chu (1976), the simulated conditions precisely match the  $\pm 15$  cm/s and  $\pm 7.5$  cm/s linear vection steps used during experimentation (D). (A): Negative Vection Field Velocity (-x). (B): Estimated linear velocity (C): Estimated pitch angle. Vection field velocity (D) and subjective linear vection reports (E) from Chu (1976).

## Roll circular vection.

VEST		VISUAL			
$\vec{\omega}$	$\vec{a}$	$\vec{x}$	$\vec{v}$	$\vec{g}$	$\vec{\omega}$

In the previous two simulations of circular vection (sections “Earth vertical rotation [circular vection]” and “Optokinetic nystagmus [OKN] & optokinetic after-nystagmus [OKAN]”) the angular velocity vector of the vection field was aligned with gravity and produced only illusory self motion about an upright yaw axis. For both of these examples, the CNS was able to estimate angular velocity without interaction or stimulation of the otolith organs. If we shift the orientation of the vection field, we can induce self-motion about a roll or pitch body axis. In this scenario the visual system, semicircular canals, and otoliths all interact to form an estimate of both orientation and angular self-motion. During circular vection about a roll or pitch body axis, a paradoxical sensation of limited displacement in tilt (Mast, Berthoz, & Kosslyn, 2001) while experiencing a continuous tumbling velocity sensation is often reported (Allison, Howard, & Zacher, 1999). This sensation is commonly described as velocity without displacement or tumbling without getting anywhere. The degree of tumbling and angle of tilt are dependent on the strength of the visual cue and the size of the visual field.

To model this example, we position a simulated subject in front of a wide field of view roll vection field that rotates at a velocity of 45°/s. We assume that the subject can extract a visual angular velocity cue from the vection field but cannot extract a strong visual orientation cue.

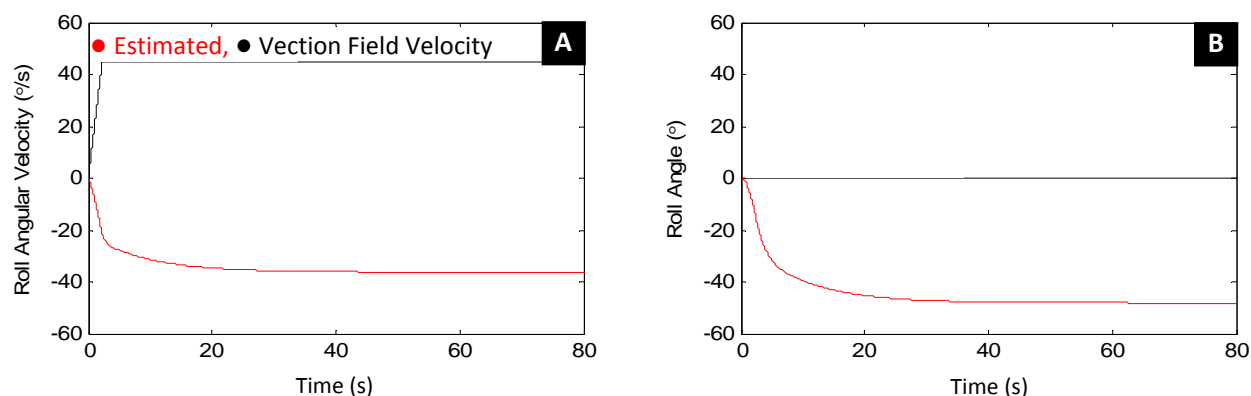


*Figure 41.* Model response to a 45°/s circular roll vection stimulus. **(A)**: Estimated roll angular velocity. **(B)**: Estimated roll angle. The drum velocity is also shown in pane A.

Results (Figure 41) show that the model is able to successfully predict the paradoxical sensations that are typically experienced during circular roll vection. For this simulation, the subject estimates a steady state static tilt angle of -48° (Figure 41B) and a persistent angular velocity, or tumbling sensation, at a rate of -36°/s (Figure 41A). The Perception Toolbox provides a tool to visualize this paradoxical sensation (Figure 42). During the simulation, the actual orientation of the subject remains constant (only the visual scene changes orientation) (Figure 42A). The estimated orientation, however, is comprised of two individual sensations: static tilt, represented by the solid avatar in Figure 42B, and constant tumbling, represented by

the translucent rotating avatar. When viewed in real time, this visualization tool provides a powerful illustration of the combined perceptual response.

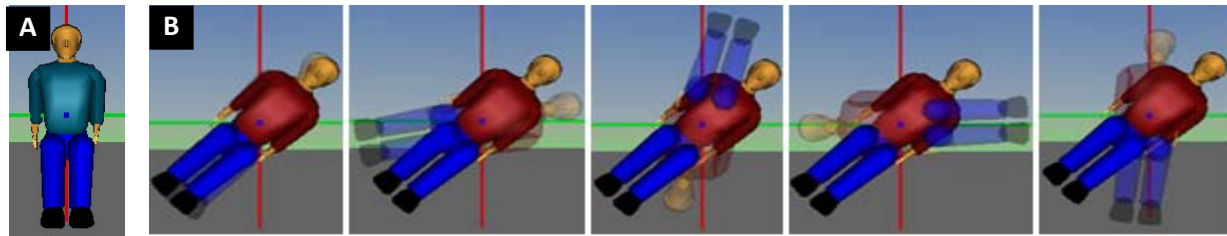


*Figure 42.* Perception Toolbox tilting and tumbling visualization tool during constant velocity roll circularvection. **(A):** Actual subject orientation throughout simulation. **(B):** Screenshots of the animated avatar showing the constant tilt angle (solid avatar) and persistent tumbling sensation (translucent avatar) experienced.

It is important to note that if a strong visual orientation cue is present during simulation (i.e., a polarized floor and ceiling), the model would predict a 360° rotating tilt angle that coincides closely with the rotation of the visual scene. These results are consistent with the research of Allison et al. (1999), who demonstrated that almost 80% of subjects positioned in a furnished rotating room experienced complete 360° tumbling sensations.

## Practical Aviation Applications

### Post-turn illusion in degraded visual conditions.

VEST	VISUAL
$\vec{\omega}$ $\vec{a}$	$\vec{x}$ $\vec{v}$ $\vec{g}$ $\vec{\omega}$

The passage below, reproduced from Lawrence Young's chapter of the 2003 edition of *Principles and Practice of Aviation Psychology*, provides a thorough description of the post-turn illusion.

When a pilot banks the airplane into a right wing down constant rate level turn in the clouds, the information is registered by the horizontal semicircular canals, which register the initial yaw rate, and by the vertical canals, which measure the brief roll rate on entry into the turn [...]. Assuming a coordinated turn with no sideslip, the otolith organs and the haptic receptors continue to register the net gravito-inertial force direction along the z-axis of the aircraft, although at a magnitude greater than 1 G. Several seconds into the turn, the horizontal semicircular canals signal a steadily reduced yaw rate, which finally drops below subjective threshold at a time determined by the initial turn rate. At this point, in the absence of any confirming out-the-window visual cues, a passenger would feel the airplane to be neither banked nor turning, but flying straight and level. And so would the pilot if no reference were made to the artificial horizon or the turn indicator. When the pilot then rolls back left to straight and level flight, with the GIF still directed into the seat, the passenger's vertical semicircular canals

correctly detect a brief roll to the left. The horizontal canals, however, which had been indicating no yaw rate, now experience a sudden change in angular velocity to the left, which they now duly signal to the brain. Pilot and passenger alike feel that they have begun a left turn. (Young, 2003, p. 84-86)

In the next two sections (“Post-turn illusion in degraded visual conditions” and “Post-turn illusion with artificial visual horizon orientation cue”), we simulate two examples of the post-turn illusion following a coordinated two-minute-turn. For simplicity, we only consider the forces that are produced due to aircraft rotation and centripetal acceleration and do not attempt to model atmospheric interactions, lift, drag, or other more complicated aerodynamic characteristics of the flight profile. These factors are important to flight control but are not important to illustrate this particular illusion.

We assume that the pilot is situated in an aircraft that rolls about the center of the head. At time  $t = 0$ , the pilot enters a coordinated two-minute-turn with a true airspeed of 120 knots and a subsequent bank angle of  $18.25^\circ$  (resultant radius of the turn is equal to 0.6366 nautical miles). A 2-min turn under these conditions will result in a total turn velocity of  $3^\circ/\text{s}$  ( $360^\circ$  in 120 seconds =  $3^\circ/\text{s}$ ). As the aircraft banks into the coordinated turn, the roll- or x-axis semicircular canal will register the aircraft bank rate ( $18.25^\circ/\text{s}$  for this example). Simultaneously, the  $3^\circ/\text{s}$  angular velocity of the turn will be projected along the y- and z-axes of the semicircular canals. The net GIF vector throughout the simulation will remain directed into the seat; however, the y- and z-axes of the otolith organs will be stimulated by the centripetal acceleration of the turn. This acceleration is directed toward the center of rotation. Figure 43 summarizes all of the forces acting on the semicircular canals and otolith organs during the coordinated 2-min turn.

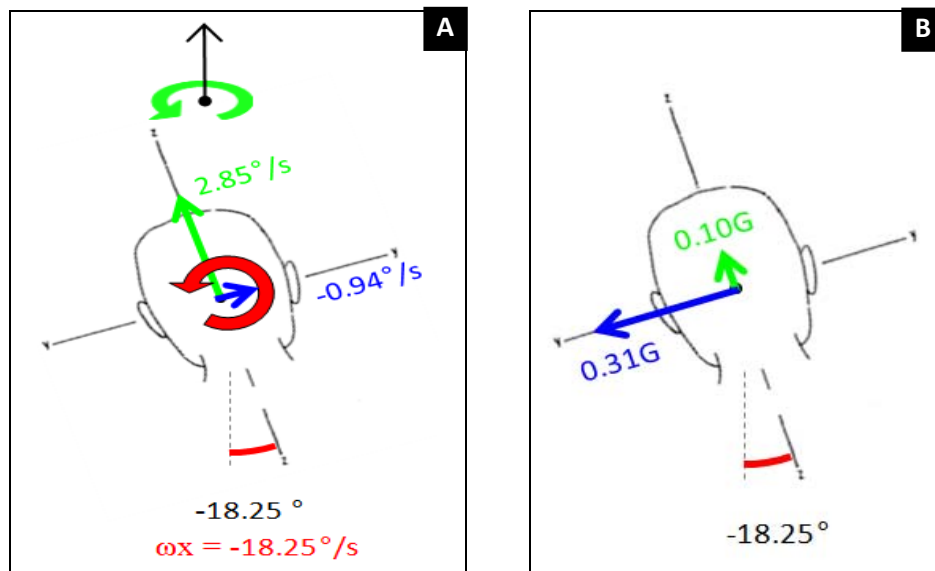


*Figure 43.* Model input to the semicircular canal (A) and otolith organs (B) during a coordinated 2-min turn. (A): Semicircular canal angular velocity projection. (B): Otolith linear acceleration projection. The radius of curvature of the coordinated turn was equal to 0.637 nautical miles.

For this simulation, we assumed that the pilot was flying under degraded visual conditions and failed to look (or attend to) the attitude indicator sufficiently during the turning maneuver. Under these conditions, the model successfully predicts the dynamics of the post-turn illusion as described by Young (Figure 44). As the pilot enters the turn, he initially experiences a sensation of roll tilt in the proper direction of aircraft bank. This cue quickly washes out and soon the pilot feels as if he is flying straight and level. After 2 min, as he begins to roll out of the turn, he perceives that he is banking in the opposite direction (magnitude of illusory bank  $\approx 18^\circ$ ) of actual aircraft motion and entering a right turn. This illusion is relevant to spatial disorientation that can occur during “go around” maneuvers following a missed approach (McGrath, Newman, Lawson, & Rupert, 2015).

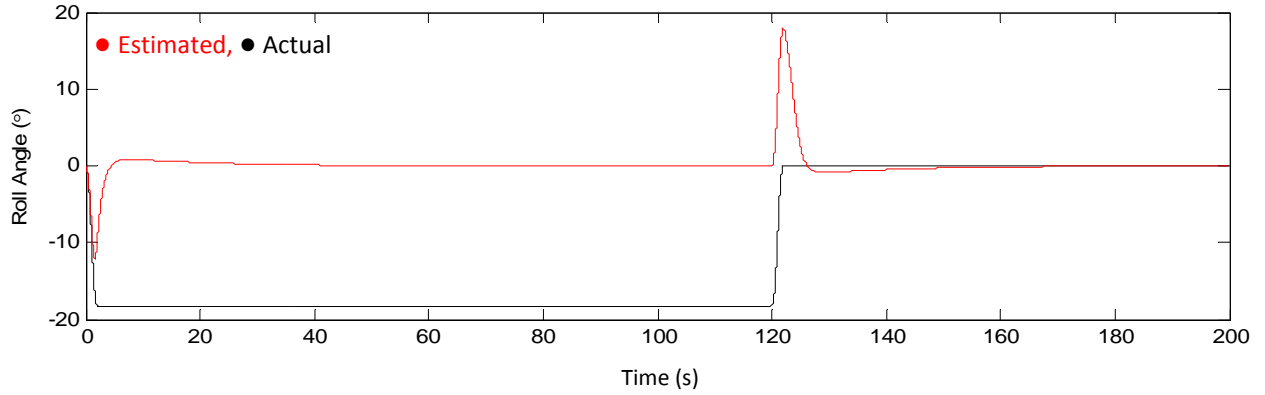


Figure 44. Estimated roll angle during coordinated turn without visual sensory input.

#### Post-turn illusion with artificial visual orientation cue.

VEST		VISUAL			
$\vec{\omega}$	$\vec{a}$	$\vec{x}$	$\vec{v}$	$\vec{g}$	$\vec{\omega}$

In this simulation, we repeat the coordinated 2-min turning profile used in the section “Post-turn illusion in degraded visual conditions” but add a visual orientation cue from an artificial horizon indicator such as an attitude display. We model this visual input as a unit vector that maintains alignment with the true aircraft bank angle. Perception of aircraft bank angle is now driven by the rotation of the aircraft registered by the semicircular canals, the resultant acceleration vectors due to circular motion acting on the otolith organs, and a visual orientation vector that steers the central estimate of bank towards the true orientation. The estimated roll angle of the aircraft under these conditions is shown in Figure 45.



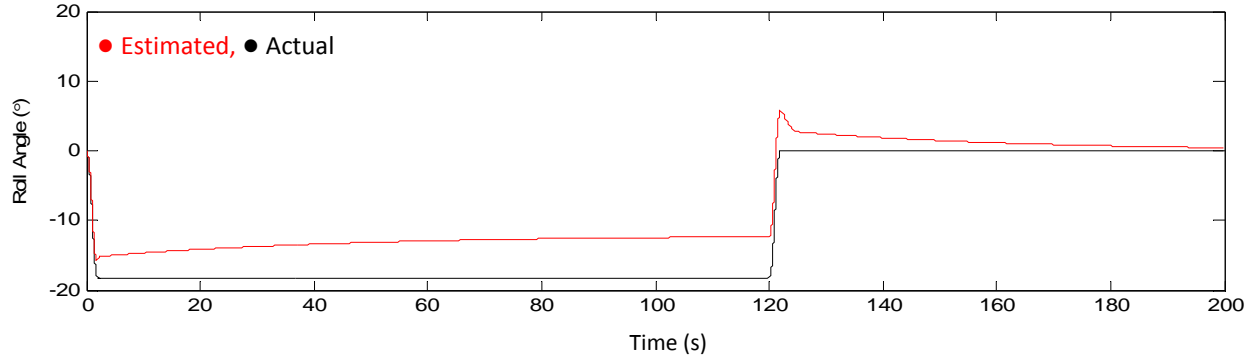


Figure 45. Estimated roll angle during coordinated turn with a visual orientation cue from an artificial horizon indicator.

The magnitude of the post-turn illusion is drastically reduced with a visual orientation cue. As the pilot rolls out of the coordinated turn, he experiences a brief, 4.5° banking roll tilt in the opposite direction of the original turn. This corresponds to a 75% reduction (4.5° vs. 18°) in the magnitude of the post-turn illusion compared with the simulation under degraded visual conditions.

#### Coriolis head movement during a coordinated turn.

VEST	VISUAL
$\vec{\omega}$ $\vec{a}$	$\vec{x}$ $\vec{v}$ $\vec{g}$ $\vec{\omega}$

For the final example, we simulate a head tilt made during a 3.6 Gz constant rate level turn. At 250 knots, the bank angle for the turning maneuver is 33.4°. Once the aircraft has entered the coordinated turn, we assume that the pilot makes a 30° rolling head movement in the opposite direction of the turn to approximately align the head with the true horizon line. Such behavior is commonly observed in flight and on the ground, and is attributable to well-known visually-mediated righting reflexes (Magnus, 1926; Young et al., 1986; Merryman & Cacioppo, 1997), which incorporate visual frame of reference information into the control of body posture and orientation perception.

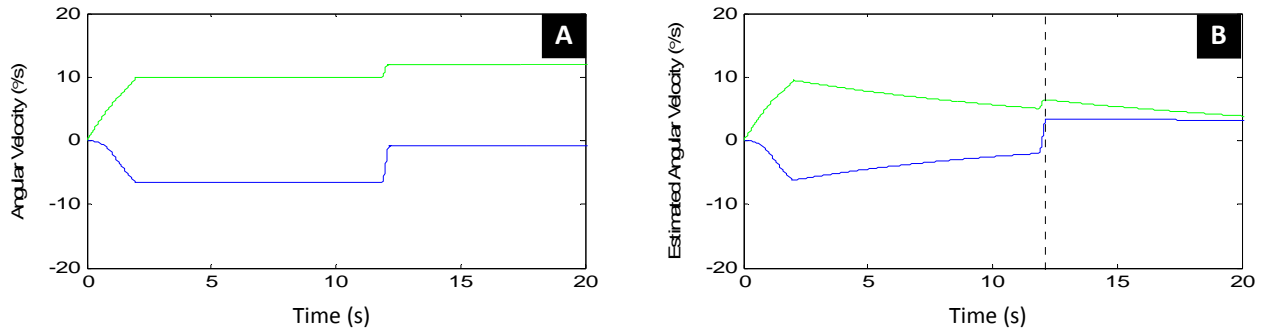
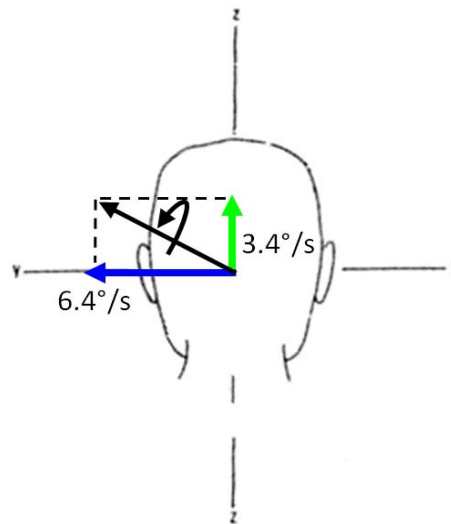


Figure 46. Angular velocity perception following a cross-coupled head movement during a coordinated turn. Actual (A) and estimated (B) angular velocity.

The angular velocity of the aircraft and the estimated angular velocity perceived by the pilot are shown in Figure 46A and Figure 46B, respectively. A vector analysis of the angular velocity impulse immediately following the head tilt reveals a small forward, pitch down, tumbling velocity of magnitude  $7.25^\circ/\text{s}$  (Figure 47). This small angular rate is unlikely to induce a strong sensation of tumbling, vertigo, or spatial disorientation. An increased turn rate would intensify the cross-coupled illusion. Even under the moderately stressful conditions simulated in this example; the response is not very provocative. We would expect pilots to minimize these types of head movements if they were particularly disorienting. Angular velocity of the aircraft is not usually the reason for disturbance during head movement (Gilson et al., 1973; Guedry & Rupert, 1991).



*Figure 47. Vector analysis of estimated angular velocity immediately following 30° roll tilt.*

Note that the tilted orientation of the pilot's head is offset from the true horizon line by only  $2^\circ$ . The resultant magnitude of the angular velocity tumbling vector (Figure 47) (black arrow) is equal to  $7.25^\circ/\text{s}$  forward (into the page), and the estimated illusory sensation of pitch is equal to approximately  $4^\circ$  nose down.

## **Case Study: F18 Mishap Analysis**

### **Mishap summary.**

On August 10th 2011, two U.S. Marine aviators ejected from a McDonnell Douglas F/A-18D Hornet during a night "2v2 intercept" exercise<sup>5</sup>, 35 miles off the coast of Ensenada, Mexico. Both pilots survived the incident, which is rare for a spatial disorientation (SD) mishap; however, the aircraft was damaged beyond repair, costing the U.S. Government approximately 70 million dollars. Flight incident recording data indicated a series of extreme maneuvers preceding the mishap, with high G-loading. An average of 5.5 Gz was sustained during the final 15 s of the

<sup>5</sup> 2 versus 2 intercept exercise: The pilots involved in this mishap were practicing maneuvers wherein two aircraft investigated two other unidentified aircraft that were in their airspace and essentially escorted the unidentified aircraft out of the territory or take necessary defensive action.

flight. This value peaked at 7.46 Gz immediately prior to pilot ejection, but G-induced loss of consciousness was not indicated. According to MAJ Thomas Mondeaux, an Aviation Safety Officer who evaluated the mishap, “There was no evidence of loss of consciousness, because control inputs were made throughout the end of the flight, the pilot communicated and ejected successfully...” (personal communication, September 19, 2011; Newman, Lawson, Rupert, & McGrath, 2012). Given that the incident occurred at night, over the ocean, and with such extreme forces acting on the body, it is likely SD played a role in causing or exacerbating this accident. A re-creation of the aircraft’s orientation, instrumentation, and pilot control input was created by NAVAIR (Naval Air Systems Command) ASIST (Aircraft Ship Integrated Secure and Traverse System) from the DFIR (Digital Forensics and Incident Response) recording. We used the same data as NAVAIR to simulate the final 42.5 s of the mishap with the OMS.

### **Data preparation.**

Data from the DFIR recording was up-sampled to 100 Hz using cubic spline interpolation (Figure 48). This data was converted to the proper coordinate frame and used to generate a series of OMS input files. All files consider the final 42.5 seconds of flight (the same time frame considered in the NAVAIR video recreation).

Three different sensory cueing scenarios were produced in order to dissociate the influence of each sensory system on pilot orientation perception. For all three examples, we assumed that the pilot was facing forward and that the pilot lacked continuous information concerning his visual position (i.e., out-the-window estimate of altitude), linear velocity (i.e., moving visual scene over the ground) and orientation (i.e., a natural or artificial attitude clue or horizon line). These assumptions appear to agree with the visual conditions and other circumstances of the mishap.

In our initial discussion of the accelerations associated with the mishap, we consider only the angular cues acting on the aircraft. G-force values are therefore ignored and are assumed to be equal to zero for the duration of the simulation. For Case 2 (section “F18 mishap analysis [angular velocity cues + acceleration cues]”) we consider both the angular cues and the acceleration cues acting on the body. For the final case, Case 3 (section “F18 mishap analysis [G-excess parameter adjustment]”) we use the modified G-excess parameter set (introduced in section “G-Excess illusion”) and repeat the simulation with both angular and linear acceleration cues.

This section is intentionally blank.

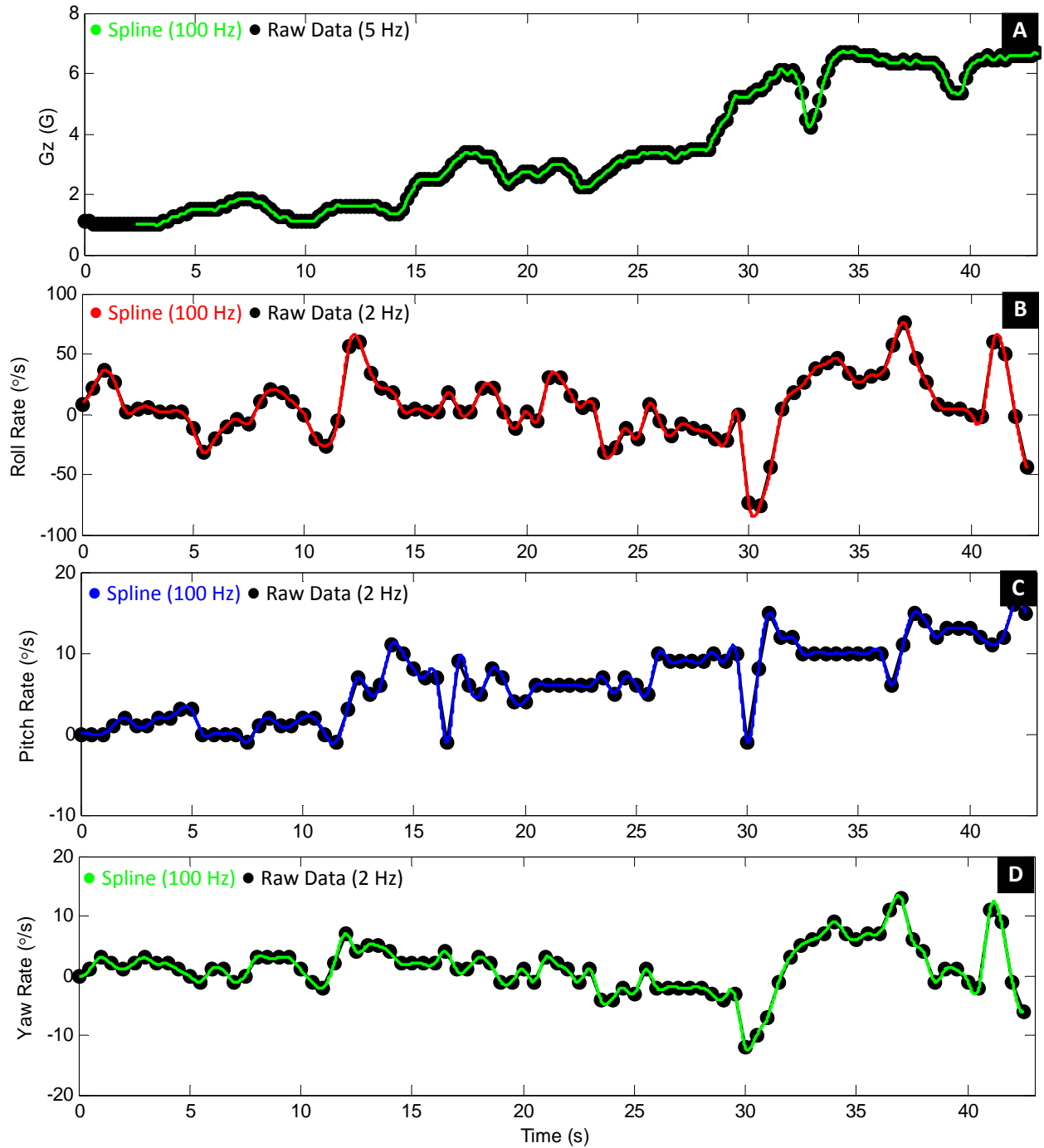
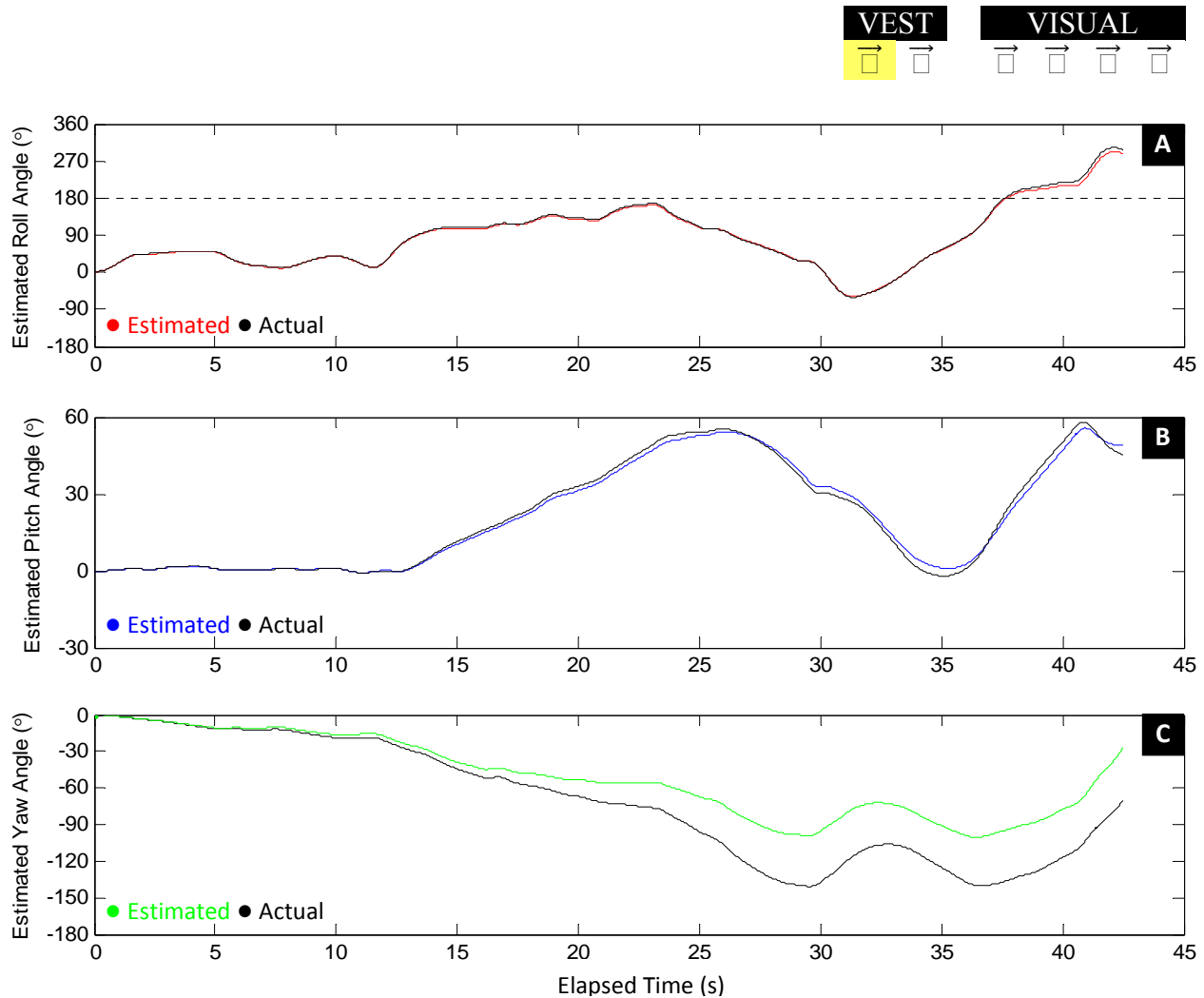


Figure 48. Spline fits for F18 mishap analysis. (A): Raw 5 Hz Gz data and 100 Hz spline fit. Raw 2 Hz angular velocity data and 100 Hz spline fits for roll (B), pitch (C) and yaw (D) angular velocity.

### F18 mishap analysis (Isolated angular velocity cues).



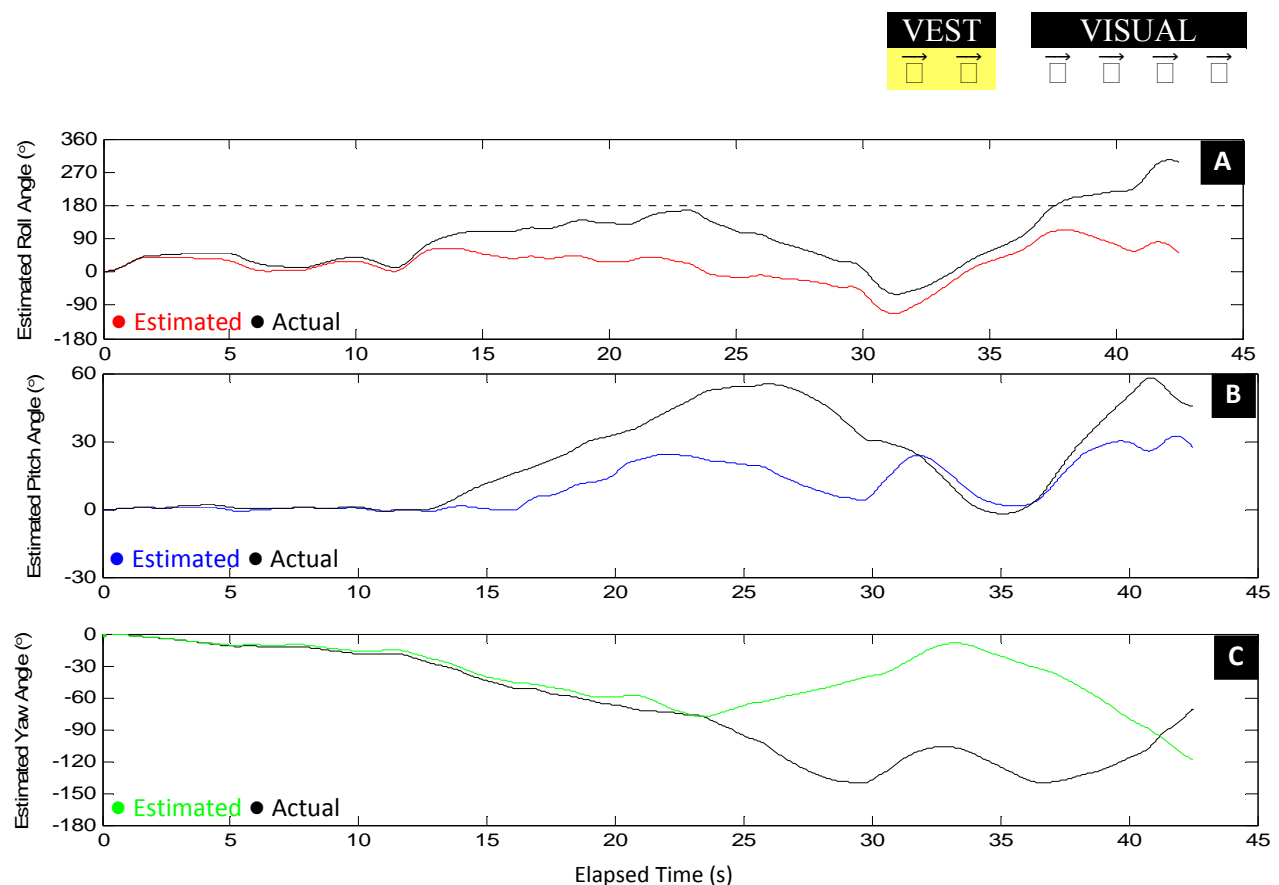
*Figure 49.* Orientation perception during F18 mishap (angular velocity). Isolated angular velocity cues (aircraft acceleration artificially set to zero, *see text for explanation*). **(A):** Estimated and actual roll angle (°). **(B):** Estimated and actual pitch angle (°). **(C):** Estimated and actual yaw angle (°).

Figure 49 shows model results for the F18 mishap pilot's estimated perception of aircraft orientation. For this example, we assume only angular velocity cues and gravity are acting on the body. By isolating the angular cues, we can determine if angular roll, pitch, and yaw velocity perceptions alone (due to canal washout or interaction with the internal estimates of gravity and acceleration) would produce appreciable disorientation or illusory self-motion.

Results suggest that pilot perception of roll (Figure 49A) and pitch (Figure 49B) angle would be nearly accurate given these conditions. While the estimated yaw angle (Figure 49C) is slightly over-estimated towards the end of the simulation, the misperception is minor, and

unlikely to produce significant disorientation or provoke the pilot response witnessed in the accident re-creation. Based on the pilot's actual behavior, it is highly unlikely that he had such an accurate perception of the aircraft's roll and pitch angle. If the pilot realized that he had become inverted (represented by the dotted line in Figure 49A), he would have taken corrective action to right the aircraft. Likewise, if the pilot realized he was nose-down with greater than 60° of pitch, he would have most likely taken a different course of corrective action. Based on these modeling results, we can therefore conclude that the angular rates of the mishap alone cannot account for significant disorientation of the pilot. Below, we expand our consideration beyond linear acceleration.

### F18 mishap analysis (Angular velocity + linear acceleration cues).



*Figure 50.* Orientation perception during F18 mishap (angular velocity and linear acceleration). **(A):** Estimated and actual roll angle (°). **(B):** Estimated and actual pitch angle (°). **(C):** Estimated and actual yaw angle (°).

Once we consider the G-forces acting on the body during the mishap, the OMS predicts a significant misperception of spatial orientation (Figure 50). A recreation of the pilot's actual and estimated orientation is reproduced below to help visualize the extreme disorientation predicted by the OMS (Figures 51, 52, 53). This recreation displays the mishap in 2-s increments and corresponds with the plots in Figure 50.

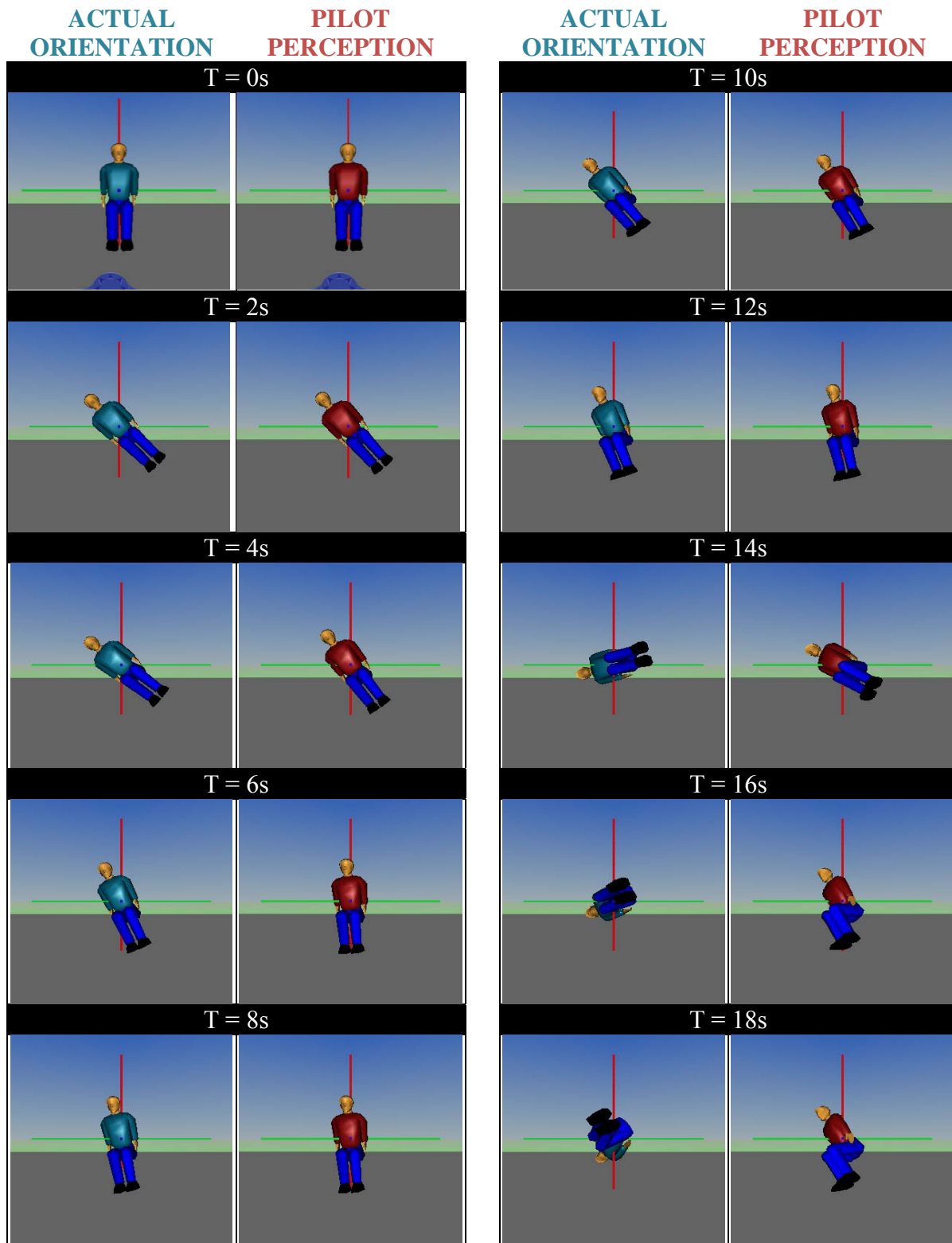


Figure 51. Actual and estimated pilot orientation during F18 mishap (Part I of III).

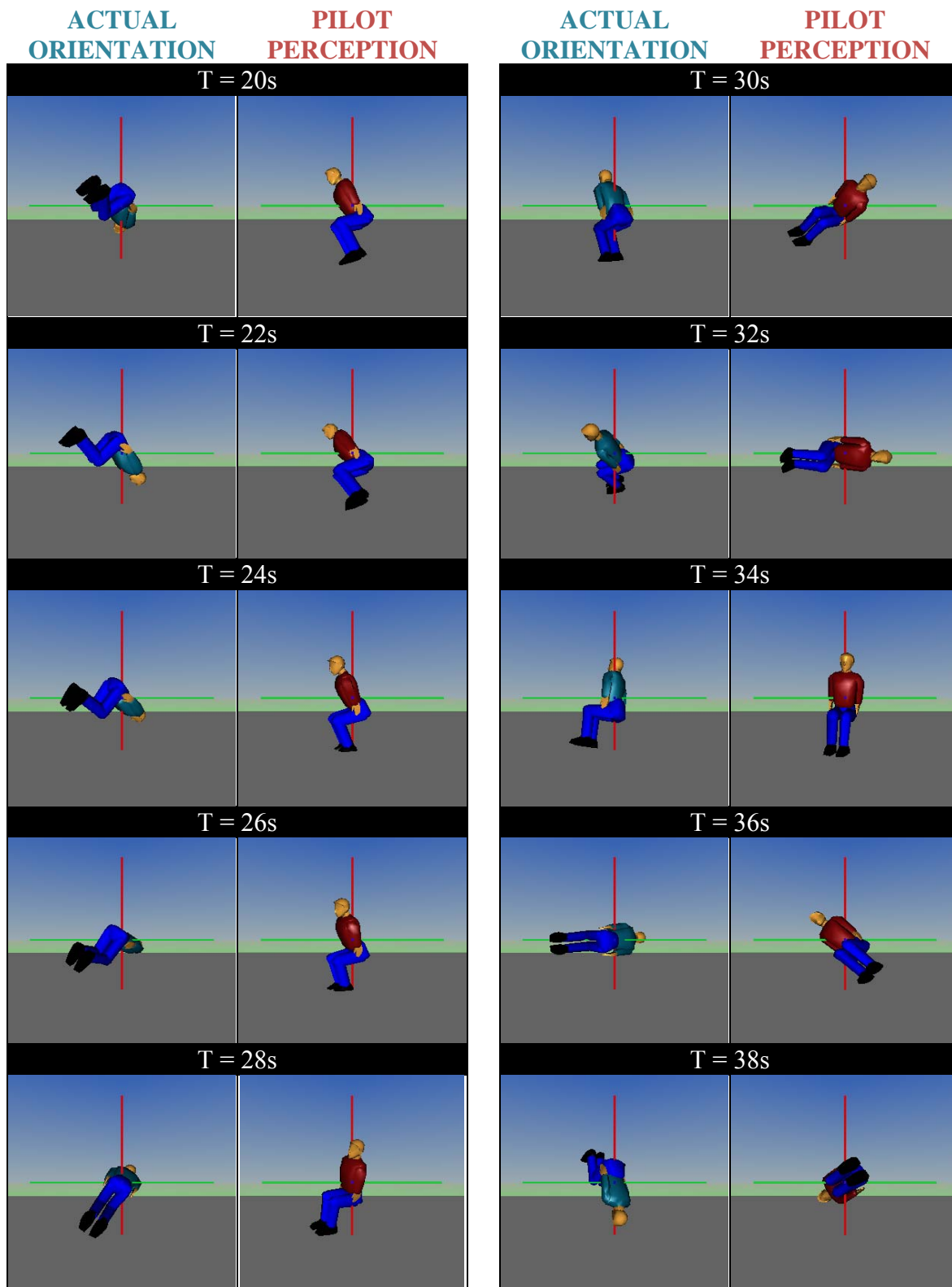


Figure 52. Actual and estimated pilot orientation during F18 mishap (Part II of III).



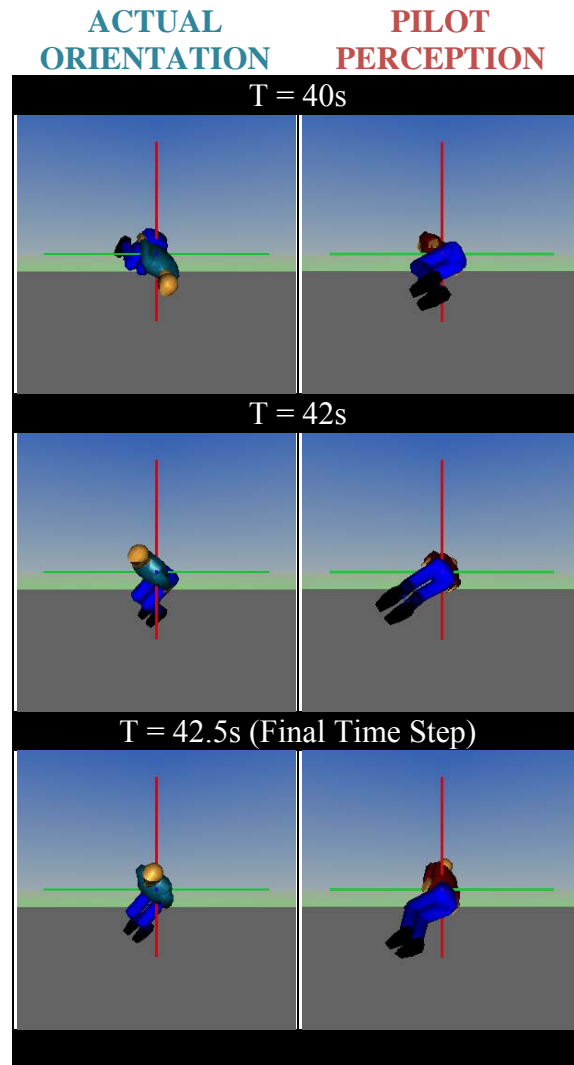


Figure 53. Actual and estimated pilot orientation during F18 mishap (Part III of III).

The model predicts that the most extreme errors in attitude perception would have occurred about the roll axis (Figure 50). The OMS predicts that from about 16 s into the simulation until 28 s have elapsed, the pilot would feel upright, even though he was actually inverted or nearly inverted (roll angle  $> 90^\circ$ ). Errors in roll, pitch, and yaw perception are plotted in Figure 54 along with the G level at each time step. Predicted roll error peaks at 24 s ( $143^\circ$  error) and immediately prior to ejection ( $225^\circ$  error) (Figure 54B). From 29 to 31 s, as the pilot “unloads” some G ( $6 \text{ Gz} \rightarrow 4 \text{ Gz}$ ), accurate roll and pitch perception begin to recover somewhat (Figures 54A, 54B, and 54C). Roll perception errors drop by almost 50%, and pitch errors drop by almost 90%. At 32 s, in an attempt to either gain attitude or stabilize the airplane, the pilot begins to pull back on the stick once again. The aircraft reaches and sustains more than 6 Gz for the remainder of the simulation. Roll and pitch perception degrade again, and roll misestimation reaches its maximum value ( $225^\circ$  error).

The OMS confirmed that pitch perception was highly compromised during the moments preceding the mishap (Figure 50B). Maximum misestimation of pitch angle coincided with the 16 → 30 s time interval where roll perception was most erroneous. During this time, true aircraft pitch angle approached 60° nose down, with an average pitch angle greater than 30°. The model predicted that pitch perception would indicate an orientation that is approximately upright, resulting in profound disorientation. Pitch error peaked at 28 s (39° pitch error).

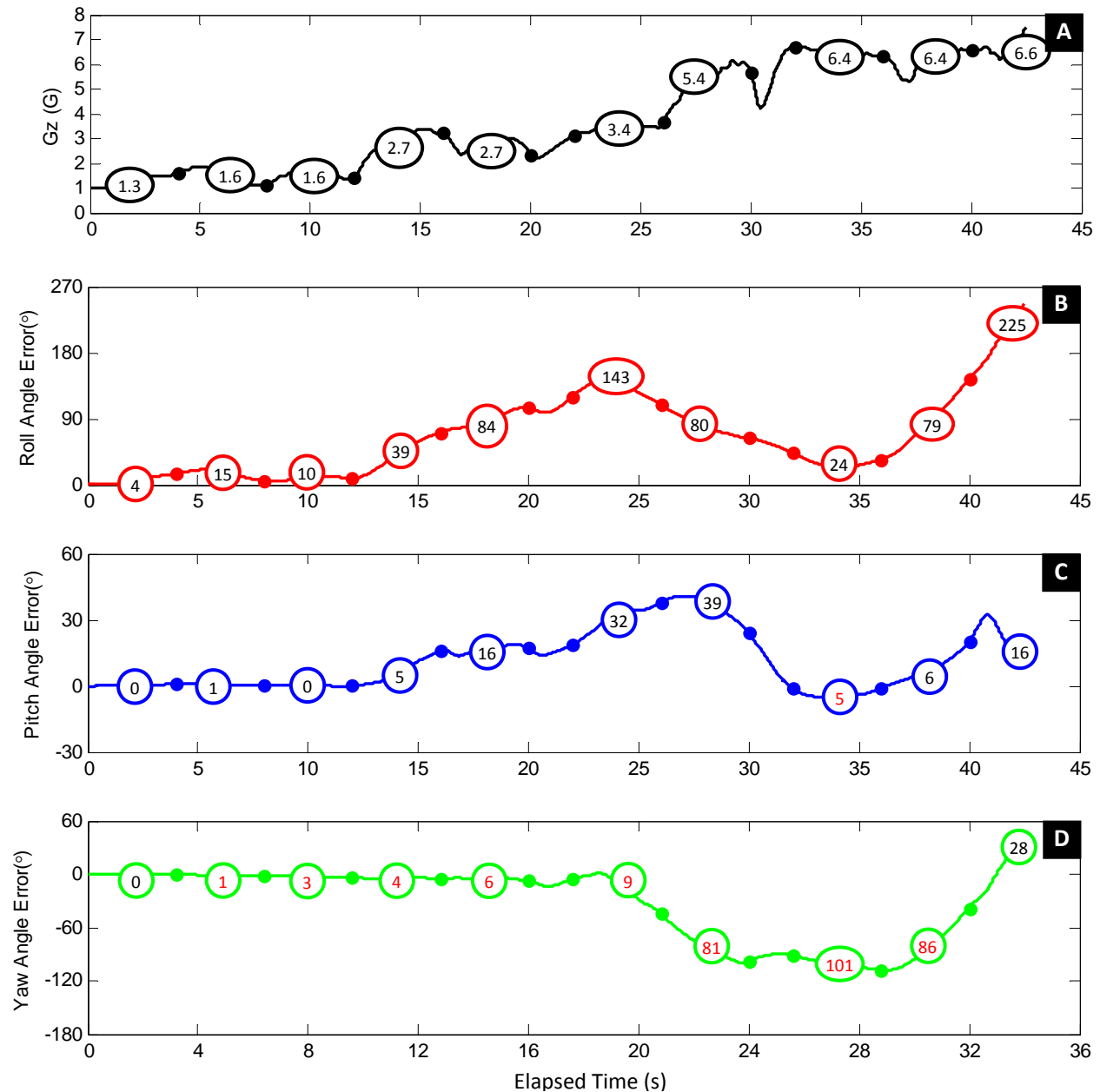


Figure 54. Errors in roll, pitch, and yaw perception. Values in **RED** are negative. (A): G loading (Gz). (B): Roll angle error (°). (C): Pitch angle error (°). (D): Yaw angle error (°).

Errors in heading, or yaw angle, do not at first appear to cause significant disorientation. However, if we step through the animated frames presented in Figures 51, 52, and 53, we notice that misestimation of yaw angle is more insidious than it first appears. When combined with roll and pitch misestimation, yaw errors serve to exacerbate perceptual errors. This is especially dangerous when the pilot is partially or fully inverted. As perception of yaw angle began to degrade from 19 to 24 s, the pilot's incorrect perception of being upright was reinforced, even though he was actually rolled greater than 100°.

Based on these model predictions, we conclude that a significant spatial disorientation event occurred from 16 to 28 s into the simulation. This corresponds to the reports of the aviators, who said they experienced SD prior to ejection. The event was likely initiated by the large roll misestimation that occurred at time  $t = 14$  s as the pilot began to pull significant Gs. The added G forces reinforced the feelings of being upright, as the aircraft began to invert. A complete loss of spatial orientation followed this inversion. At  $t = 30$  s, perception began to improve due to G unloading, however, it was likely too late to recover the aircraft.

### F18 mishap analysis (G-excess parameter adjustment).

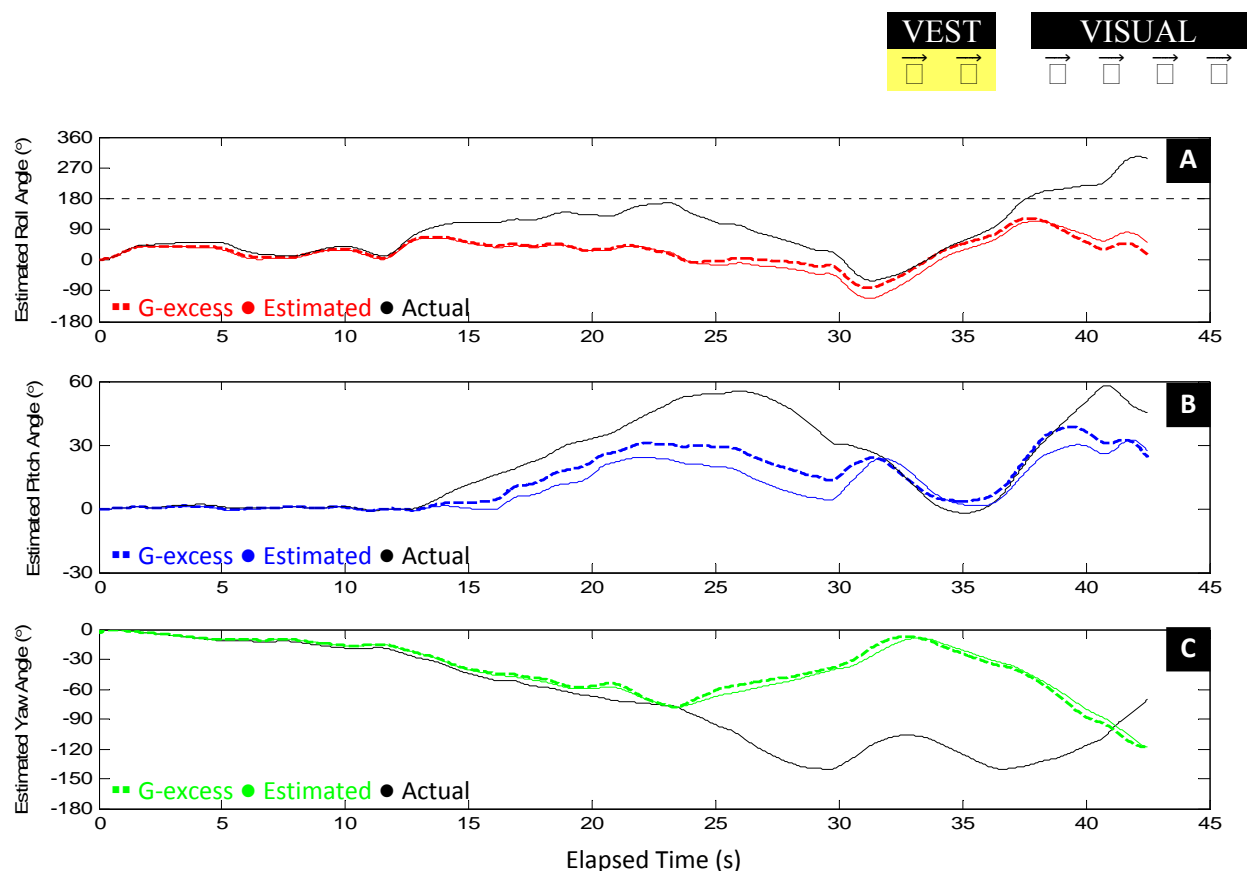


Figure 55. Comparison of orientation perception during F18 mishap with and without G-excess parameter adjustment. (A): Estimated, G-excess and actual roll angle (°). (B): Estimated, G-excess and actual pitch angle (°). (C): Estimated, G-excess and actual yaw angle (°).

For completeness, we included a simulation that uses the modified G-excess parameters (Figure 55). Since we do not have information regarding pilot head movements and head orientation, we cannot fully utilize the G-excess parameter set. Nevertheless, limited head movements would be expected during the high-G forces preceding the mishap, and results from the G-excess simulation are very much in agreement with the results presented in the previous section (“F18 mishap analysis [angular velocity cues + acceleration cues]”). The G-excess parameter set predicts a slightly reduced perception of pitch angle (Figure 55B). In this particular case, the G-excess results do not change the estimated cause or severity of the overall spatial disorientation event.

### Visualization tool.

A visualization tool was created as a companion to the NAVAIR accident recreation video (Figure 56B). This tool allows the user to visualize the angular rates, G level, and actual and predicted pilot orientation, moment-by-moment, throughout the simulation. Screen shots of the companion tool were used to generate Figures 51, 52, and 53.

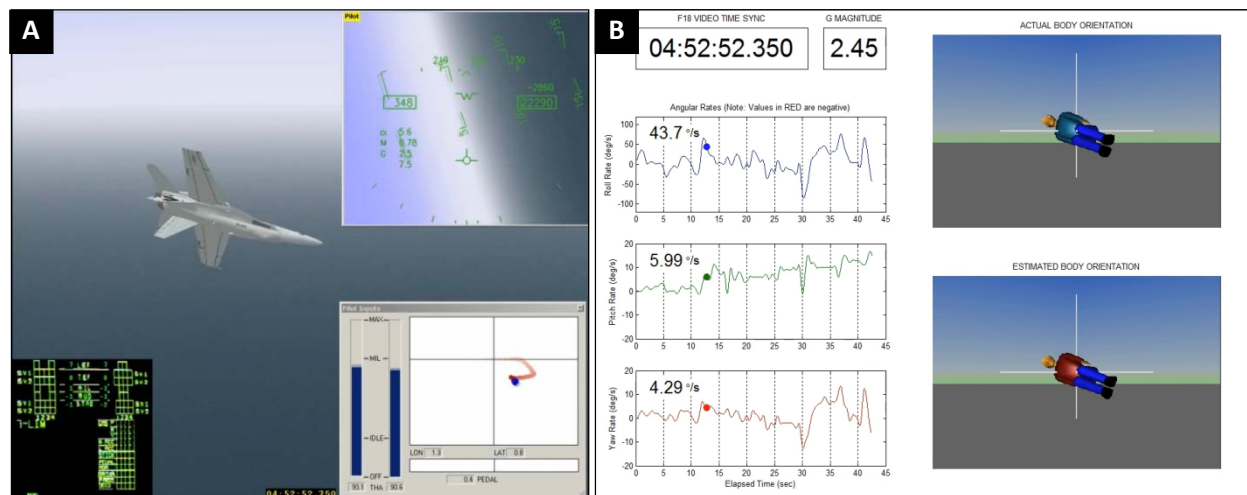


Figure 56. F18 mishap visualization tools. (A): NAVAIR re-creation. (B): Companion perception modeling visualization tool.

### Further considerations.

Simulation results could be improved in the future by incorporating real-time eye and head tracking recordings of pilot motion during the mishap. These variables would allow the model to better estimate the importance of G-excess and cross-coupled effects and better determine visual cues derived from the aircraft instrument panel. For example, if we knew that the pilot looked at the attitude indicator at time  $t = 34$  seconds, we could model both the head movement required to accomplish that action, and input a visual cue to the model that represents an improved awareness of overall orientation.

## Conclusions

A spatial OMS and perception analysis toolbox (Perception Toolbox) were developed and refined to aid in the processing, simulation, and visualization of human perception in response to three-dimensional, complex, multisensory motion stimuli. The OMS was capable of reproducing human perceptual response to more than a dozen classic laboratory sensory paradigms, and it successfully predicted several common spatial disorientation illusions (viz., Coriolis cross-coupling, post-turn, somatogravic, and G-excess).

The Perception Toolbox successfully integrated novel visualization techniques with specialized tools for modeling high-G perceptual environments. The OMS and six other classic perception models were programmed into the Perception Toolbox to facilitate comparison with previous research and modeling results.

The OMS and Perception Toolbox were used to perform a case study of an F18 mishap. Model results imply that profound SD was present throughout the final 42.5 s of flight. The case study highlights the strength, functionality, and crucial integration of the OMS and the Perception Toolbox. Together, these modeling tools elucidated the time course of SD during the mishap, the sensory cues that played a pivotal role in producing the SD, and the likely role of G-excess effects. The modeling tools also helped to visually represent the disorientation as it unfolded in real time.

The Perception Toolbox and the OMS were also designed to accommodate additional sensory information that is not presently available from the cockpit recorder. In the future, head, eye, and gaze tracking data could be directly integrated into the model without model modification and used to further improve simulation accuracy, once they become available.

The model potentially has wide applications for aviation mishap modeling and simulation. For example, the human inability to accurately detect and estimate certain kinds of vertical motion is relevant for vertical take-off-and landing. Since the model concerns human orientation perception rather than flight control per se, the model also has the potential to positively impact other aspects of orientation perception, e.g., by modeling of human perception of standing balance and equilibrium in the terrestrial setting or following the sort of G transitions astronauts face.

The applications of the OMS described in this paper are being expanded upon and elucidated by our other work. For example, Newman, Lawson, McGrath, & Rupert (2014) elaborated upon the need for the addition of gaze prediction capabilities to the model, which can be achieved through the use of eye tracking technology. The incorporation of gaze tracking into the model would make it possible to improve inferences concerning the visual focus of attention of the pilot during the onset of SD (Newman, Lawson, Rupert, & McGrath, 2014). McGrath et al. (2015) discussed advanced SD training applications that would be feasible through the use of a simulator that takes into account the pilot's perceived attitude and location of the ground, to teach pilots SD detection and recovery techniques. In addition to the reports above, Lawson et al. (2015) and McGrath et al. (2015) describe the model's ability to analyze post-hoc flight mishaps to determine causation, which may contribute to the development of a potential future in-flight

spatial disorientation detection capability. Finally, the description of the OMS in this report is supplemented by the description of the interface and instructional user-guide presented in Newman, Lawson, Rupert, Thompson, and McGrath (2014).

Increased understanding of the situations that induce spatial disorientation and contribute to mishaps should tremendously decrease the number of spatial disorientation mishaps in the future. The model described in this paper was initially developed by Newman (2009) as a Master's Thesis at the Massachusetts Institute of Technology, then revitalized and expanded under a USAARL In-House Independent Laboratory Research Effort to the state that it is reported here and elsewhere (Newman, Lawson, Rupert, Thompson, & McGrath, 2014). The model is currently undergoing many further improvements in preparation for transition via triservice (Defense Health Program) research and Small Business Innovation Research (SBIR). Subsequent reports will detail further model improvements.

## **Recommendations**

While our model has expanded the perceptual phenomenon that can be predicted, a number of future model refinements are recommended, some of which are underway:

- Improved head movement model: The current head movement model included in the OMS simplifies the coordinate transformation between the reference frame of the input stimuli and the head. A more complex model based on true head-neck kinematics should be developed to improve simulation results and accuracy.
- Integration of canal and otolith thresholds: The OMS needs to model the mechanical thresholds of the semicircular canal or otolith organs. Integration of thresholds would improve simulation of SD illusions such as the leans.
- Improved visual sensor models: The OMS does not dissociate between focal and ambient visual function. An improved, physiologically-validated vision model would improve vection simulation results and provide more realistic processing of visual sensory information. For example, the model should simulate the fact that vection onset is not always immediate, and that a subject cannot always estimate a rotating or translating visual velocity cue accurately. Visual model refinements will improve the performance of the model.

Additional research is recommended to improve the model:

- G-excess: Further experimentation would be beneficial to validate the G-excess parameter modification discussed in the section "G-Excess illusion." For example, further data is desired concerning the time course and dynamics of the illusion under different G environments. Such work is already underway as a result of the SBIR effort mentioned above (see Conclusions section). Some of these results will be published soon.
- Coriolis cross-coupling: Further data on the time course, magnitude, direction and duration of the Coriolis cross-coupling illusion would help to validate several of the predictions presented in this report.
- Vertical Motion Perception: In order to validate the limbic coordinate frame velocity and displacement integrator aspects of the model, a large amplitude vertical vs. horizontal motion experiment is recommended. The experiment should test vertical motion with the human body z-axis aligned with and perpendicular to the gravity axis, measuring perceived

displacement amplitude and phase. An identical experiment could be performed for horizontal motion with the body z-axis aligned with and perpendicular to the direction of displacement.

This section is intentionally blank.

This page is intentionally blank.



## References

- Allison, R. S., Howard, I. P., & Zacher, J. E. (1999). Effect of field size, head motion, and rotational velocity on roll vection and illusory self-tilt in a tumbling room. *Perception*, 28, 299-306.
- Aoki, H., Ohno, R., & Yamaguchi, T. (2003). A study of spatial orientation in a virtual weightless environment: Part 2 Causes of spatial cognition errors. *Journal of Architecture, Planning, and Environmental Engineering*, 563, 85-92.
- Aoki, H., Ohno, R., & Yamaguchi, T. (2005). The effect of the configuration and the interior design of a virtual weightless space station on human spatial orientation. *Acta Astronautica*, 56, 1005-1016.
- Benson, A. J. (1966a). Modification of the pre- and post-rotational responses by the concomitant linear acceleration. *Proceedings of the 2nd Symposium on the Role of the Vestibular Organs in Space Exploration*. Washington, DC: US Government Printing Office, 199–213.
- Benson, A. J. (1966b). Post-rotational sensation and nystagmus as indicants of semicircular canal function. *Proceedings of the 3rd Symposium on the Role of the Vestibular Organs in Space Exploration*, Washington, DC: US Government Printing Office, 421–432.
- Benson, A. J., Bodin, C. B., & Bodin, M. A. (1966). Comparison of the effect of the direction of the gravitational acceleration on post-rotational responses in yaw, pitch, and roll. *Aerospace Medicine*, 37(9), 889-897.
- Best, P. J., White, A. M., & Minai, A. (2001). Spatial processing in the brain: The activity of hippocampal place cells. *Annual Review of Neuroscience*, 24, 459-86.
- Bilien, V. (1993). *Modeling human spatial orientation perception in a centrifuge using estimation theory*. (S. M. Thesis). Massachusetts Institute of Technology: Cambridge, Massachusetts.
- Borah, J., Young, L. R., & Curry, R. E. (1978). *Sensory mechanism modeling* (Final Report AFHRL-TR-78-83). Brooks Air Force Base, Texas: Air Force Human Resources Laboratory, Air Force Systems Command.
- Borah, J., Young, L. R., & Curry, R. E. (1988). Optimal estimator model for human spatial orientation. *The Annals of the New York Academy of Sciences*, 545, 51-73.
- Calton, J. L., & Taube, J. S. (2005). Degradation of head direction cell activity during inverted locomotion. *Journal of Neuroscience*, 25(9), 2420-2428.

- Chelette, T. L., Martin, E. J., & Albery, W. B. (1995). The effect of head tilt on perception of self-orientation while in a greater than one G environment. *Journal of Vestibular Research*, 5(1), 1-17.
- Chu, W. (1976). *Dynamic response of human linearvection*. (S.M. Thesis). Massachusetts Institute of Technology: Cambridge, Massachusetts.
- Clark, B., & Graybiel, A. (1963). Contributing factors in the perception of the oculogravic illusion. *American Journal of Psychology*, 76, 18-27.
- Clark, B., & Graybiel, A. (1966). Factors contributing to the delay in the perception of the oculogravic illusion. *American Journal of Psychology*, 79, 377-388.
- Clark, T.K. (2013). *Human Perception and Control of Vehicle Roll Tilt in Hyper-Gravity*. (Ph.D. Thesis), Man-Vehicle Laboratory, Cambridge, Massachusetts: Massachusetts Institute of Technology.
- Cohen, B., Henn, V., Raphan, T., & Dennett, D. (1981). Velocity storage, nystagmus and visual-vestibular interactions in humans. *Annals of the New York Academy of Sciences*, 374, 421-33.
- Cohen, M. M., Crosby, R. H., & Blackburn, L. H. (1973). Disorienting effects of aircraft catapult launchings. *Aerospace Medicine*, 44, 37-39.
- Correia, M. J., Hixson, W. C., & Niven, J. I. (1968). On predictive equations for subjective judgments of vertical and horizon in a force field. *Acta Otolaryngologica, Suppl*, 230, 1-20.
- Cowings, P. S., Toscano, W. B., DeRoshia, C. & Tauson, R. A. (2001). Effects of the command and control vehicle (C2V) operational environment on soldier health and performance, *Human Performance in Extreme Environments*, 5(2), 66-91.
- Fang, A. C., & Zimmerman, B. G. (1969). *Digital simulation of rotational kinematics* (Final Report NASA TN D-5302). Washington D.C: Goddard Space Flight Center, 1-27.
- Fernandez C., & Goldberg, J. M. (1976). Physiology of peripheral neurons innervating otolith organs of the squirrel monkey. I. Response to static tilts and to long-duration centrifugal force. *Journal of Neurophysiology*, 39(5), 970-984.
- Fernandez C., & Goldberg, J. M. (1976). Physiology of peripheral neurons innervating otolith organs of the squirrel monkey. II. Directional selectivity and force-response relations. *Journal of Neurophysiology*, 39(5), 985-995.
- Fernandez C., & Goldberg, J. M. (1976). Physiology of peripheral neurons innervating otolith organs of the squirrel monkey. III. Response dynamics. *Journal of Neurophysiology*, 39(5), 996-1008.

- Fernandez, C., & Goldberg, J. M. (1971). Physiology of peripheral neurons innervating semicircular canals of the squirrel monkey. II. Response to sinusoidal stimulations and dynamics of peripheral vestibular system. *Journal of Neurophysiology*, 34(4), 661-675.
- Gibb, R., Ercoline, B., & Scharff, L. (2011). Spatial Disorientation: Decades of Pilot Fatalities. *Aviation, Space and Environmental Medicine*, 82(7), 717-724.
- Gilson, R. D., Guedry, F. E., Hixson, W. C., & Niven, J. I. (1973). Observations on perceived changes in aircraft attitude attending head movements made in a 2-g bank and turn. *Aerospace Medicine*, 44(1), 90-91.
- Goldberg, J., & Fernandez, C. (1971). Physiology of peripheral neurons innervating the semicircular canals of the squirrel monkey. I. Resting discharge and response to constant angular accelerations. *Journal of Neurophysiology*, 34(4), 635-660.
- Graybiel, A. (1966). *Orientation in aerospace flights* (Special Report 66-6, NASA order R-93). Pensacola, FL: Naval Aerospace Medical Institute, NASA.
- Graybiel, A., & Brown, R. (1951). The delay in visual reorientation following exposure to a change in direction of resultant force on a human centrifuge. *Journal of General Psychology*, 45, 143-150.
- Graybiel, A., & Knepton, J. (1976). Sopite syndrome: A sometimes sole manifestation of motion sickness. *Aviation, Space and Environmental Medicine*, 47(8), 873-82.
- Groen, E. L., Smaili, M. H., & Hosman, R. J. A. W. (2007). Perception model analysis of flight simulator motion for a decrab maneuver. *Journal of Aircraft*, 44(2), 427-435.
- Guedry, F.E., & Rupert, A. H. (1991). Steady-state and transient G-excess effects. *Aviation Space and Environmental Medicine*, 62(3), 252-253.
- Guedry, F. E., & Benson, A. J. (1978). Coriolis cross-coupling effects: Disorienting and nauseogenic or not?. *Aviation, Space and Environmental Medicine*, 49(1), 29-35.
- Guedry, F. E., & Harris, C. S. (1963). *Labyrinthine function related to experiments on the parallel swing* (Bureau of Medicine and Surgery Project MR005.13-6001, NASA Joint Report No. 86) Pensacola, FL: Naval School of Aviation Medicine.
- Guedry, F. E., & Oman, C. M. (1990). *Vestibular Stimulation During a Simple Centrifuge Run* (Report No. ADA227285). Pensacola, FL: Naval Aerospace Medical Research Lab.
- Haslwanter, T., Curthoys I. S., Black, R. A., Topple, A. N., & Halmagyi, G. M. (1996). The three-dimensional human vestibulo-ocular reflex: Response to long duration yaw angular accelerations. *Experimental Brain Research*, 109(2), 303-311.

- Haslwanter, T., Jaeger, R., Mayr, S., & Fetter, M. (2000). Three-dimensional eye-movement responses to off-vertical axis rotations in humans. *Experimental Brain Research*, 134(1), 96-106.
- Hafting, T., Fyhn, M., Molden, S., Moser, M. B., & Moser, E. I. (2005). Microstructure of a spatial map in the entorhinal cortex. *Nature*, 436(7052), 801-806.
- Israël, I., Grasso, R., Georges-François, P., Tsuzuku, T., & Berthoz, A. (1989). Spatial memory and path integration studied by self-driven passive linear displacement. I. Basic properties. *Journal of Neurophysiology*, 77(6), 3180-3192.
- Jell, R. M., Ireland, D. J., & Lafortune, S. (1984). Human optokinetic after-nystagmus. Slow-phase characteristics and analysis of the decay of slow phase velocity. *Acta Otolaryngologica*, 98(5-6), 462-471.
- Jones, G. M., & Young, L. R. (1978). Subjective detection of vertical acceleration: A velocity dependent response?. *Acta Otolaryngologica*, 85(1-2), 45-53.
- Knierim, J. J., McNaughton, B. L., and Poe, G. R. (2000). Three –dimensional spatial selectivity of hippocampal neurons during space flight. *Nature Neuroscience*, 3, 209-210.
- Knierim, J. J., Poe, G. R., & McNaughton, B. L. (2003). Ensemble neural coding of place in zero-g. In J.C. Buckey, Jr., and J.L. Homick, (Eds.), *The Neurolab Spacelab Mission: Neuroscience Research in Space: Results from the STS-90 Neurolab Spacelab Mission* (pp.63-68). NASA SP-2003-535.
- Kynor, D. B. (2002). *Disorientation Analysis and Prediction System*. (Final Report AFRL-HE-WP-TR-2002-0179). Wright-Patterson Air Force Base, Ohio: United States Air Force Research Laboratory.
- Lafortune, S., Ireland, D., Jell, R., & DuVal, L. (1986). Human optokinetic after-nystagmus. Stimulus velocity dependence on the two-component decay model and involvement in pursuit. *Acta Otolaryngologica*, 101(3-4), 183-192.
- Lathan, C. E., & Clement, G. (1997). Response of the neurovestibular system to spaceflight. In S. Churchill (Ed.), *Fundamentals of Space Life Sciences* (Volume 1) (pp. 65-82). Malabar, FL: Krieger Publishing Co.
- Lawson, B. D., Guedry, F. E., Rupert, A. R., & Anderson, A. M. (1994). Attenuating the disorienting effects of head movement during whole-body rotation using a visual reference: Further tests of a predictive hypothesis. In *Advisory Group for Aerospace Research and Development: Virtual Interfaces: Research and Applications* (pp. 15-1 to 15-14). Neuilly- Sur Seine, France: AGARD.
- Lawson B. D. (2005). “Exploiting the illusion of self-motion (vection) to achieve a feeling of ‘virtual acceleration’ in an immersive display,” in Stephanidis C. (Ed.), *Proceedings of*

- the 11th International Conference on Human-Computer Interaction*, (Las Vegas, NV), 1-10.
- Lawson, B. D., & Mead, A. M. (1998). The sopite syndrome revisited: drowsiness and mood changes during real or apparent motion. *Acta Astronautica*, 43(3-6), 181-192.
- Lawson, B.D., McGrath, B.J., Newman, M.C., & Rupert, A.H. (2015). Requirements for developing the model of spatial orientation into an applied cockpit warning system. *Proceedings of the 18<sup>th</sup> International Symposium on Aviation Psychology, Dayton, OH, 4-7 May. Symposium: Technical Countermeasures for Spatial Disorientation*, 22-30.
- Lawson, B. D., Rupert, A. H., Guedry, F. E., Grissett, J. D., & Mead, A. M. (1997). The human-machine interface challenges of using virtual environment (VE) displays aboard centrifuge devices. In M. J. Smith, G. Salvendy, & R. J. Koubek (Eds.), *Design of computing systems: Social and Ergonomic Considerations*, Vol. 2, (pp. 945-948). New York, NY: Elsevier.
- Lawson, B. D., Smith S. A., Kass, S. J., Kennedy R. S., & Muth, E. R. (2003). Vestibular stimuli may degrade situation awareness even when spatial disorientation is not experienced. *Spatial Disorientation in Military Vehicles: Causes, Consequences and Cures*, RTO-MP-086, ADP013883, 43-1 to 43-21.
- Loomis, J. M., Klatzky, R. L., Golledge, R. G., Cicinelli, J. G., Pellegrino, J. W., & Fry, P. A. (1993). Non-visual navigation by blind and sighted: Assessment of path integration ability. *Journal of Experimental Psychology*, 122(1), 73-91.
- Luenburger, D. G. (1971). An introduction to observers. *IEEE Transactions on Automatic Control*, 16(6), 596-602.
- Malcolm, R., & Jones, G. M. (1973). Erroneous perception of vertical motion by humans seated in the upright position. *Acta Otolaryngologica*, 77(4), 274-283.
- Magnus, R. (1926). Some results of studies in the physiology of posture. *The Lancet*, 531-536.
- Mast, F. W., Berthoz, A., & Kosslyn, S. M. (2001). Mental imagery of visual motion modifies the perception of roll-vection stimulation. *Perception*, 30(8), 945-957.
- Mayne, R. (1974). A systems concept of the vestibular organs. In H. Kornhuber (Ed.) *Handbook of Sensory Physiology, The vestibular system. Psychophysics, Applied Aspects and General Interpretations. Part 2*, 493-580. Berlin-Heidelberg: Springer Berlin Heidelberg.
- McGrath, B.J., Newman, M.C., Lawson, B.D., & Rupert, A.H. (2015) An algorithm to improve ground-based spatial disorientation training. *Proceedings of the American Institute of Aeronautics and Astronautics*, 7 Jan., Virginia Beach, 9 Pages.

- McGrath, B. J., Oman, C. M., Guedry, F. E., & Rupert, A. H. (1993). *Human vestibulo-ocular response during 3 Gz centrifuge stimulation* (Report No. NAMRL-1388). Pensacola Florida: Naval Aerospace Medical Research Laboratory.
- McGrath, B. J., Rupert, A. H., & Guedry, F. E. (2003). Analysis of spatial disorientation mishaps in the US Navy. In *Spatial Disorientation in Military Vehicles: Causes, Consequences and Cures: Proceedings from the RTO Human Factors and Medicine Panel (HFM) Symposium* (pp.10-1 to 10-12). La Coruna, Spain.
- Merfeld, D. M., Young, L. R., Oman, C. M., & Shelhamer, M. J. (1993). A multidimensional model of the effects of gravity on the spatial orientation of the monkey. *Journal of Neurophysiology*, 3(2), 141-161.
- Merfeld, D. M., Zupan, L., & Peterka, R. (1999). Humans use internal models to estimate gravity and linear acceleration. *Nature*, 398, 615–618.
- Merfeld, D. M., & Zupan, L. H. (2002). Neural processing of gravito-inertial cues in humans. III Modeling tilt and translation response. *Journal of Neurophysiology*, 87(2), 819-833.
- Merfeld, D. M., Zupan, L. H., & Gifford, C. A. (2001). Neural processing of gravito-inertial cues in humans. II. Influence of the semicircular canals during eccentric rotation. *Journal of Neurophysiology*, 85(4), 1648–1660.
- Merryman, R.F.K. & Caciopo, B.S. (1997). The opto-kinetic cervico reflex in pilots of high performance aircraft. *Aviation, Space, and Environmental Medicine*, 68, 479-487.
- Miller, E. F., & Graybiel A. (1971). Effect of gravito-inertial force on ocular counter-rolling. *Journal of Applied Physiology*, 31(5), 697-700.
- Mittelstaedt, M. L., & Glasauer, S. (1991). Idiothetic navigation in gerbils and humans. *Zoologische Jahrbucher Abteilung fur Allgemeine Zoologie und Physiologie der Tiere*, 95, 427–435.
- Mittelstaedt, M. L., & Mittelstaedt, H. (2001). Idiothetic navigation in humans: Estimation of path length. *Experimental Brain Research*, 139(3), 318–332.
- Newman, M. C. (2009). *A Multisensory Observer Model for Human Spatial Orientation Perception*. (S. M. Thesis). Massachusetts Institute of Technology: Cambridge, Massachusetts.
- Newman, M.C., Lawson, B.D., McGrath, B.J., & Rupert, A.H. (2014) Perceptual modeling as a tool to prevent aircraft upset associated with spatial disorientation. *Proceedings of the AIAA Guidance, Navigation, and Control Conference*, 13 Jan, National Harbor, MD.
- Newman, M.C., Lawson, B.D., Rupert, A.H., & McGrath, B.J. (2012). The role of perceptual modeling in the understanding of spatial disorientation during flight and ground-based

- simulator training. Proceedings of the American Institute of Aeronautics and Astronautics, 15 Aug., Minneapolis, MN, 14 pages.
- Newman, M.C., Lawson, B.D., Rupert, A.H., Thompson, L.B., & McGrath, B.J. (2014). *The orientation modeling system (OMS): Description of the user interface* (Report No. 2014-09). Fort Rucker, AL: U.S. Army Aeromedical Research Laboratory.
- Oman, C. M. (2007). Spatial processing in navigation, imagery and perception. In F. Mast & L. Jancke (Eds.), *Spatial Orientation and Navigation in Microgravity* (pp. 209-247), New York: Springer.
- Pommellet, P. E. (1990). *Suboptimal estimator for the spatial orientation of a pilot*. (S. M. Thesis). Massachusetts Institute of Technology: Cambridge, Massachusetts.
- Raphan, Th., Matsuo, V., & Cohen, B. (1977). A velocity storage mechanism responsible for optokinetic nystagmus (OKN), optokinetic after-nystagmus (OKAN) and vestibular nystagmus. In R. Baker & A. Berthoz (Eds.), *Control of gaze by brain stem neurons* (pp. 37-47). Amsterdam: Elsevier/North-Holland Biomedical Press.
- Raphan, Th., Matsuo, V., & Cohen, B. (1979). Velocity storage in the vestibulo-ocular reflex arc (VOR). *Experimental Brain Research*, 35(2), 229-248.
- Robinson, D. A. (1977). Vestibular and optokinetic symbiosis: An example of explaining by modeling. In R. Baker & A. Berthoz (Eds.), *Control of Gaze by Brain Stem Neurons* (pp. 49-58). Amsterdam: Elsevier/North-Holland Biomedical Press.
- Schöne, H. (1964). On the Role of Gravity in Human Spatial Orientation. *Aerospace Medicine*, 35, 764-772.
- Seidman, S. H. (2008). Translational motion perception and vestibulo-ocular responses in the absence of non-inertial cues. *Experimental Brain Research*, 184(1), 13-29.
- Selva, P. (2009). *Modeling of the vestibular system and nonlinear models for human spatial orientation perception*. Universite de Toulouse, Toulouse.
- Singer, G., Purcell, A.T., & Austin, M. (1970). The effect of structure and degree of tilt on the tilted room illusion. *Attention, Perception, & Psychophysics*, 7(4), 250-252.
- Small, R. L., Keller, J. W., Wickens, C. D., Socash, C. M., Ronan, A. M., & Fisher, A. M. (2006). *Multisensory integration for pilot spatial orientation* (Report No. A253074). Boulder, Colorado: Micro Analysis and Design.
- Small, R. L., Oman, C. M., Wickens, C. D., Keller, J. W., Curtis, B., Jones, T. D., & Brehon, M. (2011). *Modeling and mitigating spatial disorientation in low-G environments* (Final Report NSBRI Project SA-01302). Houston, TX: National Space Biomedical Research Institute.

- Tokumaru, O., Kaida, K., Ashida, H., Mizumoto, & C., Tatsuno, J. (1998). Visual influence on the magnitude of somatogravic illusion evoked on advanced spatial disorientation demonstrator. *Aviation, Space, and Environmental Medicine*, 69(2), 111-116.
- Vidal, M., Amorim, M.A., & Berthoz, A. (2004). Navigating in a virtual three dimensional maze: How do egocentric and allocentric reference frames interact? *Cognitive Brain Research*, 19(3), 244-258.
- Vidal, M., Lipshits, M., McIntyre, J., & Berthoz, A. (2003). Gravity and spatial orientation in virtual 3D-mazes. *Journal of Vestibular Research*, 13(4-6), 273-286.
- Vingerhoets, R. A. A., Van Ginsbergen, J. A. M., & Medendorp, W. P. (2007). Verticality perception during off vertical axis rotation. *Journal of Neurophysiology*, 97(5), 3256-3268.
- Waespe, W., & Henn, V. (1977). Neuronal activity in the vestibular nuclei of the alert monkey during vestibular and optokinetic stimulation. *Experimental Brain Research*, 27(5), 523-538.
- Walsh, E. G. (1964). The perception of rhythmically repeated linear motion in the vertical plane. *Experimental Physiology*, 49, 58-65.
- Young, L. R. (2003). Chapter 3: Spatial Orientation. In P. Tsang & M. Vidulich (Eds.), *Principles and Practice of Aviation Psychology* (pp. 69-114). Mahwah, NJ: Lawrence Erlbaum Associates.
- Young, L.R., Shelhammer, M., & Modestino, S. (1986). M.I.T./Canadian vestibular experiments on the Spacelab-1 mission: 2. Visual vestibular tilt interaction in weightlessness. *Experimental Brain Research*, 64, 299-307.
- Zupan, L., Peterka, R., & Merfeld, D. M. (2000). Neural processing of gravito-inertial cues in humans. I. Influence of the semicircular canals following post-rotatory tilt. *Journal of Neurophysiology*, 84(4), 2001-2015.



This page is intentionally blank.

## Appendix A. Spatial Rotations

### A.1 Coordinate Systems

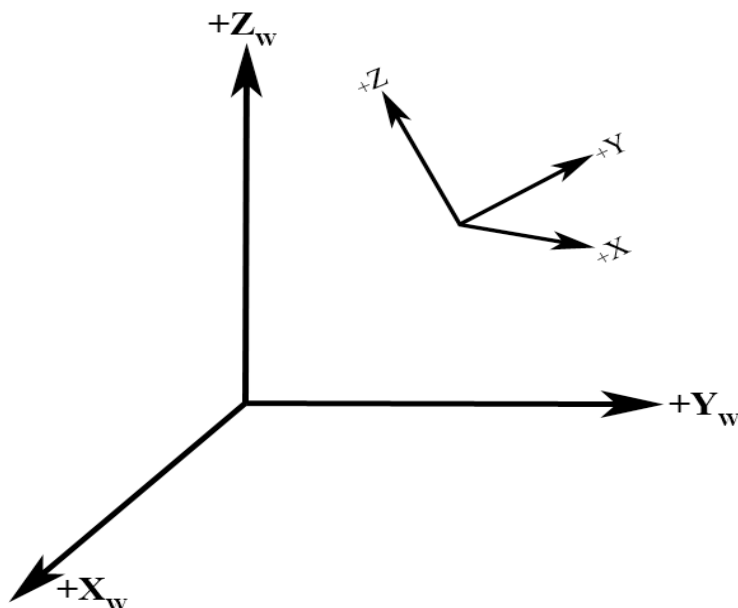


Figure A1 Head and World coordinate frames.

We define a right handed coordinate system relative to the world ( $X_w$ ,  $Y_w$ ,  $Z_w$ ) and the head ( $X$ ,  $Y$ ,  $Z$ ) (Figure A1). It is assumed that the semicircular canals and otoliths are situated at the center of the head and align with the naso-occipital  $X$ , interaural  $Y$ , and dorsoventral  $Z$ , axes. For computational simplicity, angular velocity and linear acceleration inputs to the vestibular model are processed in the egocentric head-fixed frame. It is often necessary to transform quantities between reference frames. Gravity, for instance, is inherently defined in world coordinates yet needed for the GIF (gravito-inertial force) calculation performed in the head axes. As we rotate and translate about in space, a novel description of the relationship between these coordinate frames is therefore required.

### A.2 Quaternion Representation

The quaternion provides us with a useful notation for representing spatial rotations. Quaternions eliminate gimbal lock, reduce numerical storage from nine to four digits (nine being the typical representation of a rotation matrix), and increase computational stability. A quaternion representation for our model's coordinate frames and vector rotations is therefore preferred. We can define a unit quaternion in the following form:

$$\vec{q} = q_0 + q_1 i + q_2 j + q_3 k$$

$$\text{with } i^2 = j^2 = k^2 = -1$$

In order to update the quaternion vector as we rotate in inertial space the initial quaternion  $\vec{q}_0$ <sup>1</sup> must be integrated with respect to the angular velocity input,  $\vec{\omega}(t) = [\omega_x(t), \omega_y(t), \omega_z(t)]^T$ . A stable algorithm to perform this integration was developed by Fang & Zimmerman (1969).

$$\dot{q}_0 = -\frac{1}{2}(q_2\omega_x + q_1\omega_y + q_3\omega_z) + k\lambda q_0 \quad (1)$$

$$\dot{q}_1 = -\frac{1}{2}(q_1\omega_x - q_0\omega_y - q_2\omega_z) + k\lambda q_1 \quad (2)$$

$$\dot{q}_2 = \frac{1}{2}(q_0\omega_x + q_3\omega_y - q_1\omega_z) + k\lambda q_2 \quad (3)$$

$$\dot{q}_3 = \frac{1}{2}(q_1\omega_x - q_2\omega_y + q_0\omega_z) + k\lambda q_3 \quad (4)$$

$$\lambda = 1 - (q_0^2 + q_1^2 + q_2^2 + q_3^2) \quad (5)$$

Integrating Equations 1 – 5 yields a complete time history for the quaternion vector  $\vec{q}$ . This particular formulization uses an algebraic constraint to minimize the constraint error. For alternate integration schemes using normalization or derivative constraints, refer to Fang & Zimmerman (1969). Constraint errors represent a non-orthonormality in the transformation matrix and are thus extremely problematic for the decomposition of vectors. The proportionality constant “ $k$ ” ensures stability such that  $k > 0$  and the product  $hk \leq 1$ , where  $h$  is defined as the integration time step. A value of  $k = 0.8 - 0.9$  worked best for our input file sample rates and Simulink ODE45 differential equation solver.

The integrated quaternion now provides us with all the necessary information to transform vectors between the head and world coordinate frames. At each time step a rotation of the gravity vector  $\vec{g}_W = [g_{xw}, g_{yw}, g_{zw}]^T$  is accomplished with the transformation matrix  $\mathbf{T}$ ;

---

<sup>1</sup> The initial quaternion is calculated based on the initial gravitational state. Assuming the subject is oriented upright, inline with the gravitational vertical, and in a 1G environment  $\vec{g}_W = [0, 0, -1]^T$  and  $\vec{q}_0 = [1, 0, 0, 0]^T$ .

$$T = \begin{bmatrix} q_0^2 + q_1^2 - q_2^2 - q_3^2 & 2(q_1q_2 + q_0q_3) & 2(q_1q_3 - q_0q_2) \\ 2(q_1q_2 - q_0q_3) & q_0^2 - q_1^2 + q_2^2 - q_3^2 & 2(q_0q_1 + q_2q_3) \\ 2(q_0q_2 + q_1q_3) & 2(q_2q_3 - q_0q_1) & q_0^2 - q_1^2 - q_2^2 + q_3^2 \end{bmatrix}$$

such that the current direction of gravity in head coordinates can be expressed as the premultiplication of  $\vec{g}_w$  with  $\mathbf{T}$ .

$$\vec{g}(t) = T(\vec{q}) \cdot \vec{g}_w \quad (6)$$

Likewise, we can integrate Equations 1 – 5 with respect to the internal estimate of angular velocity,  $\hat{\vec{\omega}}$ , and obtain a similar representation for the estimated gravity state.

$$\hat{\vec{g}}(t) = T(\hat{\vec{q}}) \cdot \hat{\vec{g}}_w \quad (7)$$

The estimated initial gravity vector,  $\hat{\vec{g}}_w$ , and the true initial gravity vector,  $\vec{g}_w$ , are assumed to be equivalent. A discrepancy between these vectors would result in a perceived sustained acceleration inconsistent with actual human perception literature. In any gravity environment, the CNS is therefore modeled to maintain an initially veridical estimate of the direction and magnitude of gravity.

### A.3 Limbic Coordinate Frame Calculation and Quaternion Transformation

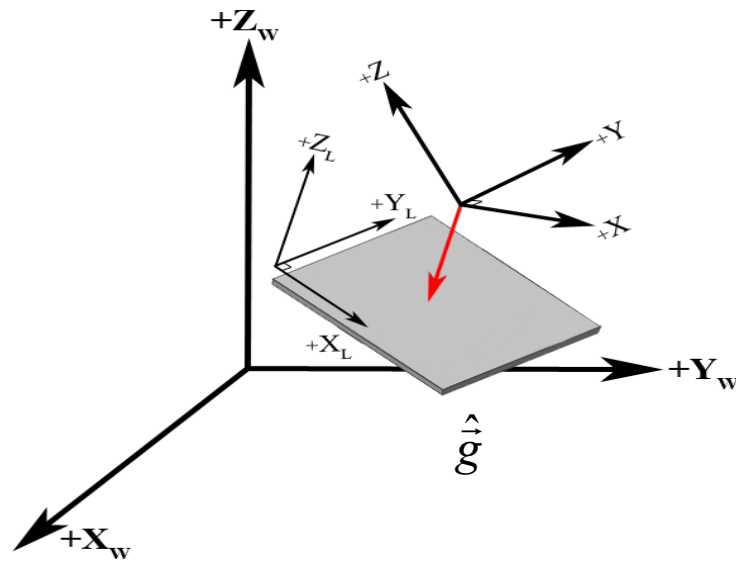


Figure A2 Limbic coordinate frame.

The quaternion vector,  $\hat{\vec{q}}$ , from the estimated gravitational state completely defines the limbic coordinate frame. As shown in Figure A.2, the limbic frame confines to the same right handed orientation and sign conventions of the other coordinate systems. The  $X_L$ - $Y_L$  horizontal plane is perpendicular to the direction of estimated gravity and acts as our natural plane of 2D navigation. Just as  $\mathbf{T}$  was used to transform vectors from world to head coordinates, its inverse can be used to perform the opposite duty. Driven by the estimated quaternion,  $\hat{\vec{q}}$ ,  $\mathbf{T}^{-1}$  can transform any vector from head to limbic coordinates. Rearranging Equation 7, and substituting the estimated acceleration vector in place of gravity, we obtain;

$$T(\hat{\vec{q}}) \cdot \hat{\vec{a}}_L(t) = \hat{\vec{a}}(t) \quad (8)$$

Where  $\hat{\vec{a}}_L(t)$  corresponds to the estimated acceleration vector expressed in the limbic frame. Pre-multiplying both sides of Equation 8 by the inverse transformation we can solve explicitly for  $\hat{\vec{a}}_L(t)$ .

$$\begin{aligned} T^{-1}(\hat{\vec{q}}) \cdot T(\hat{\vec{q}}) \cdot \hat{\vec{a}}_L(t) &= T^{-1}(\hat{\vec{q}}) \cdot \hat{\vec{a}}(t) \\ \hat{\vec{a}}_L(t) &= T^{-1}(\hat{\vec{q}}) \cdot \hat{\vec{a}}(t) \end{aligned}$$

#### A.4 Visual position and velocity transformations

A direct conversion between the world and limbic frame is not possible with the current quaternion setup. To circumvent this potential problem, inputs are converted from world to head coordinates and then subsequently from the head to the limbic system. This rotation is performed with two transformation matrices. The expressions for visual position and velocity are shown below.

$$\begin{aligned} T^{-1}(\hat{\vec{q}}) \cdot (T(\vec{q}) \cdot \vec{x}_v) \\ T^{-1}(\hat{\vec{q}}) \cdot (T(\vec{q}) \cdot \dot{\vec{x}}_v) \end{aligned}$$

#### A.5 Visual gravity and angular velocity transformations

Visual gravity and angular velocity are transformed to head coordinates prior to processing. Rearranging equation 6 and substituting the visual inputs we obtain expressions for their coordinate frame transformations.

$$\begin{aligned} T(\vec{q}) \cdot \vec{\omega}_v \\ T(\vec{q}) \cdot \vec{g}_v \end{aligned}$$



Department of the Army  
U.S. Army Aeromedical Research Laboratory  
Fort Rucker, Alabama, 36362-0577  
[www.usaarl.army.mil](http://www.usaarl.army.mil)



U.S. Army Medical Research and Materiel Command